Eruptive stars spectroscopy
Cataclysmics, Symbiotics, Novae

Eruptive Stars
Information Letter n° 44 #2019-04 28-03-2020
Observations of Sep. - Dec. 2019

Contents

Editors:
F. Teyssier, D. Boyd, F. Sims

Authors :
F. Teyssier, D. Boyd, F. Sims, S. Shore, A. Lucy, J. Guarro, T. Lester, T. Bohlsen, U. Sollecchia, C. Boussin, P. Dubovsky, F. Campos, J. Foster, P. Somogyi, P. Berardi, P. Cazzato, O. Garde, P. McGee

"We acknowledge with thanks the variable star observations from the AAVSO International Database contributed by observers worldwide and used in this letter."
Kafka, S., 2019, Observations from the AAVSO International Database, http://www.aavso.org

Eruptive stars spectroscopy
Cataclysmics, Symbiotics, Novae

Eruptive Stars
Information Letter n° 44 #2019-04 15-02-2020
Observations of Oct. - Dec. 2019

Spectroscopic observations of novae in 2019-Q4

Editors:
F. Teyssier, D. Boyd, F. Sims

Authors:
T. Bohlsen, F. Campos, U. Sollecchia, J. Foster

Abstract:
2 classical nova events were observed during 2019-Q4: Nova LMC 2019 and nova Sct 2019 (V659 Sct)
One spectrum of nova Cyg 2019 (PGIR 19brv) in the near-IR was acquired

Stars:
V659 Sct, V2891 Cyg, AT 2019qwf

nova Sct 2019 = ASASSN-19aad = V659 Sct

Coordinates (2000.0)	
R.A.	18:39:59.8
Dec	-10:25:41.9
Mag (max)	8.3

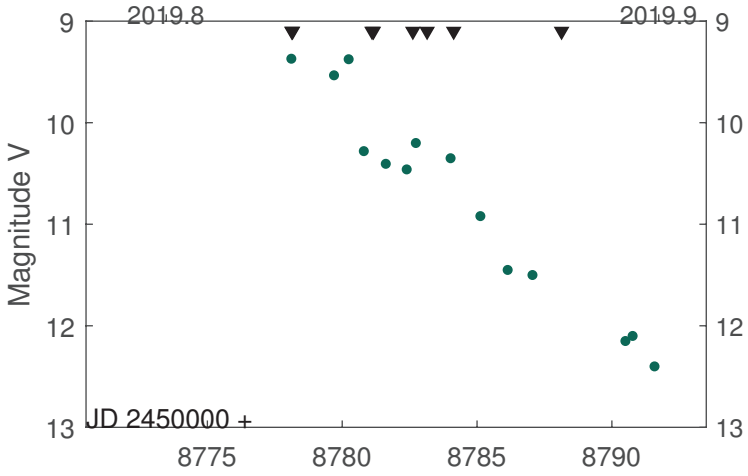

Nova Sct 2019 (ASASSN-19aad) was discovered by the All-Sky Automated Survey for Supernovae (ASAS-SN: Shappee et al. 2014; Kochanek et al. 2017) on 2019-10-29.05 UT at mag 11.5 (g-sloan).
The maximum luminosity was reached around Oct, 31 at mag 8.3 (AAVSO).

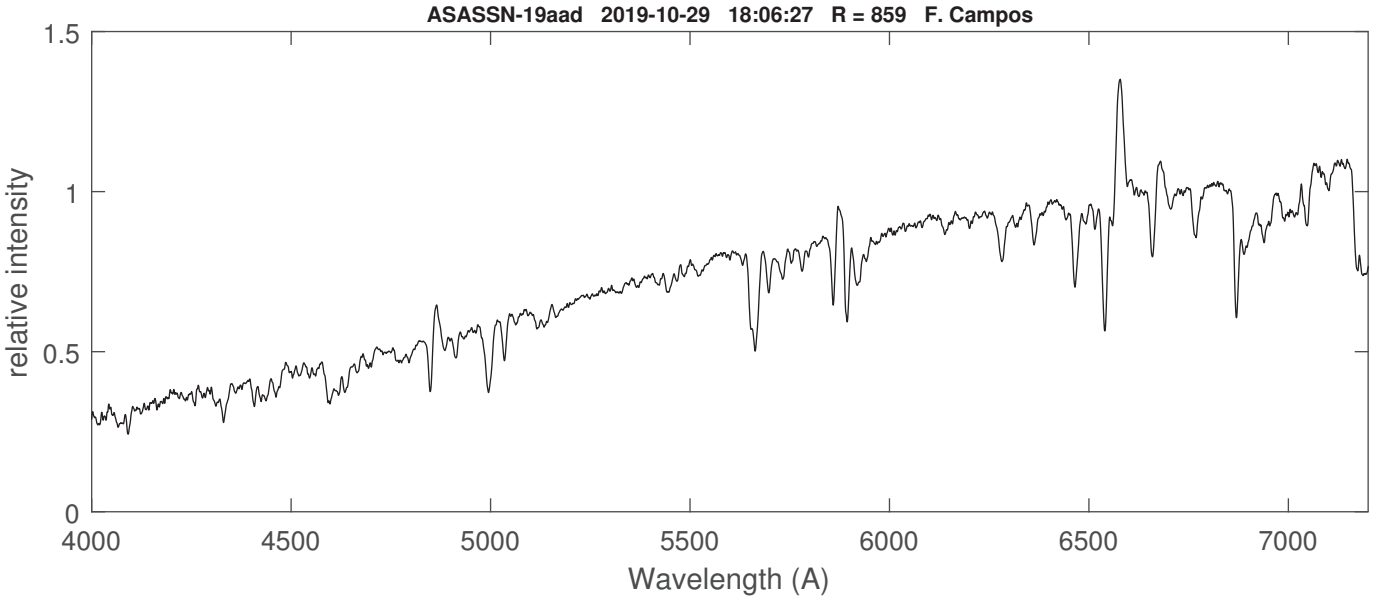

First spectrum in the database obtained by Fran Campos with DADOS-200 on 2019-10.754, 17 hours after the discovery, 1.3 day before the maximum luminosity

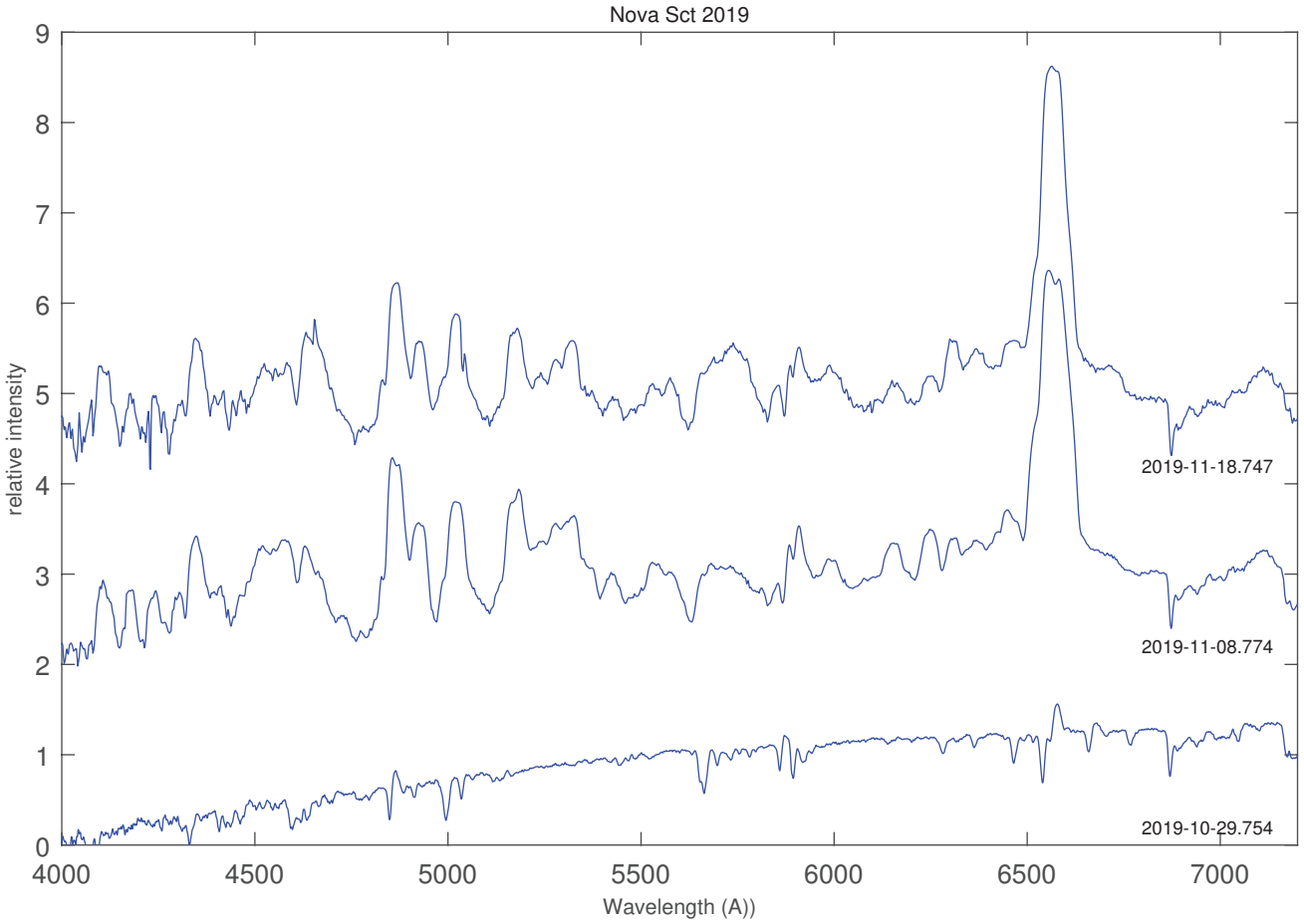

Sequence obtained by Paolo Cazzato with an Alpy (R = 600)

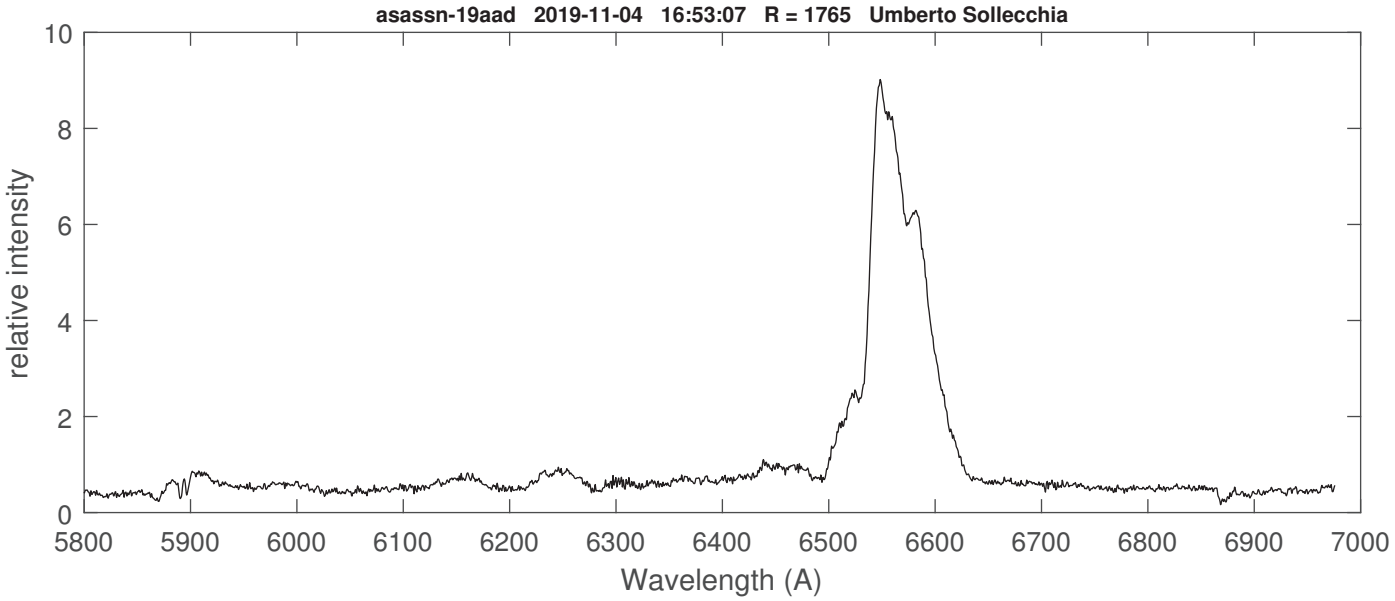

H alpha range obtained by Umberto Sollecchia with a home-made spectrograph.

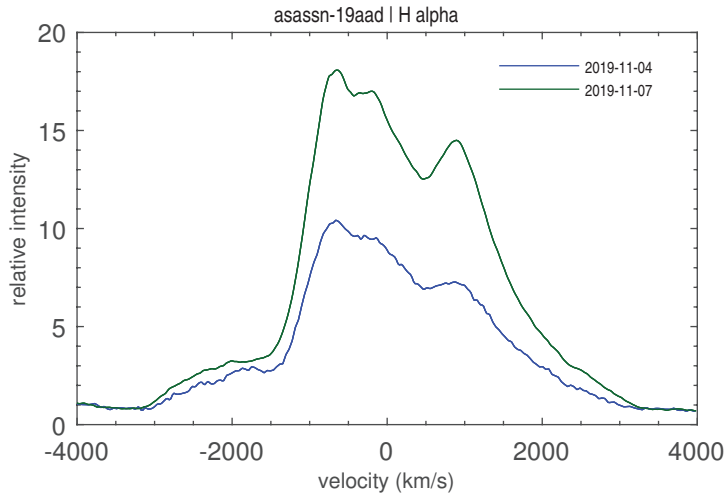

Hα profile. The range of velocities is -3000, + 3300 km.s^{-1}.

nova LMC 2019a = PNV J05145365-700948

Coordinates (2000.0)	
R.A.	05 14 53.6
Dec	-70 09 48
Mag (max)	12

PNV J05145365-7009486, reported by Patrick Schmeer in vsnet-alert 23706, was discovered by the BraTS transient search on UT 2019 Nov. 11.2263 at magnitude 12 and classified as a classical nova by F. M. Walter (ATel #13287).

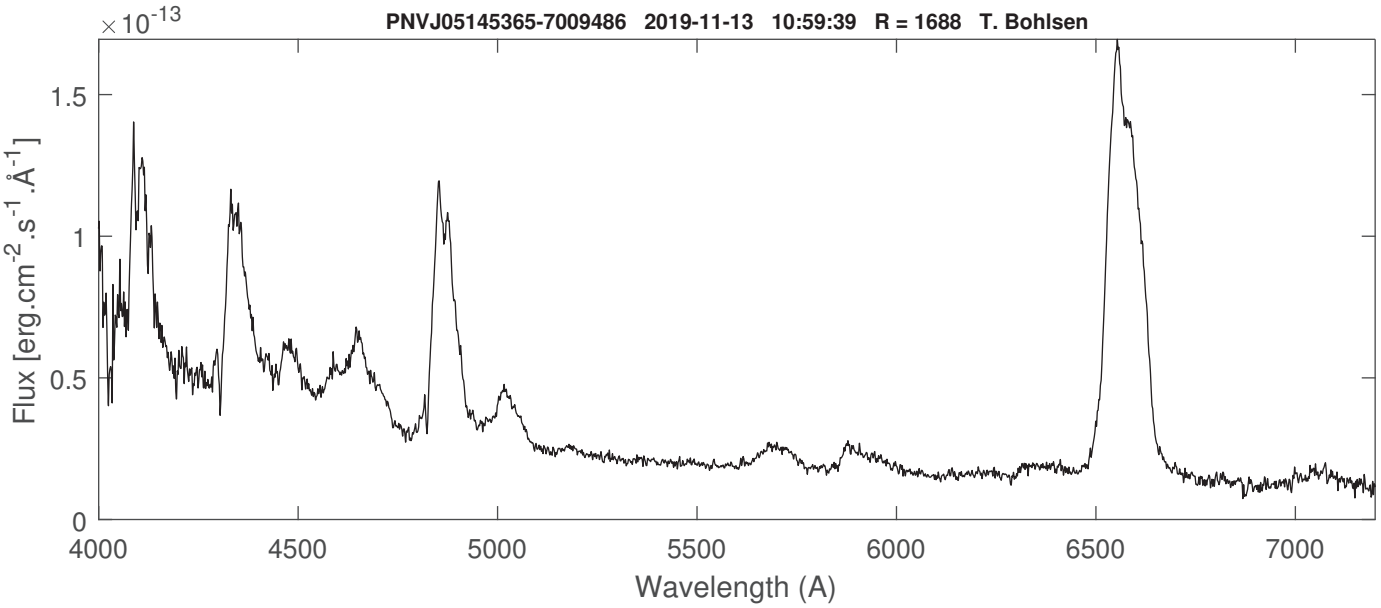

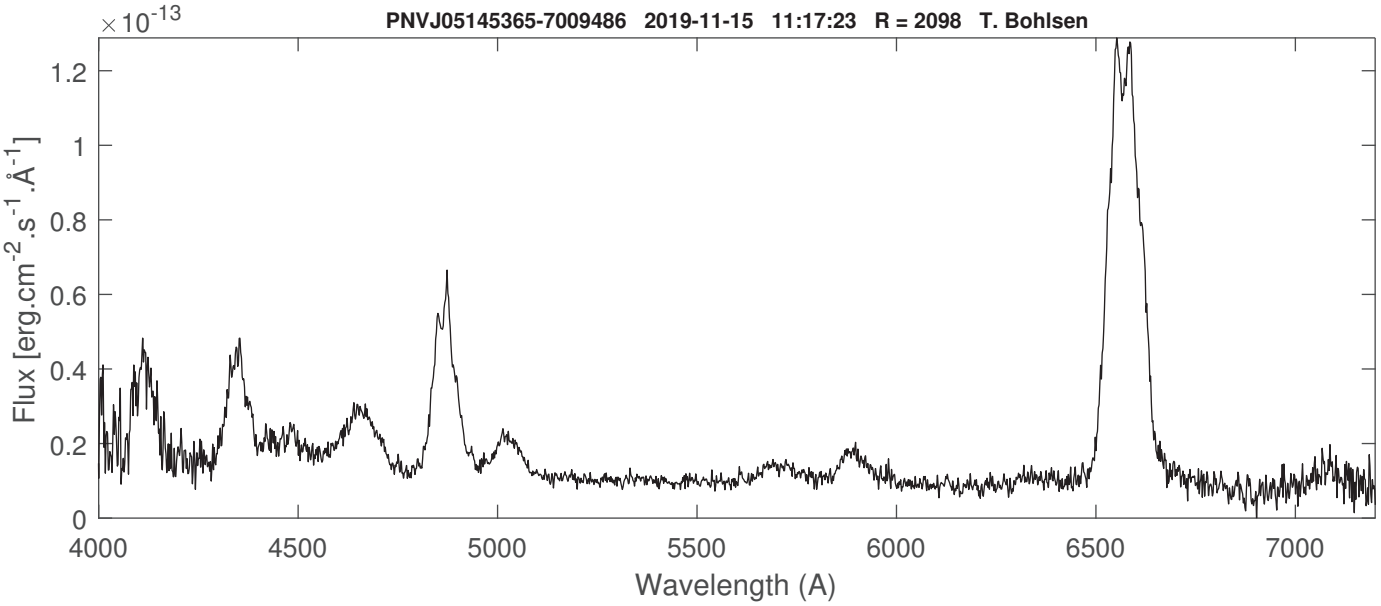

Terry Bohlsen obtained 2 spectra at R = 1000 using a LISA spectrograph on 2019-11-13 and 15, resp. 2 and 4 days after the discovery and maximum luminosity

The spectrum shows broad emission lines of Balmer, He I, Na I. The FWHM of Halpha and Hbeta are 4300 and 3400 km/s resp.

The highly reddened nova V2891 Cyg is still on its very long plateau stage.
OI λλ 7773, 8446 Å appear clearly in the near-IR spectrum obtained on November, 3 by James Foster with a LISA (IR mode)

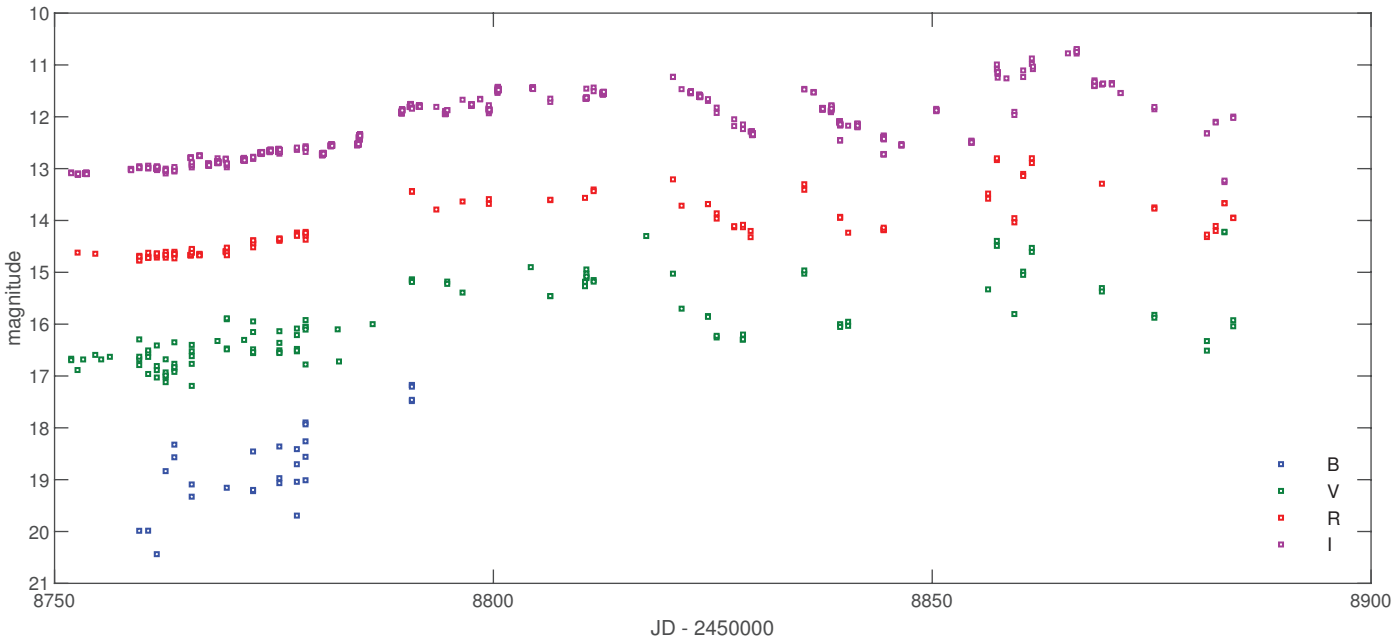

AAVSO BVRI lightcurve

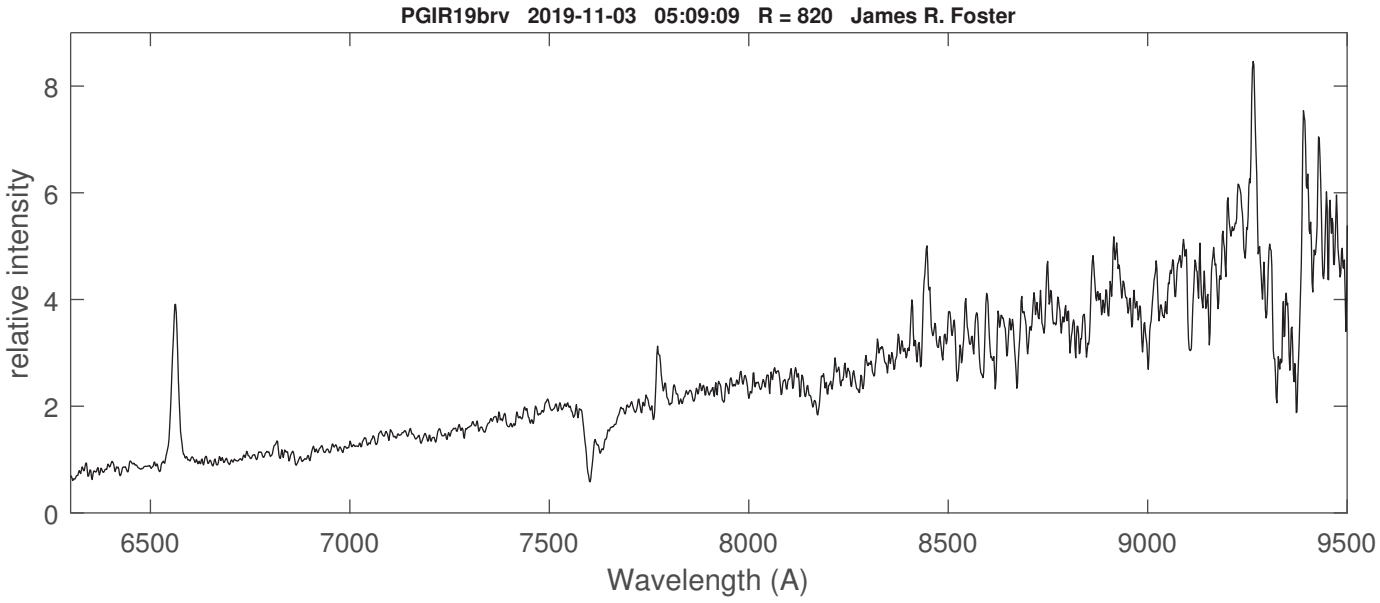

Near IR spectrum of V2891 Cyg obtained by James Foster with LISA (R = 1000)

Eruptive stars spectroscopy
Cataclysmics, Symbiotics, Novae

Eruptive Stars
Information Letter n° 44 #2019-04 15-02-2020
Observations of Oct. - Dec. 2019

Spectroscopic observations of symbiotic stars in 2019-Q4

Authors:
F. Teyssier, D. Boyd, F. Sims, A. Lucy, J. Guarro, T. Lester, C. Boussin, P. Dubovsky, F. Campos, J. Foster, P. Somogyi, P. Berardi, P. Cazzato, T. Bohlsen, O. Garde, P. McGee, U. Sollecchia,

Stars:
AG Dra, AG Peg, AX Per, BF Cyg, CH Cyg, CI Cyg, EG And, fastt1100, HbHa 1704-05, HM Sge, LT Del, omi Cet, PU Vul, R Aqr, RS Oph, stHa 32, StHa 55, SU Lyn, T CrB, V1261 Ori, V1329 Cyg, V443 Her, V471 Per, V627 Cas, V694 Mon, Z And

Abstract:
182 spectra of symbiotic stars were acquired during 2019-Q4 by 16 observers at resolution from 500 to 15000. The monitoring of the prototypical AX Per continued; at the end of 2019, [Fe VII] is still absent. CH Cygni continue to oscillate at low luminosity. R Aqr was continuously observed during the decline of the pulsation of its Mira component at a faint luminsosity suggesting an eclipse. V694 Mon still at high luminosity and low velocity of the absorptions in Balmer and Fe II (42) lines were observed in support to HST observations. FASTT 1100, showing [OIII] λ 5007, was detected as a new symbiotic star.

Request for collaborative observations

Target	Request	Objective	Notes	Status
CH Cyg	Independently A. Skopal M. Karovska	Long term monitoring of a complex and highly variable object	The most spectra as possible especially at R = 5 to 15000	Ongoing
AG Dra	R. Gàlis J. Merc L. Leedjarv	Study of outbursts and orbital variability	He II / Hβ Raman OVI	One spectrum a month
AX Per	R. Gàlis J. Merc	Ongoing outburst, declining	One spectrum aweek (low and high resolution)	Ongoing
SU Lyn	K. Ilkiewitz	Study of the orbital variations of a newly discovered symbiotic	One spectrum a week Res: 5000 to 15000 Hα and [O III] 5007	
V694 Mon	A. Lucy J. Sokolovski M. Karovska	Detection of active phases	Balmer and Fe II lines	New season
R Aqr	M. Karovska	Studying ongoing eclipse	Hα [O III]	Ongoing
RS Oph	N. Shagatova A. Skopal	See Information letter 2019-Q2	More spectra needed in 2020	Continuing until nova event (2026 ?)
T CrB	B. Schaefer	Monitoring before expected nova outburst	One spectrum aweek (low and high resolution)	Continuing until nova event (2023 ?)
Suspected	A. Lucy J. Solovski	Spectroscopic identification of new symbiotics in Southern sky	2 new symbiotics already identified by ARAS observers	Ongoing

Symbiotics ARAS Database Update: 04-01-2020

64 stars
4962 spectra

#	Name	AD (2000)	DE (2000)	Nb.	First	Last
1	EG And	0 44 37.1	40 40 45.7	136	12/08/2010	09/12/2019
2	AX Per	1 36 22.7	54 15 2.5	306	04/10/2011	29/12/2019
3	V471 Per	1 58 49.7	52 53 48.4	33	06/08/2013	03/11/2019
4	Omi Cet	2 19 20.7	-2 58 39.5	36	28/11/2015	28/12/2019
5	BD Cam	03 42 9.3	63 13 0.5	49	08/11/2011	30/08/2019
6	StHa 32	04 37 45.6	-01 19 11.8	7	02/03/2018	03/11/2019
7	UV Aur	05 21 48.8	32 30 43.1	81	24/02/2011	28/03/2019
8	V1261 Ori	05 22 18.6	-8 39 58	19	22/10/2011	03/11/2019
9	StHA 55	05 46 42	6 43 48	11	17/01/2016	02/11/2019
10	SU Lyn	06 42 55.1	+55 28 27.2	173	02/05/2016	30/12/2019
11	ZZ CMi	07 24 13.9	8 53 51.7	61	29/09/2011	21/04/2019
12	BX Mon	07 25 24	-3 36 0	64	04/04/2011	25/03/2019
13	V694 Mon	07 25 51.2	-7 44 8	336	03/03/2011	29/12/2019
14	NQ Gem	07 31 54.5	24 30 12.5	76	01/04/2013	18/04/2019
15	GH Gem	07 4 4.9	12 2 12	9	10/03/2016	15/02/2019
16	CQ Dra	12 30 06	69 12 04	38	11/06/2015	26/06/2019
17	RT Cru	12 34 53.7	-64 33 56.0	1	28/07/2019	28/07/2019
18	TX CVn	12 44 42	36 45 50.6	68	10/04/2011	21/05/2019
19	RW Hya	13 34 18	- 25 22 48.9	19	28/06/2017	05/07/2019
20	IV Vir	14 16 34.3	-21 45 50	12	28/02/2015	06/07/2019
21	T CrB	15 59 30.1	25 55 12.6	319	01/04/2012	02/10/2019
22	AG Dra	16 01 40.5	66 48 9.5	633	03/04/2013	25/12/2019
23	AS 210	16 51 20.4	-26 00 26.7	4	14/06/2018	06/07/2019
24	V503 Her	17 36 46	23 18 18	8	05/06/2013	06/07/2019
25	RS Oph	17 50 13.2	-6 42 28.4	61	23/03/2011	16/10/2019
26	V934 Her	17 06 34.5	+23 58 18.5	31	09/08/2013	07/06/2019
27	Hen 3-1341	17 08 36.5	-17 26 30.4	2	04/07/2019	07/07/2019
28	Hen 3-1342	17 08 55.0	-23 23 26.5	1	07/07/2019	07/07/2019
29	RT Ser	17 39 52.0	-11 56 38.8	3	26/06/2012	03/07/2019
30	AS 245	17 51 00.9	-22 19 35.1	1	15/07/2018	15/07/2018
31	AS 270	18 05 33.7	-20 20 38	7	01/08/2013	13/07/2019
32	AS 289	18 12 22.1	-11 40 07	3	26/06/2012	15/06/2018
33	YY Her	18 14 34.3	20 59 20	30	25/05/2011	05/07/2019
34	FG Ser	18 15 06.2	0 18 57.6	10	26/06/2012	12/07/2019
35	StHa 149	18 18 55.9	27 26 12	8	05/08/2013	31/08/2019
36	V443 Her	18 22 08.4	23 27 20	65	18/05/2011	18/10/2019
38	AS 323	18 48 35.7	-06 41 10.4	2	02/07/2019	13/07/2019
39	FN Sgr	18 53 52.9	-18 59 42	9	10/08/2013	15/07/2018
40	V919 Sgr	19 03 46.0	-16 59 53.9	9	10/08/2013	11/07/2019
41	V1413 Aql	19 03 51.6	16 28 31.7	15	10/08/2013	06/07/2019
42	V335 Vul	19 23 14	+24 27 39.7	12	14/08/2016	25/07/2019
43	BF Cyg	19 23 53.4	29 40 25.1	173	01/05/2011	02/12/2019
44	CH Cyg	19 24 33	50 14 29.1	791	21/04/2011	02/12/2019
45	HM Sge	19 41 57.1	16 44 39.9	14	20/07/2013	26/10/2019
46	QW Sge	19 45 49.6	18 36 50	12	14/08/2016	25/07/2019
47	Hen 3-1768	19 49 48.4	-82 52 37.5	2	16/05/2018	27/05/2018
48	CI Cyg	19 50 11.8	35 41 3.2	228	25/08/2010	01/12/2019
49	StHa 169	19 51 28.9	46 23 6	7	12/05/2016	30/08/2019
50	EF Aql	19 51 51.7	-05 48 16.7	1	11/11/2018	11/11/2018
51	HbHa 1704-05	19 54 42.9	+17 22 12.7	81	09/08/2018	05/10/2019
52	V1016 Cyg	19 57 4.9	39 49 33.9	25	15/04/2015	15/09/2019
53	RR Tel	20 04 18.5	-55 43 33.2	4	08/09/2017	06/09/2019
54	PU Vul	20 21 12	21 34 41.9	26	20/07/2013	01/11/2019
55	LT Del	20 35 57.3	20 11 34	22	28/11/2015	26/10/2019
56	StHa 180	20 39 20.6	-05 17 16.3	2	03/07/2019	06/07/2019
57	Hen 2-468	20 41 19.0	34 44 52.3	2	01/07/2019	11/07/2019
58	ER Del	20 42 46.4	8 40 56.4	14	02/09/2011	30/08/2019
59	V1329 Cyg	20 51 1.1	35 34 51.2	27	08/08/2015	25/12/2019
60	V407 Cyg	21 2 13	45 46 30	12	14/03/2010	18/04/2010
61	StHa 190	21 41 44.8	2 43 54.4	24	31/08/2011	26/08/2019
62	AG Peg	21 51 1.9	12 37 29.4	272	06/12/2009	09/12/2019
63	V627 Cas	22 57 41.2	58 49 14.9	38	06/08/2013	18/11/2019
64	Z And	23 33 39.5	48 49 5.4	187	30/10/2010	29/12/2019
65	R Aqr	23 43 49.4	-15 17 4.2	220	20/11/2010	01/01/2020

ARAS Data Base Symbiotics : http://www.astrosurf.com/aras/Aras_DataBase/Symbiotics.htm

Symbiotics observed in 2019-Q4 (1/2)

Id.	Observer	Date	Range		Res.
AG Dra	P. Berardi	08/10/2019	6329	6788	5445
AG Dra	F. Sims	23/10/2019	3751	7275	984
AG Dra	D. Boyd	27/10/2019	3901	7380	1040
AG Dra	D. Boyd	29/11/2019	3901	7381	1072
AG Dra	D. Boyd	25/12/2019	3900	7381	1033
AG Peg	F. Sims	30/10/2019	3719	7307	1047
AG Peg	F. Teyssier	14/11/2019	4200	7300	11000
AG Peg	J. Guarro	16/11/2019	4053	7763	9000
AG Peg	F. Sims	25/11/2019	3720	7308	1029
AG Peg	D. Boyd	29/11/2019	3900	7381	1032
AG Peg	F. Teyssier	01/12/2019	4060	7300	9000
AG Peg	F. Teyssier	09/12/2019	4100	7300	9000
AX Per	J. Foster	11/10/2018	3835	7396	685
AX Per	P. Berardi	19/10/2018	6362	6790	5634
AX Per	J. Foster	10/11/2018	3700	7400	559
AX Per	F. Sims	03/10/2019	3711	7299	1040
AX Per	T. Lester	11/10/2019	4031	7955	14000
AX Per	P. Cazzato	15/10/2019	3702	7200	543
AX Per	D. Boyd	27/10/2019	3900	7381	1132
AX Per	F. Sims	29/10/2019	3718	7308	967
AX Per	F. Campos	29/10/2019	3725	7263	1151
AX Per	J. Foster	31/10/2019	3660	7395	466
AX Per	J. Foster	03/11/2019	6256	9591	801
AX Per	F. Sims	13/11/2019	3721	7307	987
AX Per	F. Sims	23/11/2019	3726	7275	1018
AX Per	F. Teyssier	24/11/2019	4250	7200	9000
AX Per	F. Sims	02/12/2019	3718	7307	1042
AX Per	D. Boyd	04/12/2019	3901	7380	1070
AX Per	F. Teyssier	11/12/2019	4100	7300	9000
AX Per	F. Sims	18/12/2019	3714	7302	1034
AX Per	F. Sims	20/12/2019	3715	7304	1010
AX Per	F. Teyssier	25/12/2019	4100	7300	11000
AX Per	F. Sims	29/12/2019	3714	7303	1034
BF Cyg	D. Boyd	02/10/2019	3900	7380	1098
BF Cyg	F. Sims	16/10/2019	3715	7302	1059
BF Cyg	F. Campos	26/10/2019	3738	7269	909
BF Cyg	F. Sims	29/10/2019	3718	7307	1040
BF Cyg	D. Boyd	18/11/2019	3900	7381	1035
BF Cyg	F. Sims	27/11/2019	3719	7307	1042
BF Cyg	F. Sims	02/12/2019	3719	7307	1022

Id.	Observer	Date	Range		Res.
CH Cyg	F. Sims	05/10/2019	3713	7299	1054
CH Cyg	J. Guarro	05/10/2019	4053	7763	9000
CH Cyg	J. Guarro	05/10/2019	4053	7763	9000
CH Cyg	P. Berardi	08/10/2019	6329	6788	5841
CH Cyg	T. Lester	09/10/2019	4031	7955	14000
CH Cyg	J. Guarro	16/10/2019	4053	7763	9000
CH Cyg	F. Sims	18/10/2019	3716	7301	985
CH Cyg	F. Sims	21/10/2019	3715	7304	1050
CH Cyg	F. Sims	29/10/2019	3719	7307	1053
CH Cyg	F. Teyssier	14/11/2019	4400	7300	11000
CH Cyg	F. Teyssier	20/11/2019	4500	7200	11000
CH Cyg	F. Teyssier	02/12/2019	4500	7300	11000
CI Cyg	D. Boyd	16/10/2019	3901	7380	1072
CI Cyg	F. Sims	25/11/2019	3720	7306	986
CI Cyg	D. Boyd	01/12/2019	3900	7380	1036
EG And	F. Sims	13/10/2019	3714	7301	984
EG And	F. Sims	21/10/2019	3715	7304	1059
EG And	U. Sollecchia	25/10/2019	6447	6672	13525
EG And	J. Guarro	07/11/2019	4031	8984	9000
EG And	F. Teyssier	18/11/2019	4053	7763	9000
EG And	F. Teyssier	09/12/2019	4053	7763	9000
FASTT 1100	F. Sims	10/10/2019	3901	7276	1062
HbHa 1704-05	F. Sims	05/10/2019	3712	7300	1073
HM Sge	F. Campos	26/10/2019	3738	7276	915
LT Del	F. Sims	21/10/2019	3716	7302	1052
LT Del	F. Campos	26/10/2019	3749	7263	849
omi Cet	J. Foster	31/10/2019	3651	7395	463
omi Cet	J. Foster	03/11/2019	6255	9598	805
omi Cet	J. Guarro	28/12/2019	3980	9018	9000
PU Vul	J. Foster	01/11/2019	3660	7395	471

Symbiotics observed in 2019-Q4 (2/2)

Id.	Observer	Date	Range		Res.
R Aqr	F. Sims	05/10/2019	3711	7299	1047
R Aqr	J. Guarro	05/10/2019	4178	7756	9000
R Aqr	T. Lester	09/10/2019	4031	7955	14000
R Aqr	F. Sims	14/10/2019	3715	7302	1064
R Aqr	P. Cazzato	15/10/2019	3703	7199	514
R Aqr	F. Sims	16/10/2019	3714	7302	1051
R Aqr	J. Guarro	17/10/2019	4053	7763	9000
R Aqr	F. Sims	18/10/2019	3715	7301	1004
R Aqr	F. Sims	20/10/2019	3717	7305	1060
R Aqr	F. Campos	26/10/2019	3735	7267	1052
R Aqr	T. Lester	29/10/2019	4031	7955	14000
R Aqr	F. Sims	29/10/2019	3717	7308	1012
R Aqr	J. Foster	01/11/2019	3660	7395	474
R Aqr	T. Bohlsen	02/11/2019	6494	6657	14488
R Aqr	J. Foster	03/11/2019	6255	9591	815
R Aqr	F. Sims	12/11/2019	3720	7307	936
R Aqr	J. Guarro	13/11/2019	4061	9165	9000
R Aqr	T. Bohlsen	15/11/2019	3800	7400	1760
R Aqr	F. Sims	17/11/2019	3720	7306	972
R Aqr	F. Teyssier	19/11/2019	4200	7700	9000
R Aqr	F. Sims	23/11/2019	3725	7274	1044
RS Oph	F. Sims	01/10/2019	3712	7298	1073
RS Oph	F. Sims	16/10/2019	3715	7301	1010
stHa 32	J. Foster	01/11/2019	3671	7395	469
stHa 32	J. Foster	03/11/2019	6255	9501	793
StHa 55	J. Foster	02/11/2019	3676	7395	485
SU Lyn	F. Sims	13/10/2019	3712	7301	945
SU Lyn	D. Boyd	27/10/2019	3900	7381	1067
SU Lyn	F. Sims	18/11/2019	3726	7274	1026
SU Lyn	F. Teyssier	01/12/2019	4053	7763	9000
SU Lyn	D. Boyd	01/12/2019	3802	7390	1086
SU Lyn	F. Sims	21/12/2019	3713	7303	981
SU Lyn	O. Garde	30/12/2019	3972	7588	11000
SU Lyn	D. Boyd	30/12/2019	3900	7380	1027
T CrB	F. Sims	02/10/2019	3716	7274	1055
T CrB	D. Boyd	02/10/2019	3802	7390	1155
V1261 Ori	J. Foster	01/11/2019	3671	7395	476
V1261 Ori	J. Foster	03/11/2019	6255	9591	793
V1329 Cyg	D. Boyd	01/09/2019	3801	7390	1140
V1329 Cyg	D. Boyd	11/11/2019	3900	7381	944
V1329 Cyg	D. Boyd	25/12/2019	3900	7380	1068
V443 Her	F. Sims	18/10/2019	3715	7302	954
V471 Per	F. Campos	29/10/2019	3726	7264	1167
V471 Per	J. Foster	31/10/2019	3651	7395	465
V471 Per	J. Foster	03/11/2019	6256	9592	804

Id.	Observer	Date	Range		Res.
V627 Cas	F. Sims	30/10/2019	3719	7307	1044
V627 Cas	J. Foster	01/11/2019	3660	7395	478
V627 Cas	J. Foster	03/11/2019	6256	9592	817
V627 Cas	F. Sims	12/11/2019	3722	7307	883
V627 Cas	F. Sims	18/11/2019	3726	7274	953
V694 Mon	P. Somogyi	20/10/2019	6225	6932	2593
V694 Mon	P. Somogyi	20/10/2019	5424	6136	2266
V694 Mon	P. Somogyi	20/10/2019	4554	5269	1938
V694 Mon	P. Somogyi	22/10/2019	6502	6612	15837
V694 Mon	P. Somogyi	22/10/2019	4817	4961	9370
V694 Mon	F. Sims	22/10/2019	3716	7304	989
V694 Mon	F. Sims	23/10/2019	3717	7306	1055
V694 Mon	T. Bohlsen	23/10/2019	3800	7390	1333
V694 Mon	P. McGee	23/10/2019	4484	5526	1803
V694 Mon	P. Somogyi	24/10/2019	6503	6612	15792
V694 Mon	P. Somogyi	24/10/2019	4818	4962	9358
V694 Mon	J. Foster	01/11/2019	3671	7395	474
V694 Mon	J. Foster	03/11/2019	6255	9590	794
V694 Mon	F. Sims	21/12/2019	3714	7303	989
V694 Mon	F. Sims	29/12/2019	3719	7308	1042
Z And	T. Lester	05/10/2019	4031	7955	14000
Z And	F. Sims	10/10/2019	3712	7300	1052
Z And	F. Sims	20/10/2019	3715	7304	1015
Z And	D. Boyd	27/10/2019	3900	7380	1053
Z And	F. Sims	13/11/2019	3721	7307	1014
Z And	J. Guarro	16/11/2019	4053	7763	9000
Z And	F. Teyssier	19/11/2019	4060	7300	9000
Z And	F. Sims	25/11/2019	3719	7307	1035
Z And	F. Sims	02/12/2019	3718	7307	1026
Z And	F. Teyssier	02/12/2019	4200	7300	9000
Z And	D. Boyd	09/12/2019	3901	7380	1009
Z And	F. Teyssier	25/12/2019	4200	7300	11000
Z And	F. Sims	29/12/2019	3715	7304	999

AG Dra

Coordinates (2000.0)	
R.A.	16 01 41.0
Dec	+66 48 10.1
Mag V	9.8

Continuous observations of AG Dra upon the request of J. Merc and R. Gàlis.
Monitoring continues in order to acquire reference spectra according to the orbital phase in low activity.
01/10/2019: orbital phase = 0.550
31/12/2019: orbital phase = 0.716
(Fekel & al., 2000)

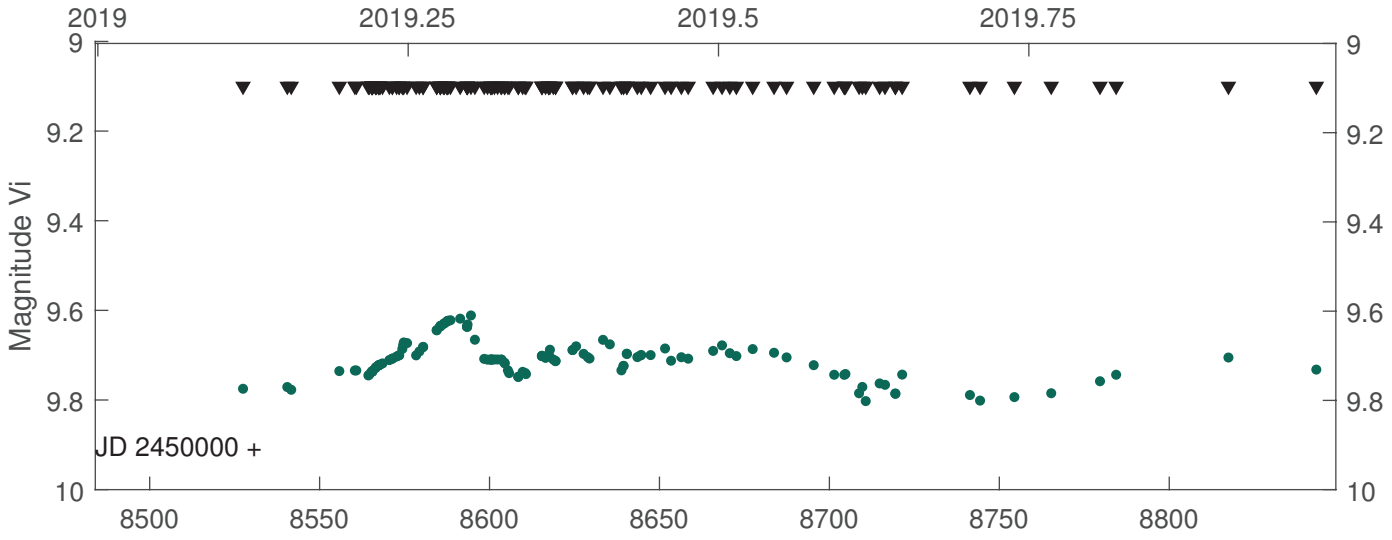

AAVSO lightcurve (selected and interpolated for the time of spectra) in 2019 and ARAS spectra (2019)
137 spectra were obtained in 2019.

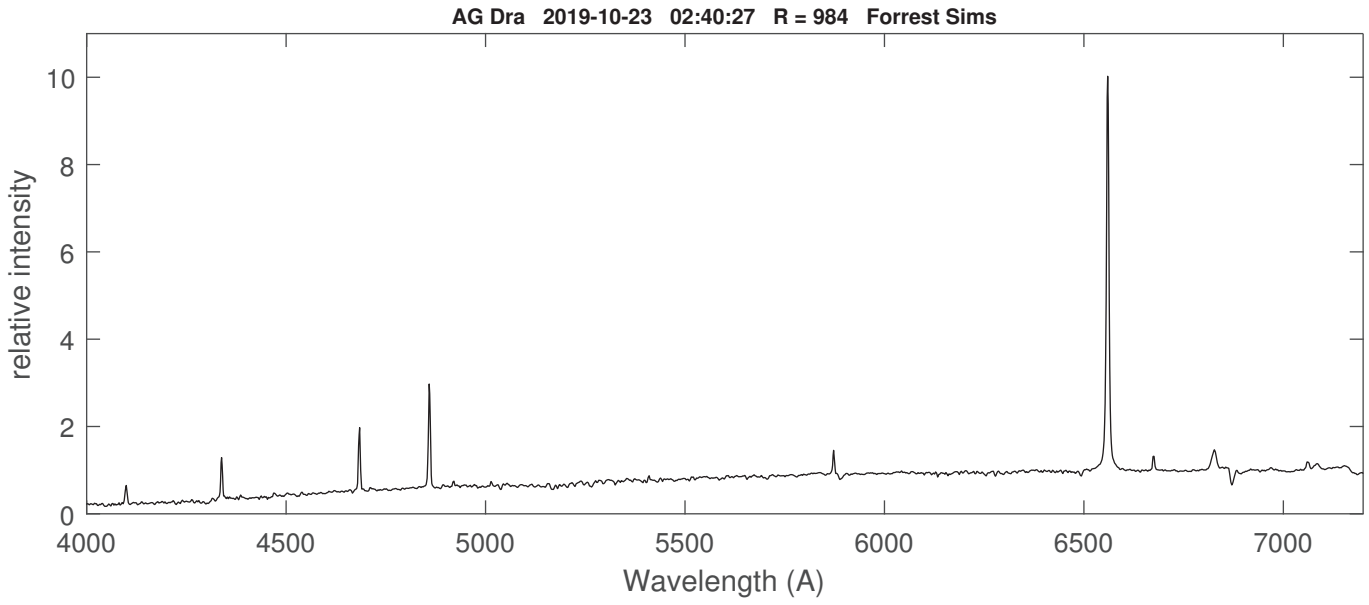

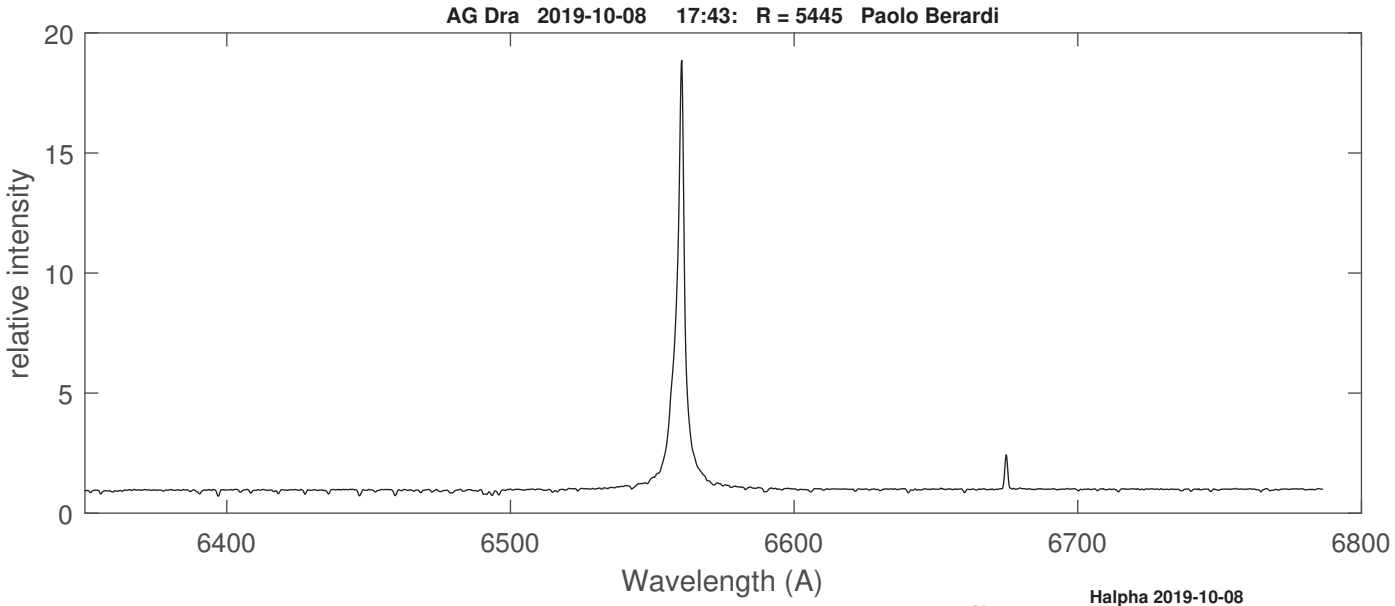

Lhires III 1200 l/mm - Paolo Berardi
Hα range and profile

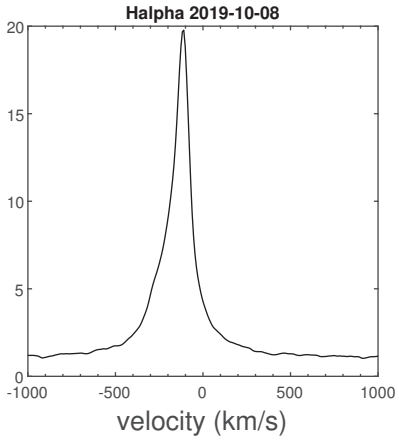

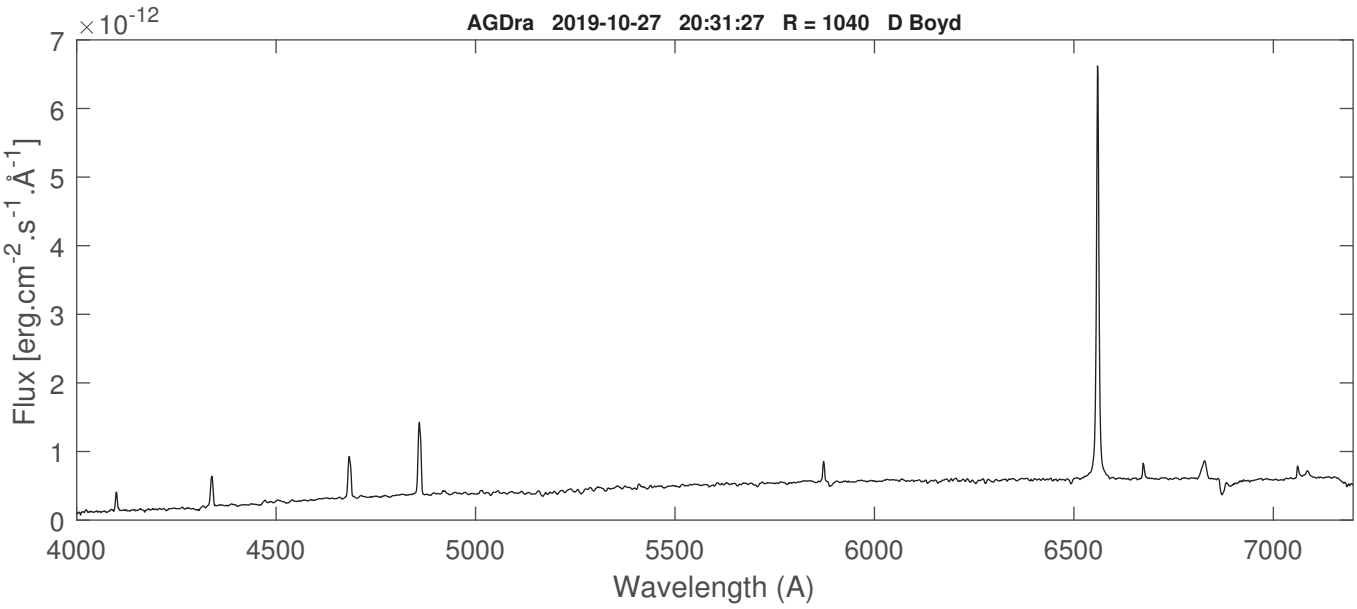
AGDra 2019-10-27 20:31:27 R = 1040 D Boyd
×10^-12
Flux [erg.cm^-2.s^-1.Å^-1]
Wavelength (A)

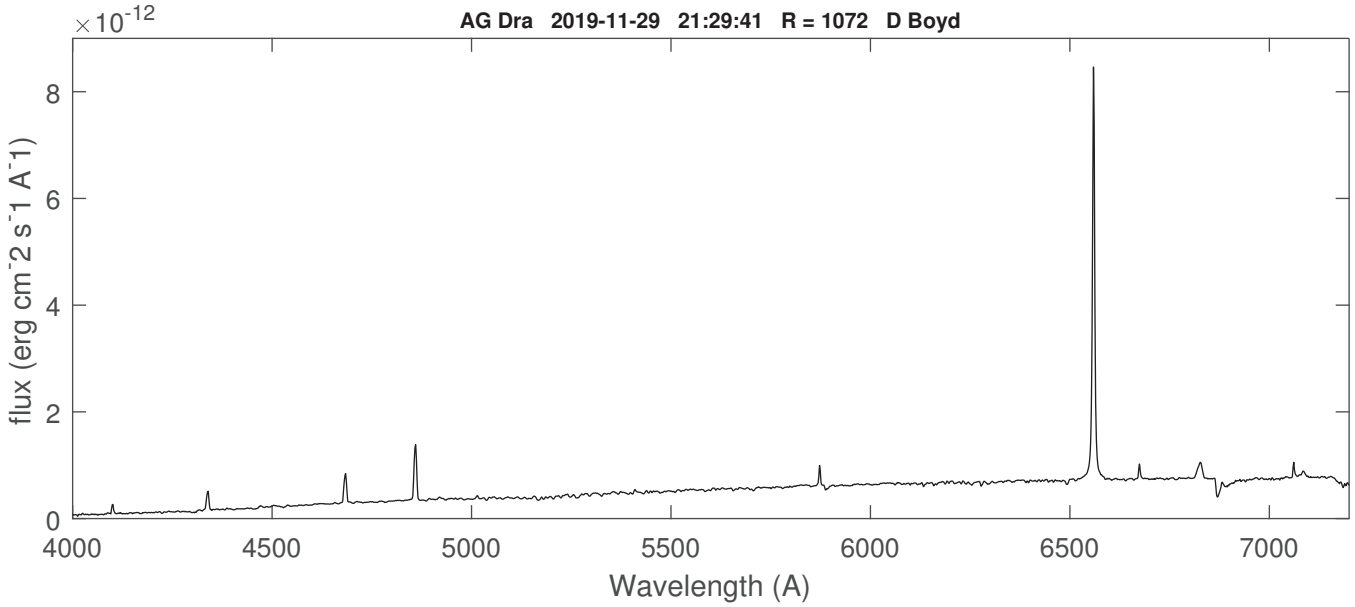
AG Dra 2019-11-29 21:29:41 R = 1072 D Boyd
×10^-12
flux (erg cm^-2 s^-1 A^-1)
Wavelength (A)

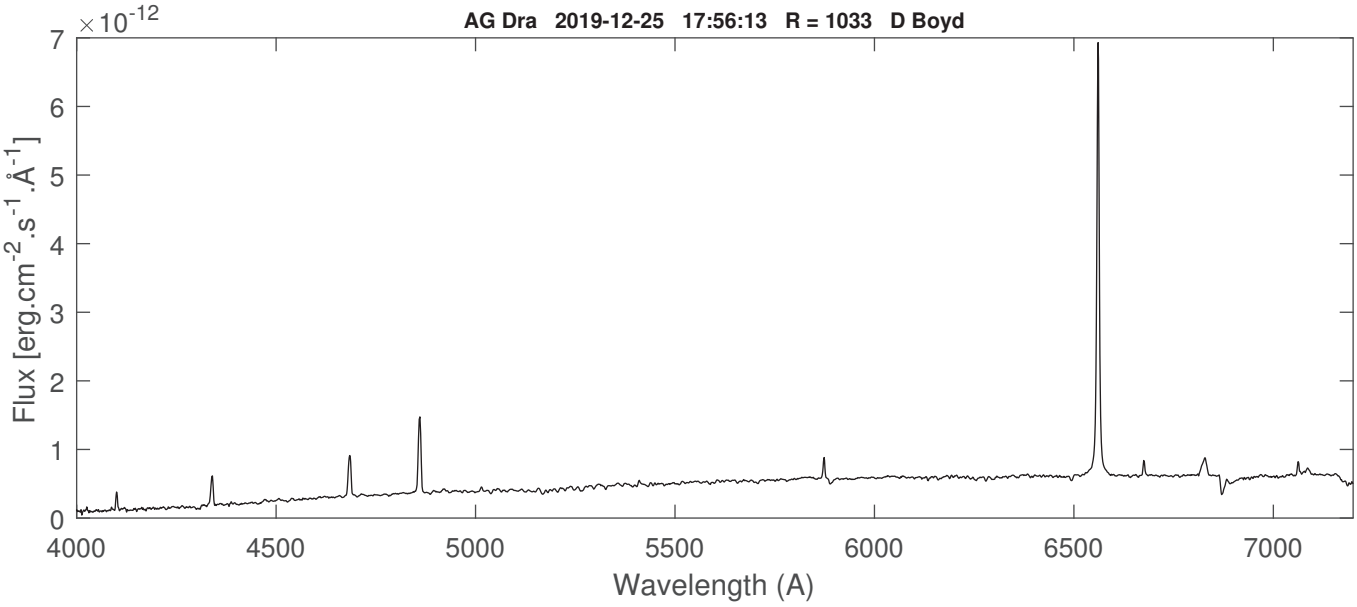
AG Dra 2019-12-25 17:56:13 R = 1033 D Boyd
×10^-12
Flux [erg.cm^-2.s^-1.Å^-1]
Wavelength (A)

AG Peg

Coordinates (2000.0)	
R.A.	21 51 01.97
Dec	+12 37 32.1
Mag	8.7

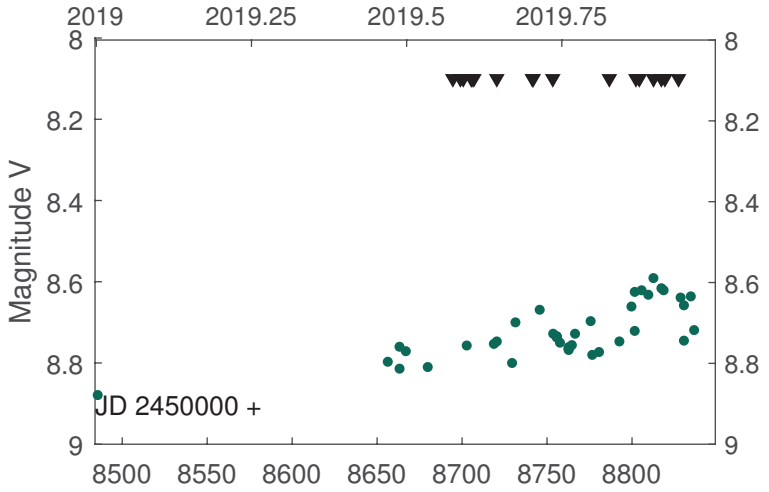

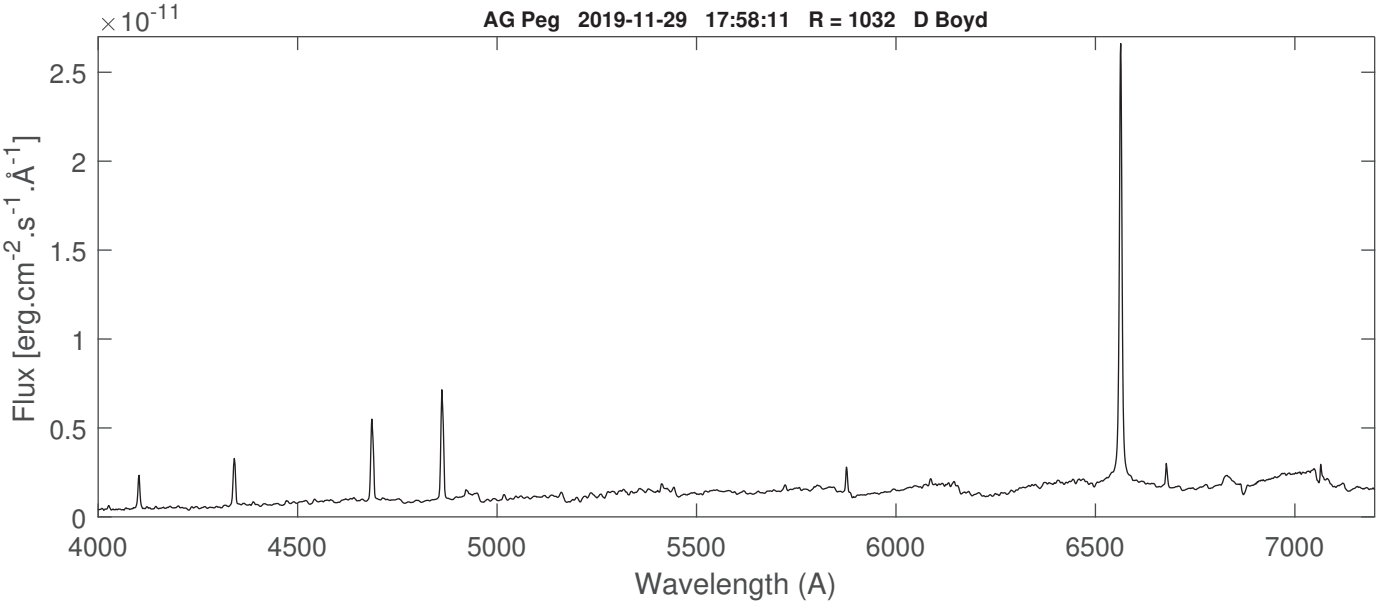

Selected lines profiles from echelle spectra (Joan Guarro, Tim Lester, François Teyssier)
30-07-2019: phase 0.101
09-12-2019: phase 0.263 (Kenyon & Garcia, 1987)

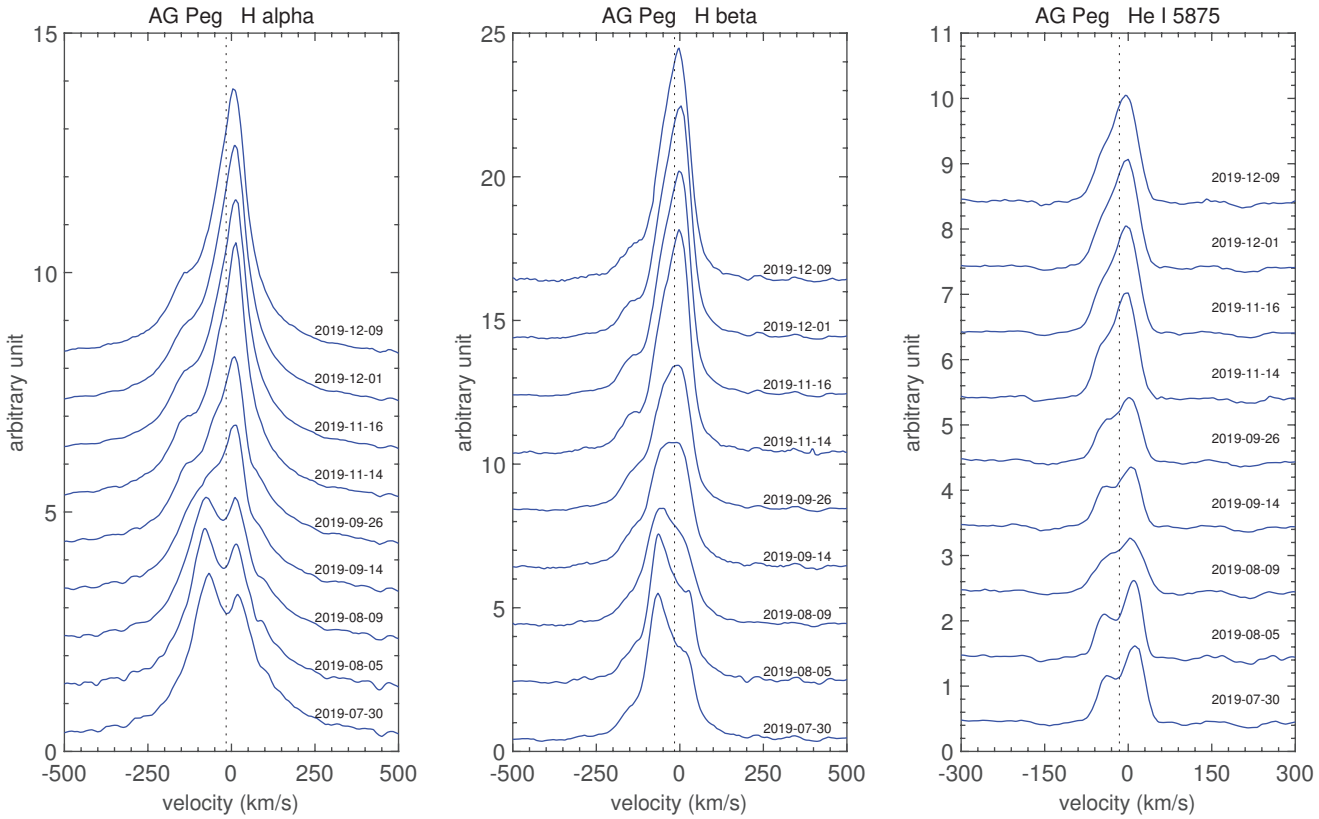

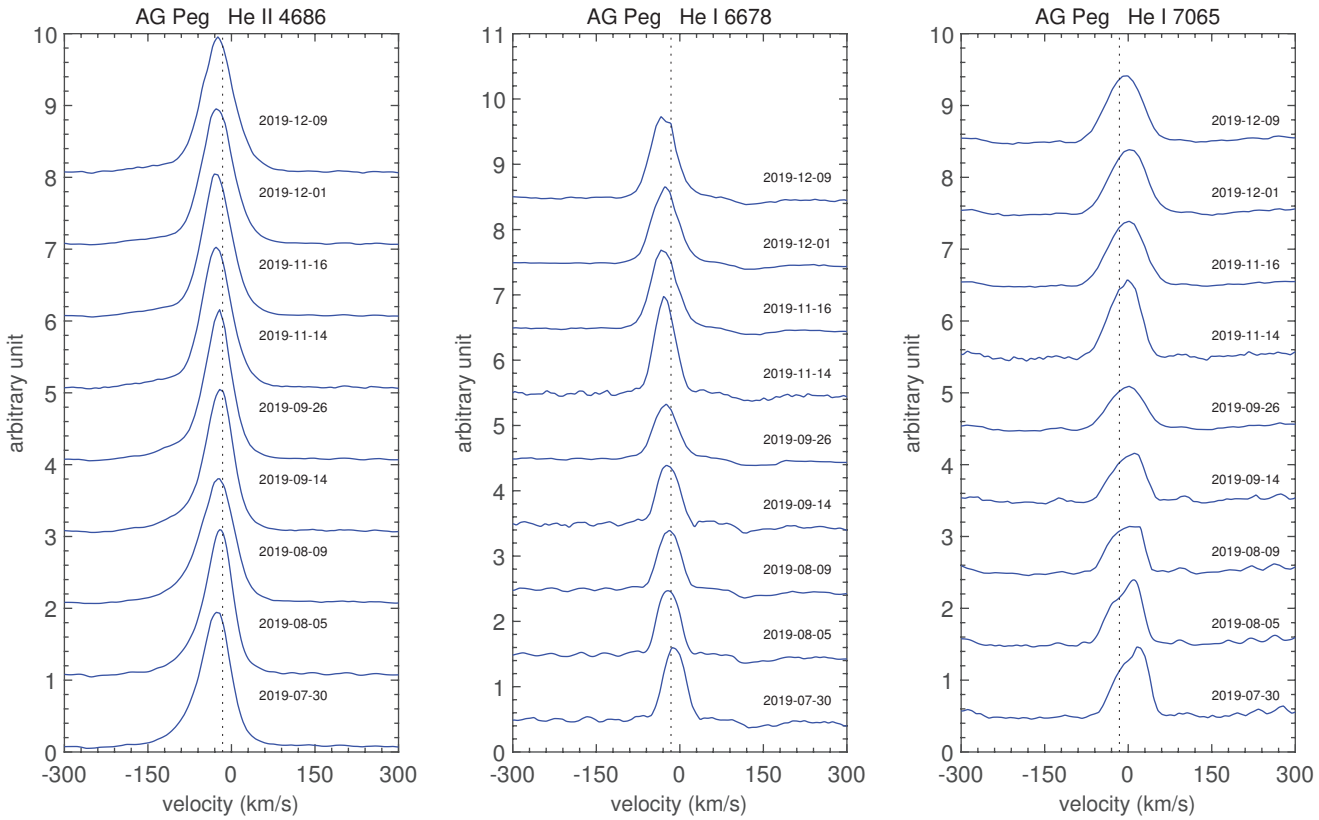

AX Per

Coordinates (2000.0)	
R.A.	01 36 22.7
Dec	+54 15 02.4
Mag	10.7 (2019-12)

Still in declining outburst. The luminosity (V) is almost stabilized since phase 0.45.
The forbidden lines [Fe VII] are still absent.

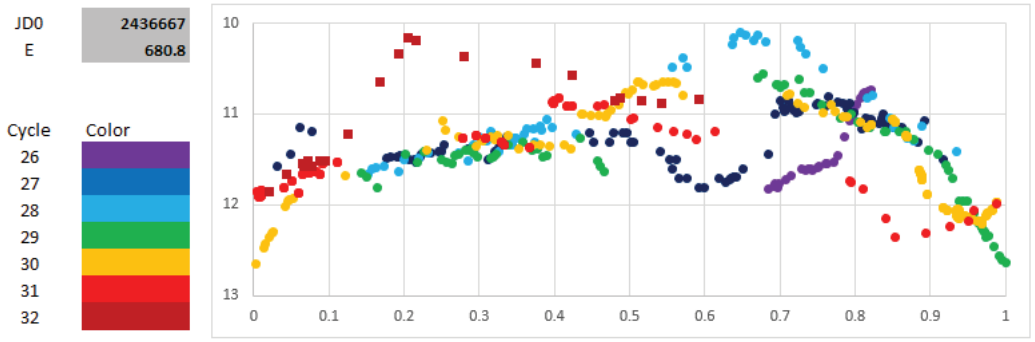

V band lightcurve according to phase (Fekel+,2000) - Current cycle: brown squares.

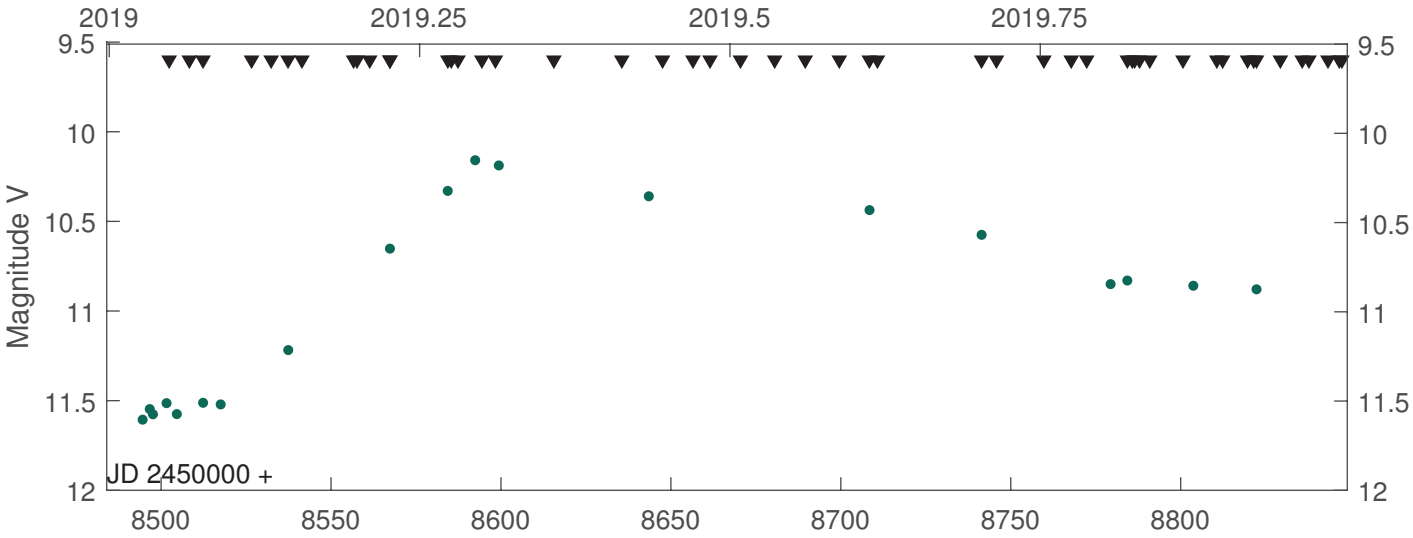

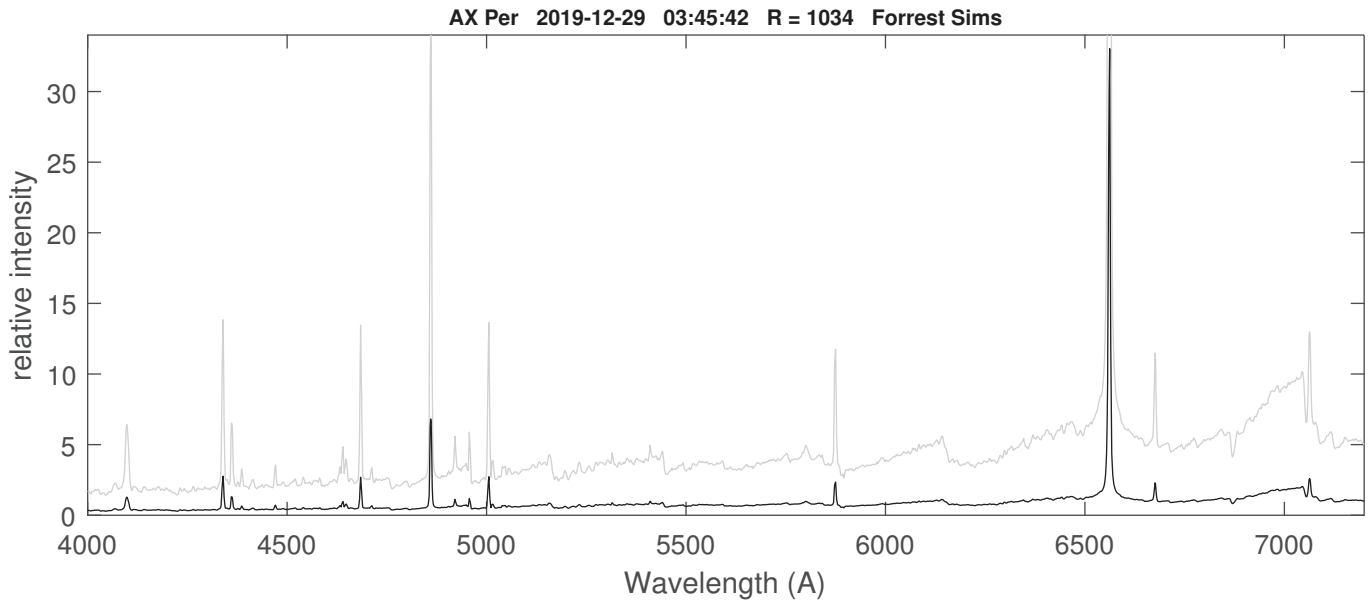

Date	J. D.	H alpha	H beta	He II 4686	He I 5876	He I 6678	[Fe VII] 6087
18/01/2019	2458502.366	224.5	22.3	22.3	12.9	7.1	6.6
24/01/2019	2458508.301	216.8	24.5	22.8	11.1	8.8	5.8
28/01/2019	2458512.339	229.2	27.0	27.2	12.3	10.0	6.8
12/02/2019	2458526.617	218.1	33.3	30.6	12.7	10.9	5.4
17/02/2019	2458532.386	271.2	30.2	27.0	13.7	13.1	6.4
22/02/2019	2458537.348	251.9	39.1	35.5	9.7	12.3	4.1
26/02/2019	2458541.429	274.3	49.5	54.5	12.5	16.1	2.5
14/03/2019	2458556.632	425.9	80.8	60.8	21.0	30.3	-
15/03/2019	2458557.631	438.1	83.0	62.8	22.2	31.7	-
18/03/2019	2458561.382	393.1	86.0	74.7	26.2	27.5	-
24/03/2019	2458567.317	543.1	101.8	73.6	25.1	44.0	-
24/03/2019	2458567.344	614.8	90.8	68.4	26.1	50.3	-
10/04/2019	2458584.372	836.3	164.8	80.6	33.3	69.7	-
11/04/2019	2458585.378	951.7	146.1	81.2	43.1	79.5	-
20/04/2019	2458594.384	941.6	158.7	85.8	46.7	69.6	-
24/04/2019	2458598.361	901.1	142.4	73.7	48.3	65.2	-
12/05/2019	2458615.564	1021.1	142.5	19.9	58.0	44.1	-
01/06/2019	2458635.565	838.0	94.2	8.3	38.2	30.6	-
13/06/2019	2458647.542	796.2	68.7	4.6	35.5	22.8	-
21/06/2019	2458656.492	711.5	67.7	5.8	32.7	21.2	-
26/06/2019	2458661.513	623.9	79.5	8.9	33.9	21.5	-
05/07/2019	2458670.467	680.7	91.5	11.1	35.5	24.2	-
16/07/2019	2458680.540	641.7	83.9	9.7	36.4	19.1	-
25/07/2019	2458689.530	527.6	81.6	11.5	30.0	15.4	-
04/08/2019	2458699.552	464.2	64.7	8.5	24.9	14.8	-
12/08/2019	2458708.394	523.0	82.6	16.7	22.8	15.0	-
15/08/2019	2458710.769	593.4	60.2	9.9	28.0	18.2	-
14/09/2019	2458741.405	531.2	87.8	20.6	22.4	15.6	-
19/09/2019	2458745.788	552.3	95.4	23.3	24.8	17.1	-
03/10/2019	2458759.743	566.4	99.0	20.9	24.2	16.9	-
11/10/2019	2458767.794	605.1	85.2	17.3	30.3	19.0	-
15/10/2019	2458772.360	702.5	85.4	14.5	29.4	22.3	-
27/10/2019	2458784.314	558.3	95.4	24.3	21.8	17.1	-
29/10/2019	2458785.755	538.1	97.0	23.5	23.5	16.6	-
29/10/2019	2458786.429	530.0	87.9	25.1	19.4	14.5	-
31/10/2019	2458787.900	400.2	57.1	16.0	19.3	16.1	-
13/11/2019	2458800.683	494.4	98.1	25.6	21.6	16.2	-
23/11/2019	2458810.639	520.4	94.2	27.0	22.7	15.9	-
24/11/2019	2458812.352	691.1	67.2	15.4	27.8	22.2	-
02/12/2019	2458819.681	500.5	98.3	30.1	21.5	15.7	-
04/12/2019	2458822.318	581.4	91.4	27.0	22.7	19.5	-
11/12/2019	2458829.326	589.7	78.0	20.9	25.3	20.3	-
18/12/2019	2458835.761	586.3	90.6	26.9	23.1	19.2	-
20/12/2019	2458837.739	615.7	91.8	25.5	24.4	19.1	-
25/12/2019	2458843.343	650.7	101.1	29.0	25.3	23.7	-
29/12/2019	2458846.673	541.5	87.8	24.8	21.6	16.5	-

Table 1. Flux of the main lines in units of 10^{-13}.erg.cm^{-1}.s^{-1}

The spectra have been calibrated in flux using AAVSO V band magnitudes (see the method described by David Boyd in ESIL#43 p. 94. The values are not derredened.

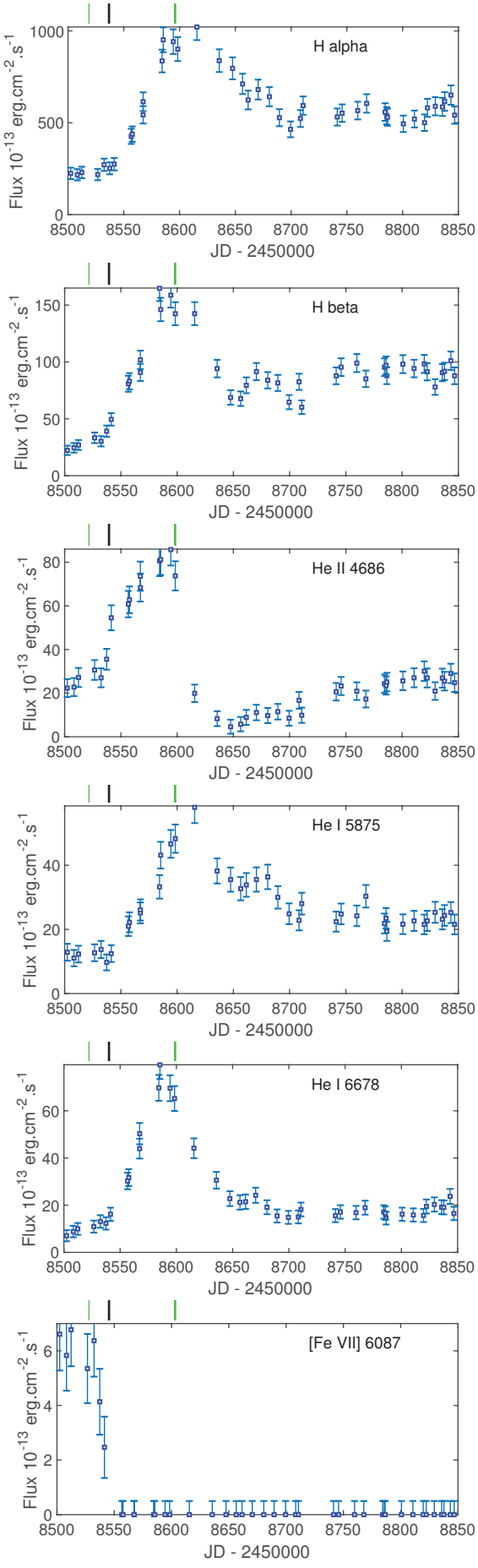

Fig. 1 - Mean lines intensity during the 2019 outburst. 3 spectra were discarded (high error due to the shape of the continuum). For each line, the error bar is the sum of a constant and a percentage of the flux.

As the system rises from JD 2458517 to visual maximum F(Hα) increases by a factor 4 from 22.10^{-11} to 95.10^{-11} erg.cm^{-2}.s^{-1}, reaching the maximum value on JD2458600 +/- 5. The flux declines to 55.10^{-11} erg.cm^{-2}.s^{-1} by a factor 2 and remains almost constant since JD 2458690, slightly increasing to 60.10^{-11} erg.cm^{-2}.s^{-1}.

Hβ follows the same trend, raising by a factor 6 from 25.10^{-13} to 150.10^{-13} erg.cm^{-2}.s^{-1} . It declines twice more quickly than Hα to 60 $.10^{-13}$ erg.cm^{-2}.s^{-1} on JD 2458650 and remains almost constant near 95.10^{-13} erg.cm^{-2}.s^{-1}.
As a result, the ratio Hα/Hβ evolves significantly during the outburst, first declining from 7(+/-1) to 4 (+/-0.5) at the begining of the outburst and remaining at this value until the peak of luminosity. At the begining of the decline, it rises again to the pre-outburst value, 7 (+/- 1) on JD2458650, 50 (+/- 10) days after the maximum luminosity.

The flux of He II λ 4686 increased by a factor 4 from 22.10^{-13} to 82.10^{-13} erg.cm^{-2}.s^{-1} reaching its maximum value at the same epoch than Hβ . During that phase, the ratio He II/Hb decreases smoothly by a factor 2 (Fig. 2c).
Just after the maximum, the flux of He II drops dramatically from to 82.10^{-13} to 20.10^{-13} erg.cm^{-2}.s^{-1} in 18 days and reaches a minimum at 5 $.10^{-13}$ erg.cm^{-2}.s^{-1} on JD 2458650. The ratio He II/Hb decreased steeply from 0.5 to its minimum 0.06 during that episode (Fig.2c).

The evolution of the flux of He I 5876 and He I 6678 differs significantly. F(He I 5876) increases by a factor of the same order of value than other recombination lines while F(He I 6678) increases by a factor 8. As a result, the diagnostic ratio F(He I 6678)/F(He I 5876) rises from ~ 0.8 to a very high value of 1.9 (+/- 0.2). This is interpreted as the result of a significant increase of the electronic density Ne (Proga+, 1990). This is consistent with the evolution of Hα/Hβ.

The intensity of the forbiden line [Fe VII] λ 6087Å collapses about 20 days after the beginning of the visual outburst from 6.10^{-13} erg.cm^{-2}.s^{-1} on JD 2458532 to ~ 0 on JD2458550 (+/-5). The decrease coincides with the increase of the ratio F(He I 6678)/F(He I 5876) and the drop of TiO_1 index. It happens while the temperature of the hot component, evaluated from the ratio He II/Hb used as proxy (Iijima, 1982), remains high (~180 kK).
We interprete the collapse of [Fe VII] as a result of the increase of the electronic density produced by ionization/recombination of a large part of the nebula rather than a decrease of the temperature of the hot component.

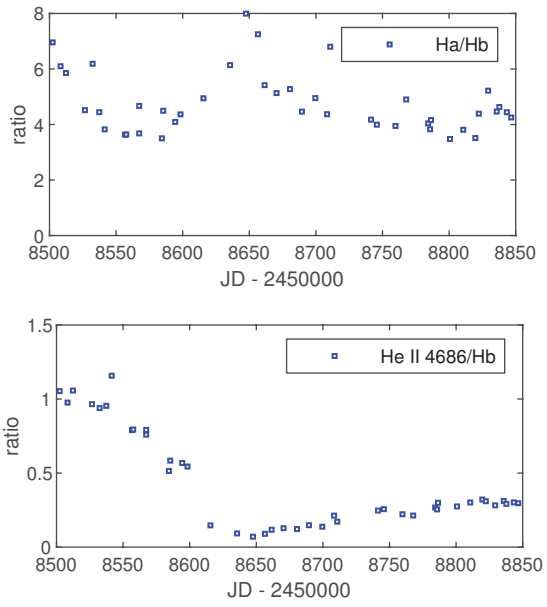

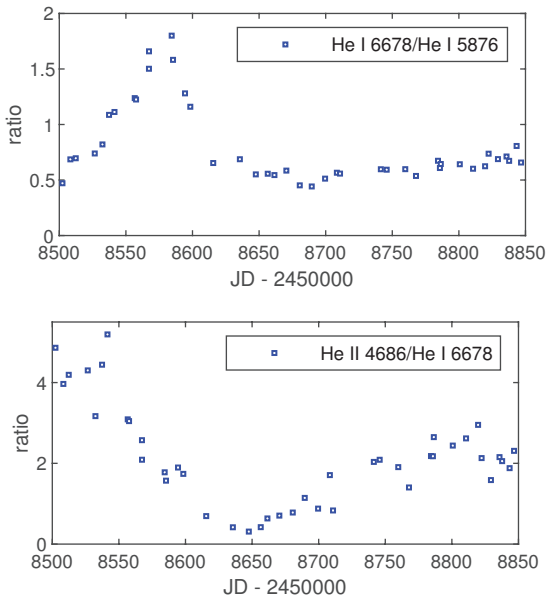

Fig. 2abcd - Diagnostic flux ratios.
a. Top left: Ha/Hβ
b. Top right: He I 5876/6678
c. Bottom left: He II 4686 / Hβ
d. Bottom right: He II 4686 / He I 6678

The ratios were derredened using
E_{B-V} = 0.27 (Mikolajewska & Kenyon, 1992)

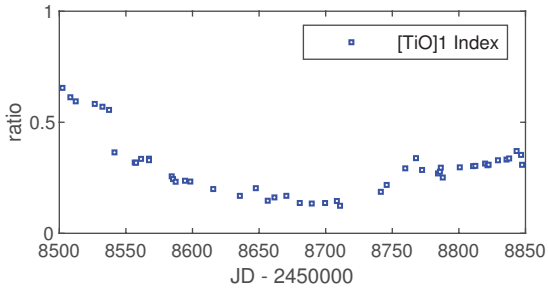

Fig. 3 - $[TiO]_1$ Index as defined by Kenyon & Fernadez-Castro (1987)

JD - 245000	Δ Days Rise	Δ days V max	error (days)	
8500	-17	-100		Balmer lines, He II, He I 6678 increases slowly at constant V luminosity (11.5). He I 5876 remains constant
8517	0	-83	4	V luminosity begins raising from 11.5 Balmer lines, He II, He I 6678 increases slowly He I 5876 remains constant
8537	+ 20	- 63	3	TiO1 index drops from 0.55 to 0.36 in less than 6 days [Fe VII] lines collapse He I 5876 begins to increase The ratio He II/ Hβ fades slowly
8550	+33	-50	5	[Fe VII] disappears The ratio F(Ha)/F(Hb) reaches its minimum ~ 4 The recombination lines increase quickly
8600	+83	0	5	Peak of luminosity in V Band Maximum luminosity of all the recombination lines The He II / Hβ ratio has decreased slowly by a factor 2 since the beginning
8616	+99	+16	3	He II / Hβ ratio drops from 0.52 to 0.14 in 16 days He I 6678/He I 5876 at it pre-outburst value
8648	+131	+48	3	He II / Hβ at its minimum (0.07) Flux(He II 4686) minimum Hα/Hβ maximum (7)

Table 2. AX Per 2019 Outburst Résumé

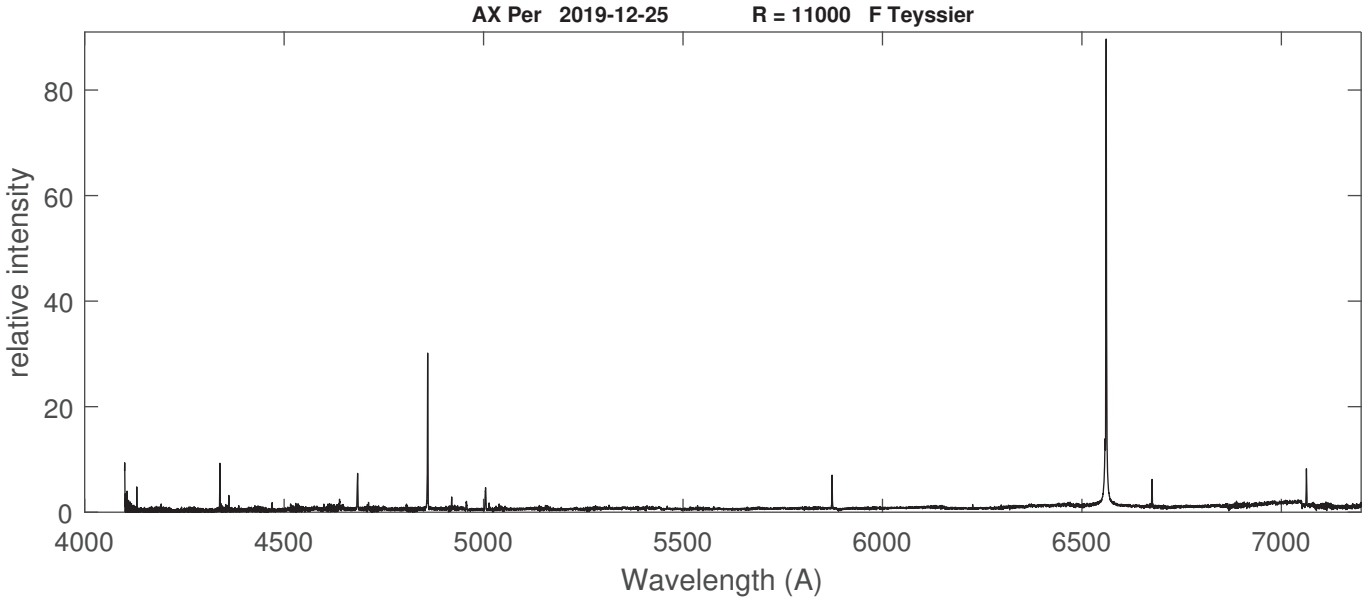
AX Per 2019-12-25 R = 11000 F Teyssier
relative intensity
Wavelength (A)

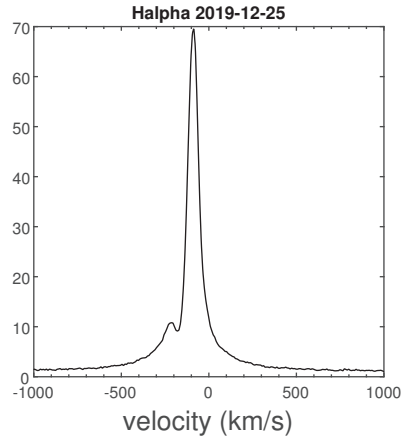
Halpha 2019-12-25
velocity (km/s)

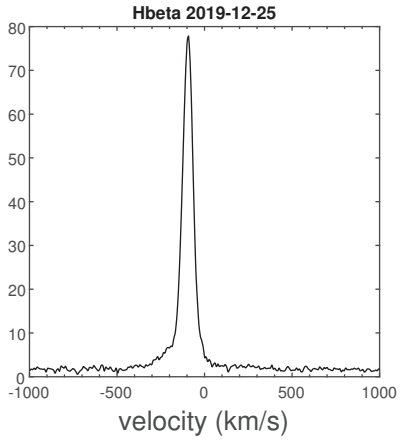
Hbeta 2019-12-25
velocity (km/s)

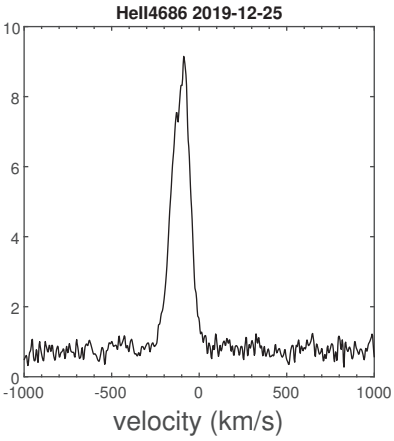
HeII4686 2019-12-25
velocity (km/s)

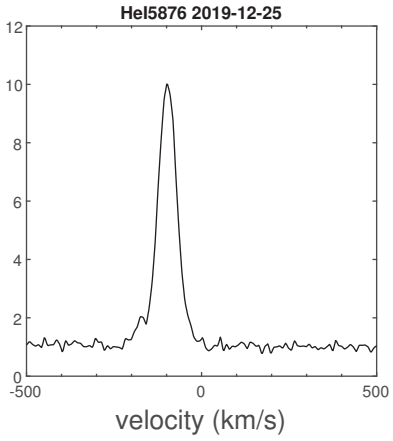
HeI5876 2019-12-25
velocity (km/s)

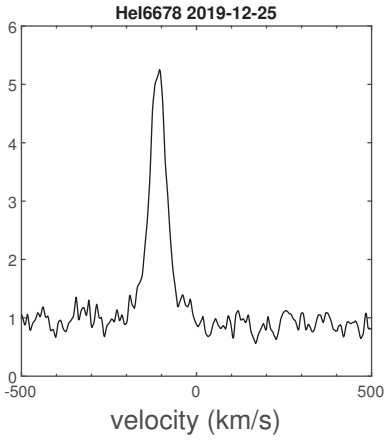
HeI6678 2019-12-25
velocity (km/s)

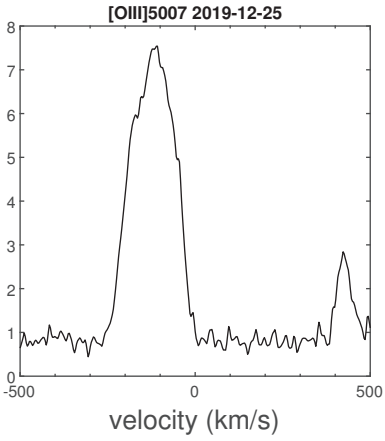
[OIII]5007 2019-12-25
velocity (km/s)

BF Cyg

Coordinates (2000.0)	
R.A.	9 21 55.3
Dec	+29 34 34.7
Mag	9.9 (2019-12)

BF Cyg still in high state.

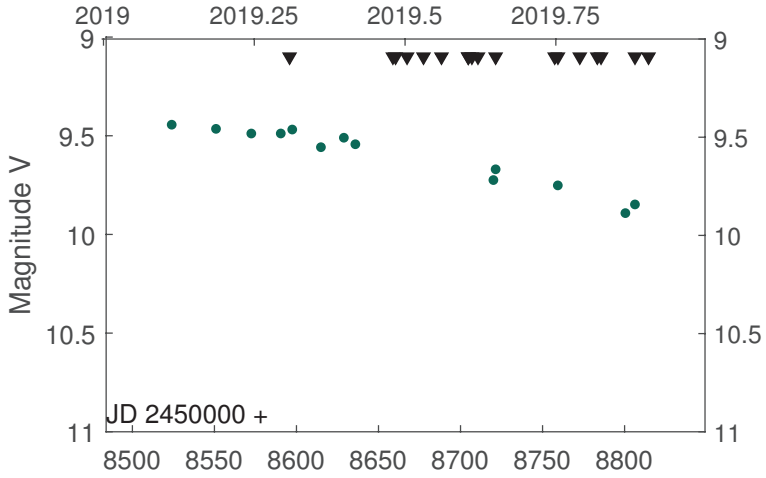

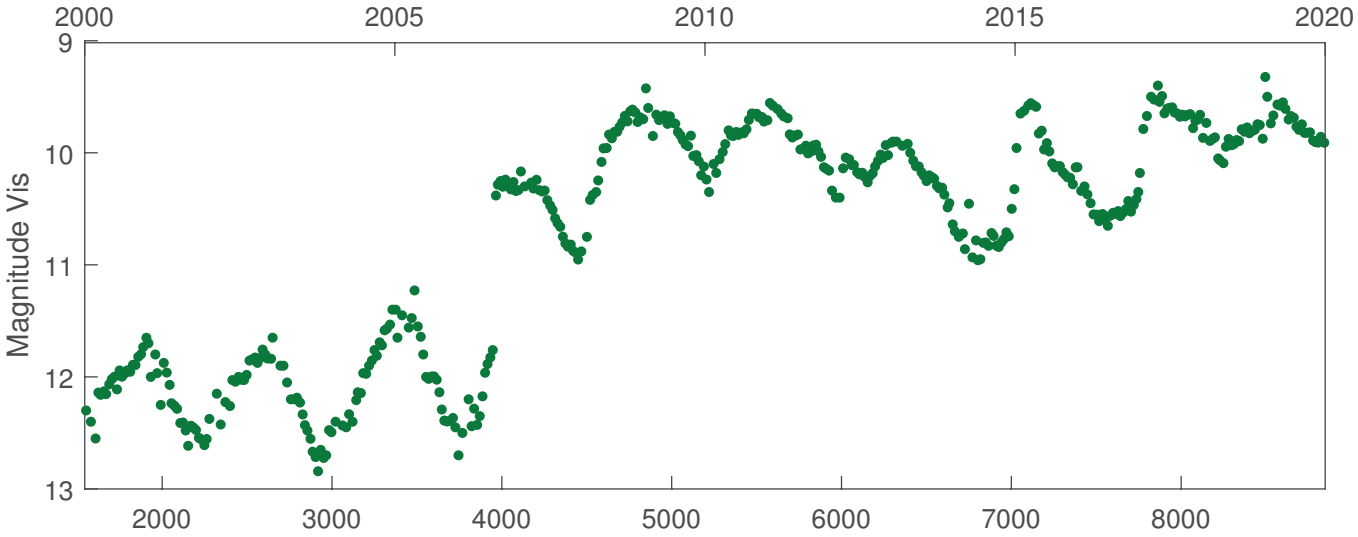

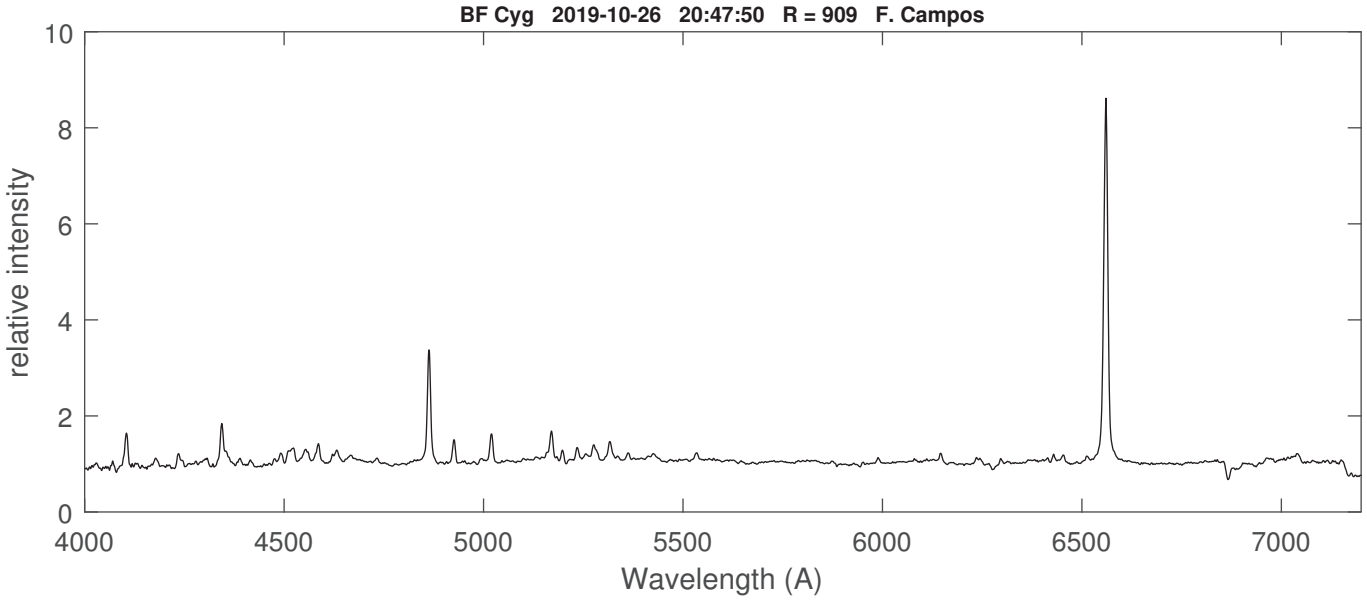

CH Cyg

Coordinates (2000.0)	
R.A.	19 24 33.1
Dec	+50 14 29.1
Mag	~ 7.2 (2017-07)

Ongoing campaign upon the request of Augustin Skopal At least one spectrum a month (high resolution and low resolution, with a correct atmospheric response)

New rise during the quarter from mag V = 8.9 to 8.2

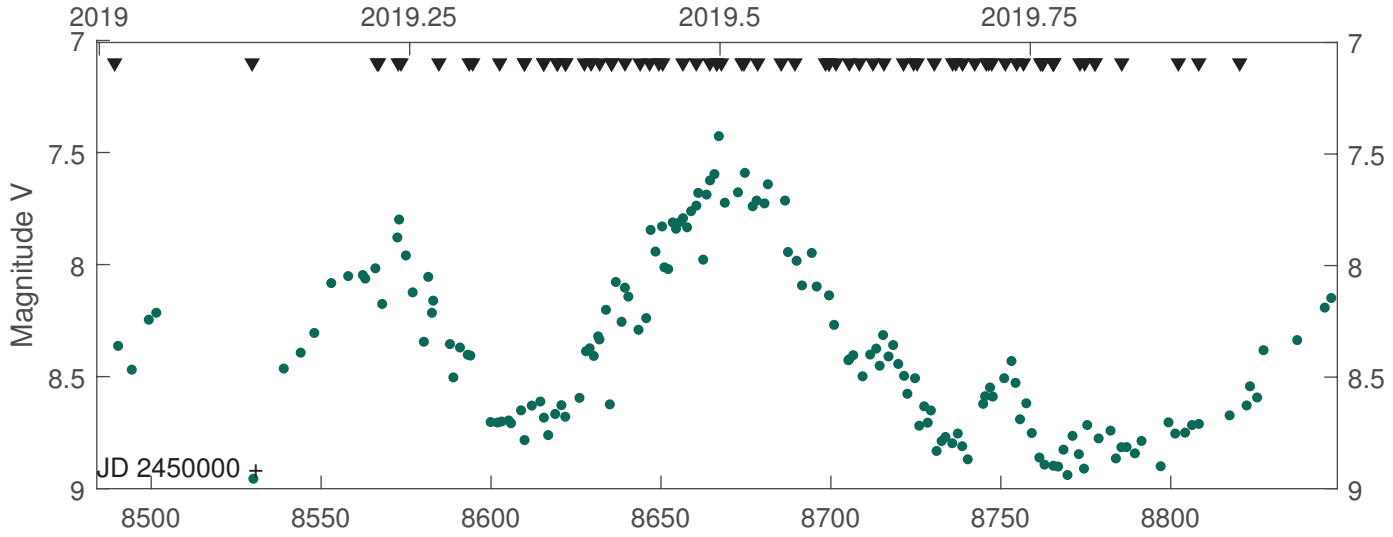

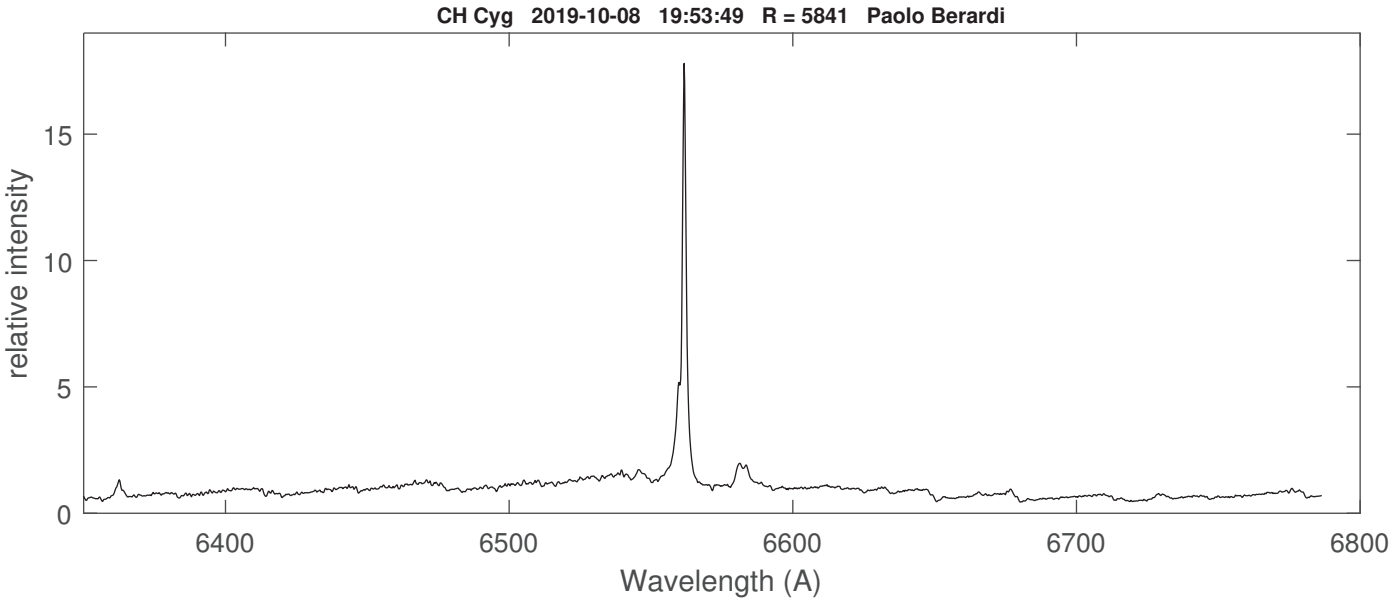

H alpha range - Paolo Berardi Lhires III 1200 l/mm R = 6000

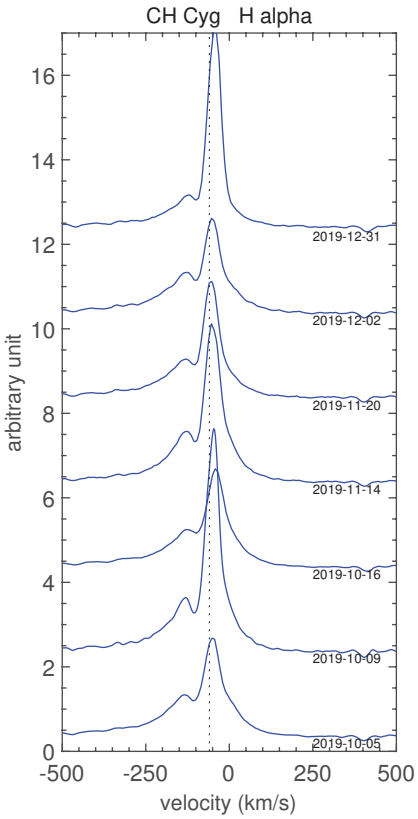

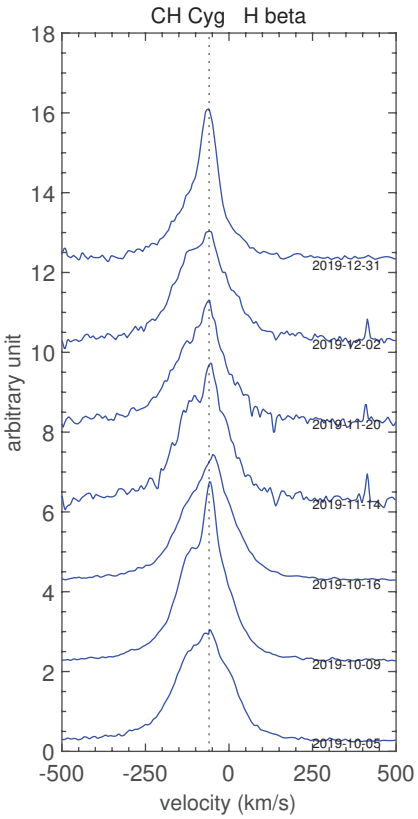

Main lines evolution during the rebrightening from echelle spectra obtained by T. Lester, J. Guarro and F. Teyssier (R = 9000 to 13000).
As usual during former rebrightnings, the emission of Na I D weakens slowly and disappears in 2020-12-31 spectrum.
We note the complex structure of [OIII] λ 5007 Å.

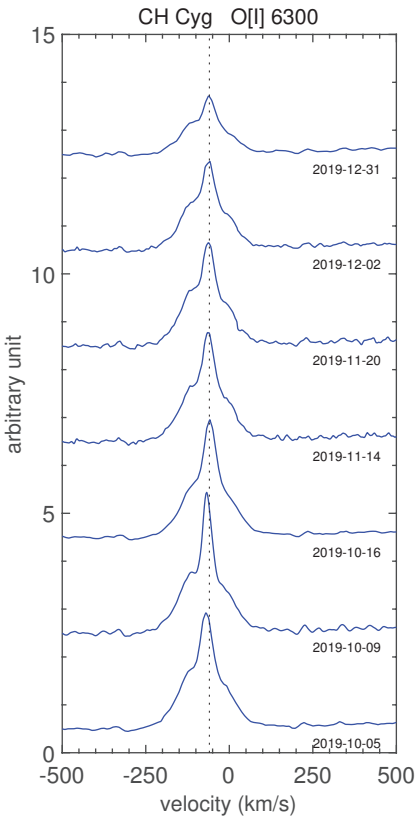

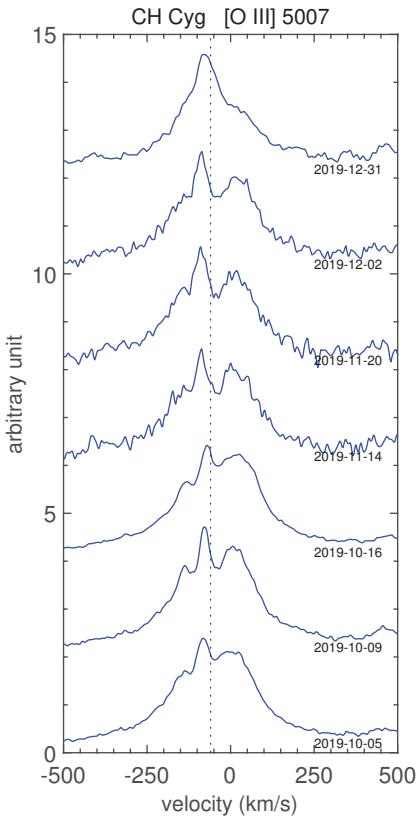

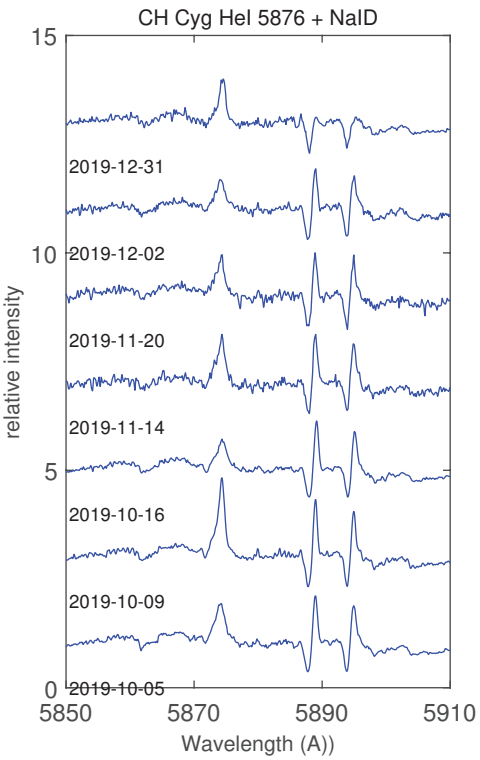

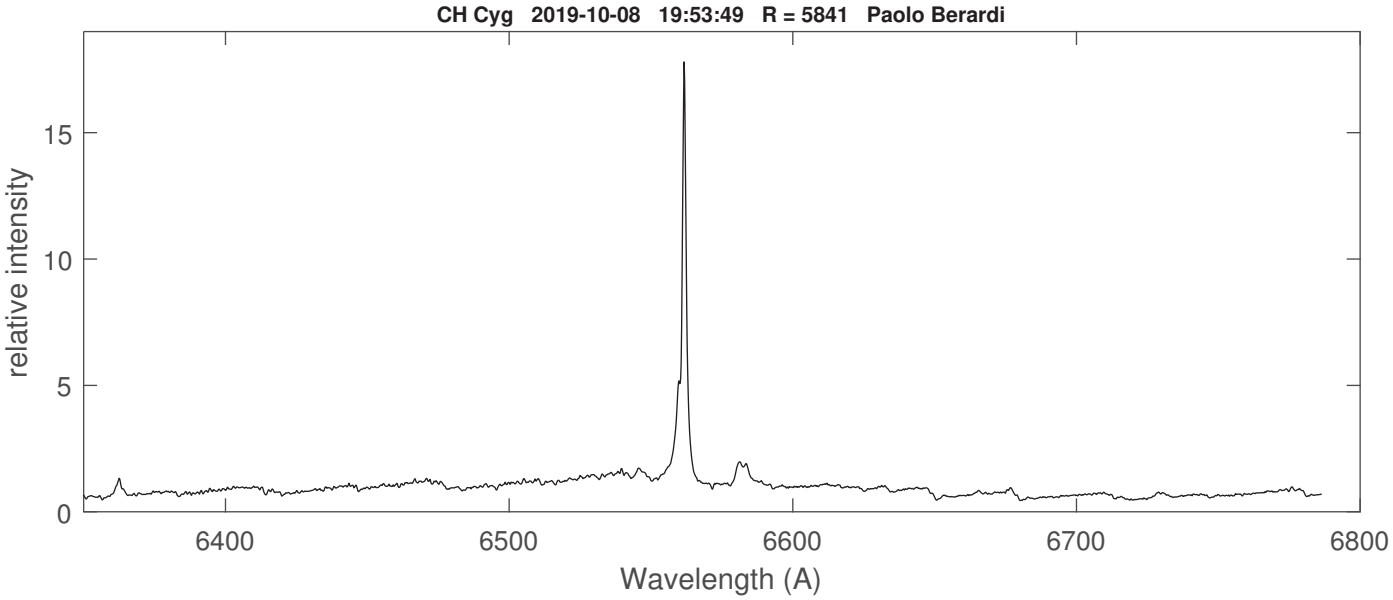

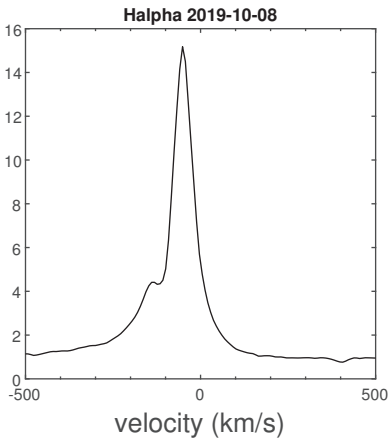

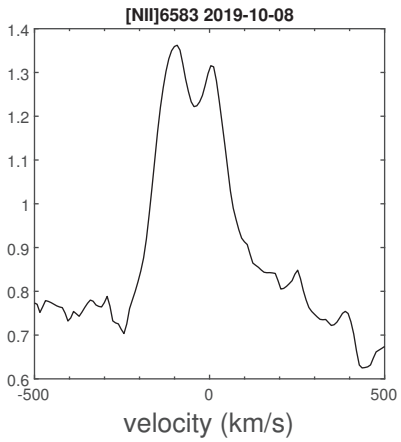

CH Cyg Hα range obtained by Paolo Berardi with Lhires III equiped with a 1200 l/mm gratings (R = 6000)

CI Cyg

Coordinates (2000.0)	
R.A.	19 23 53.5
Dec	+35 41 03.0
Mag	10.8 (2019-09)

CI Cygni before its next eclipse.
mid-eclipse: 13-04-2020
(Kenyon & Mikolajewska, 1995)

Phase = 0.88 (2019-12)

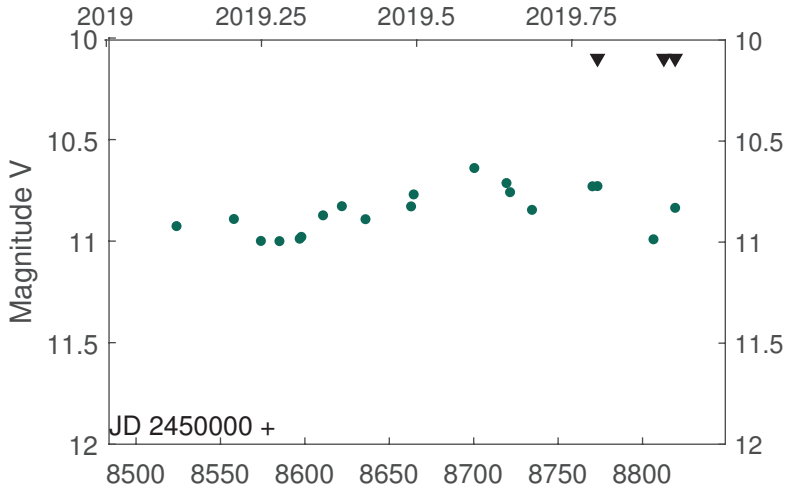

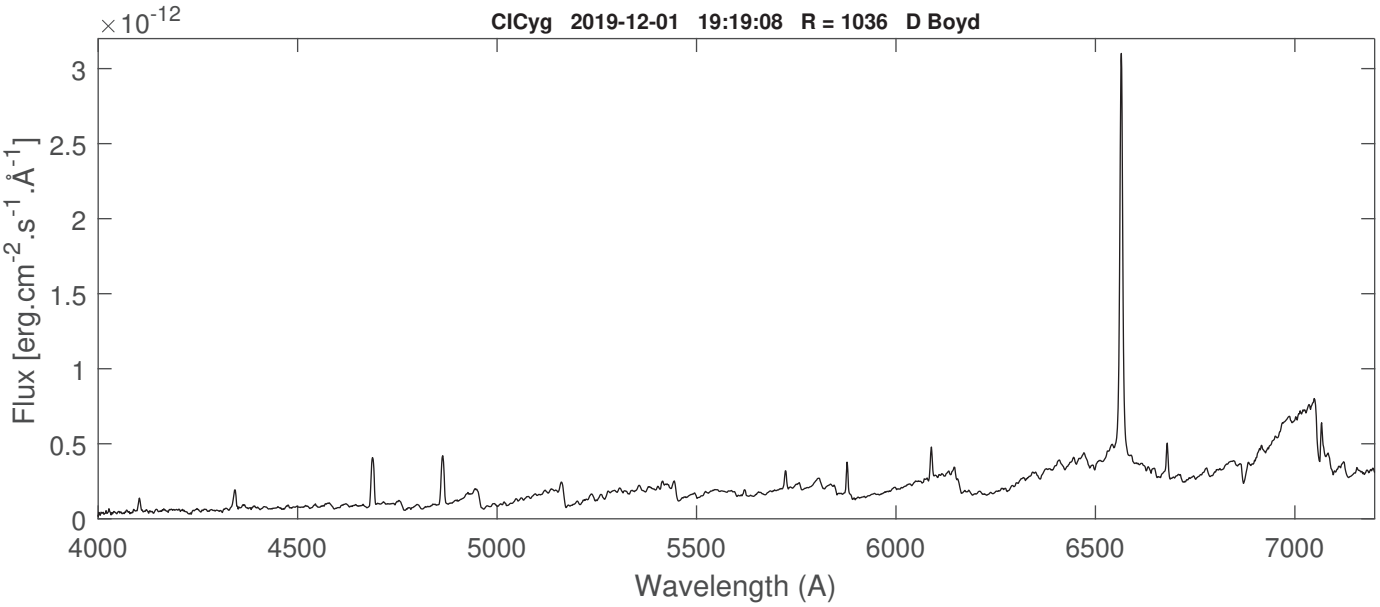

EG And

Coordinates (2000.0)	
R.A.	00 44 37.2
Dec	+40 40 45.7
Mag V	7.4

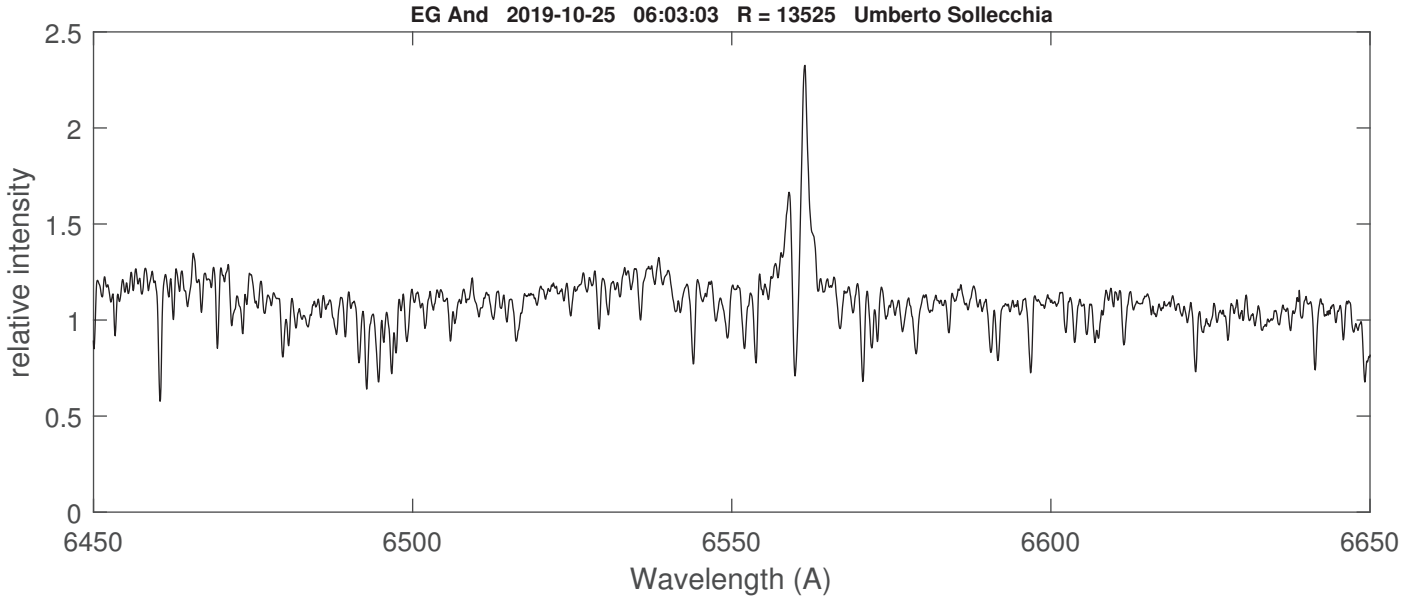

EG And Hα range obtained by Umberto Sollecchia with a home-made spectrograph (R = 13000)

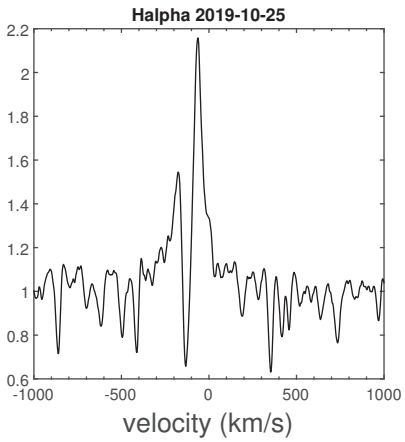

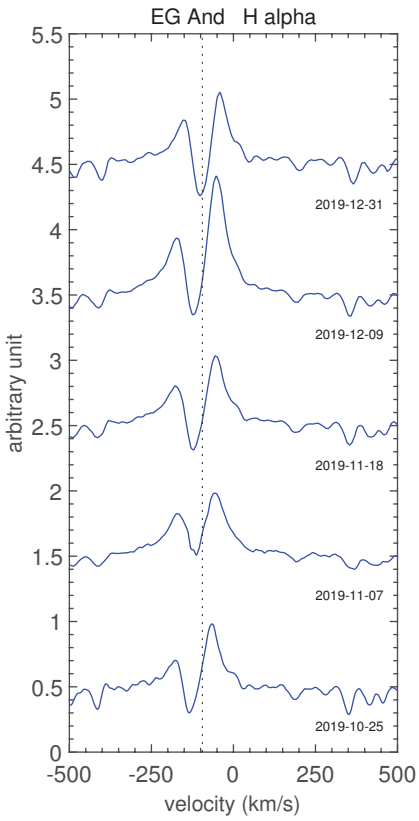

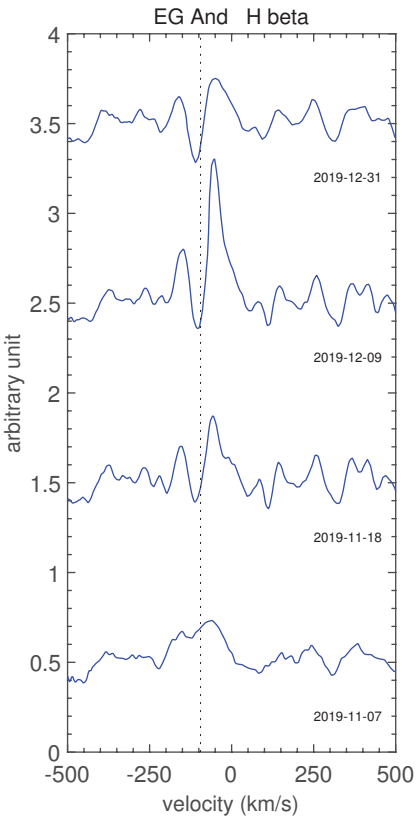

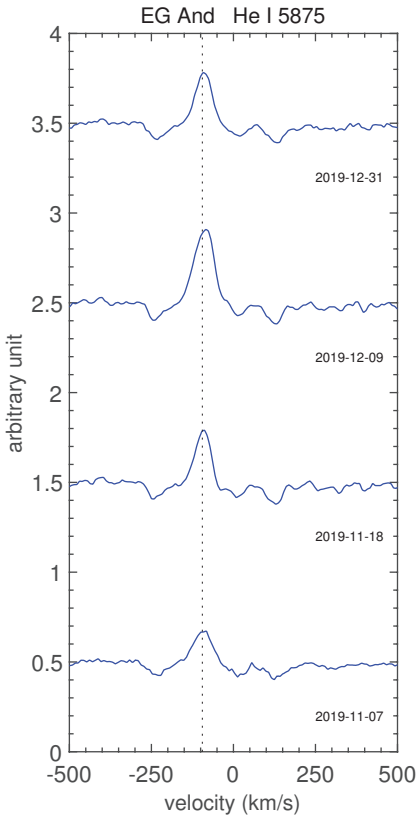

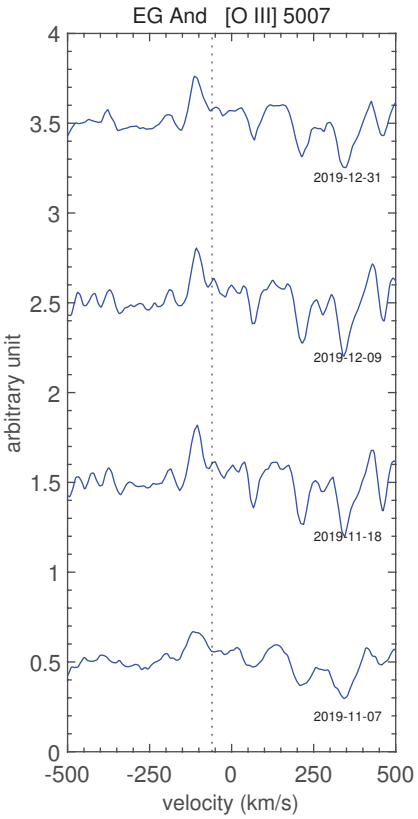

Main lines profiles from phase 0.862 to 0.001
Phase 0 = min(UV)
(Vogel, M., 1991, A&A 249, 173)
Spectra obtained by Joan Guarro, François Teyssier (Echelle, R = 9000 to 11000) and Umberto Sollecchia (Hα on 2019-10-25)

Suspected symbiotics: FASTT 1100, a new symbiotic star

Coordinates (2000.0)	
R.A.	17 53 45.30
Dec	-01 07 46.8
Mag V	~ 14 (V)

As part of the campaign for identification of symbiotic candidates in the southern sky initiated (A. Lucy and J. Sokoloski,) Forrest Sims, using a LISA spectroscope mounted on a 14" telescope operating at Desert Celestial Observatory (US), obtained a spectrum of FASTT 1100 which clearly show [OIII] in emission. In addition to Balmer and He I emission lines, the presence of the high ionisation line clearly places FASTT 1100 among the symbiotic stars according Belszinki+ (2000) definition.

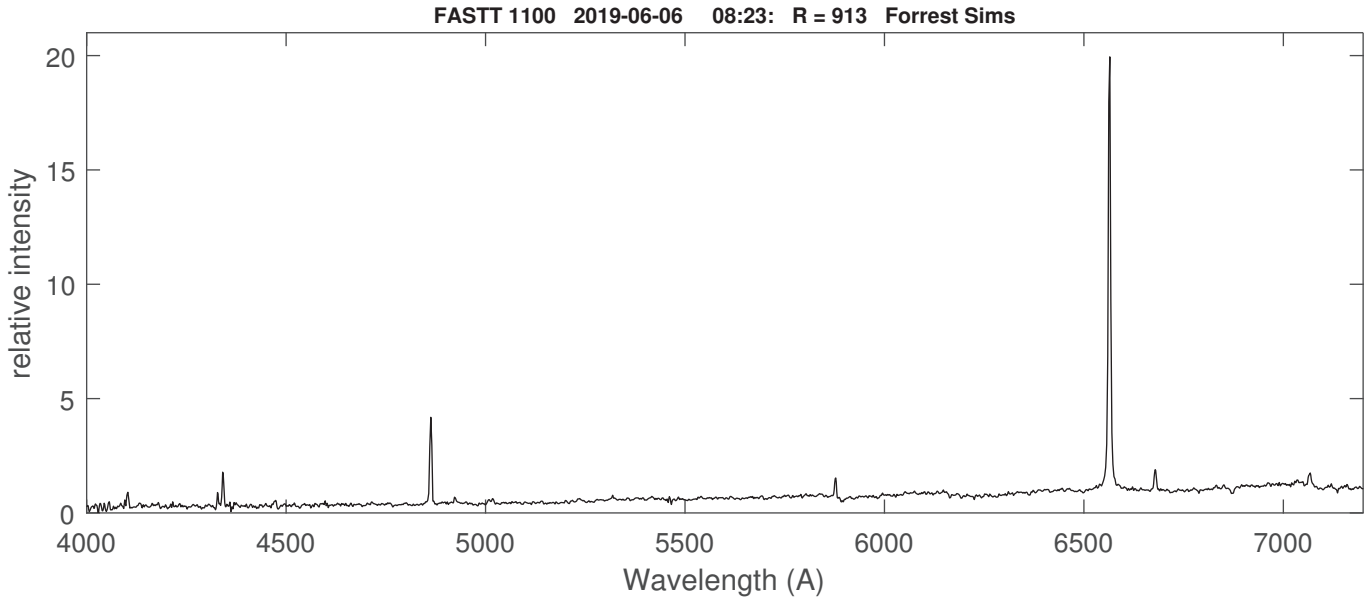

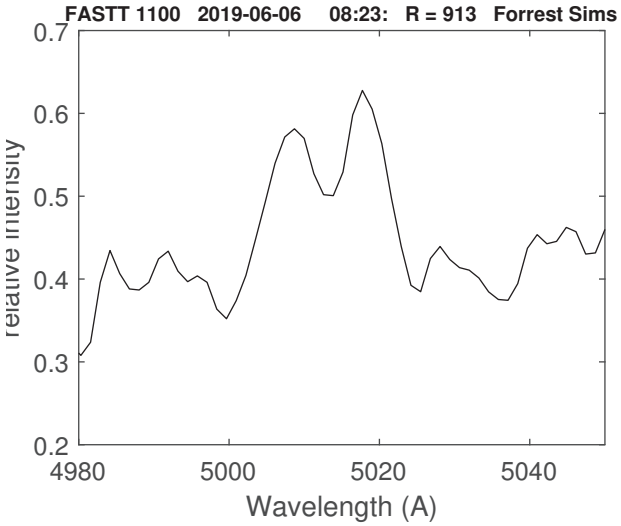

[OIII] appears clearly in emission, blended with He I 5016 and/or Fe II 5018

"An optical spectrum obtained by Forrest Sims on 2019 June 6 and October 10 confirms that symbiotic binary candidate FASTT 1100 (=EM* RJHA 101) is a symbiotic, exhibiting emission from [O III] 5007 (in a partially-resolved blend with He I 5016 and/or Fe II 5018), He I 5876, 6678, and 7066, Fe II 4923, and the Balmer series with a decrement. Preliminary spectral fits suggest that the donor star is an M0--M1 III giant. [O III] was also observed in this target exactly one year earlier, on 2018 June 6 at CASLEO by N. Nuñez, so this emission persisted for over a year at least. Additional ARAS observations were conducted by Christophe Boussin. FASTT 1100 was selected as a symbiotic candidate by A. Lucy, J. Sokoloski, N. Nuñez, et al. on the basis of its photometric behavior in the SkyMapper Southern Sky Survey, including blue ug and uv colors, alongside 1.3 magnitudes of long-term u-band variability and color variability, in a sample of cool giants selected by 2MASS photometry and GAIA distances. More results on FASTT 1100 and other candidates will be reported soon by Lucy et al. (in preparation), and the preliminary stages of the search design are briefly discussed in Lucy et al. (2018, RNAAS, 2, 229)."
Adrian Lucy (Columbia University)

HbHa 1705-04 = V426 Sge

Coordinates (2000.0)	
R.A.	19 54 42.80
Dec	+17 22 14.6
Mag V	12.5 (2019-09)

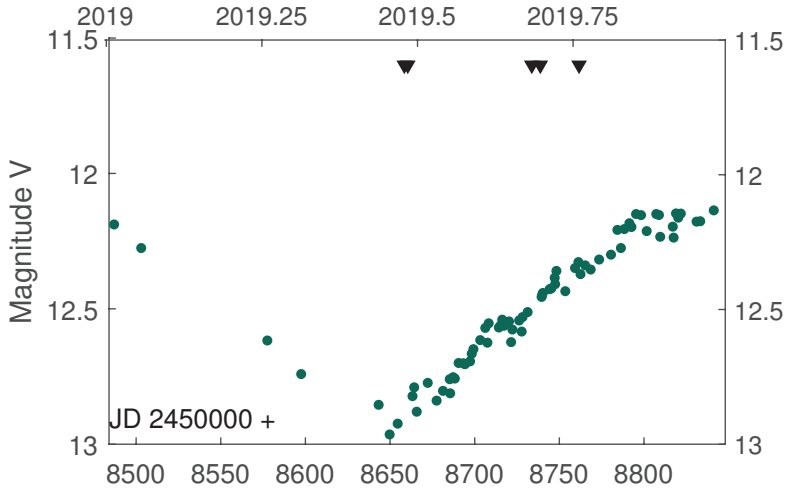

AAVSO V band lightcurve in 2019 (selected, 1 day mean) and ARAS spectra

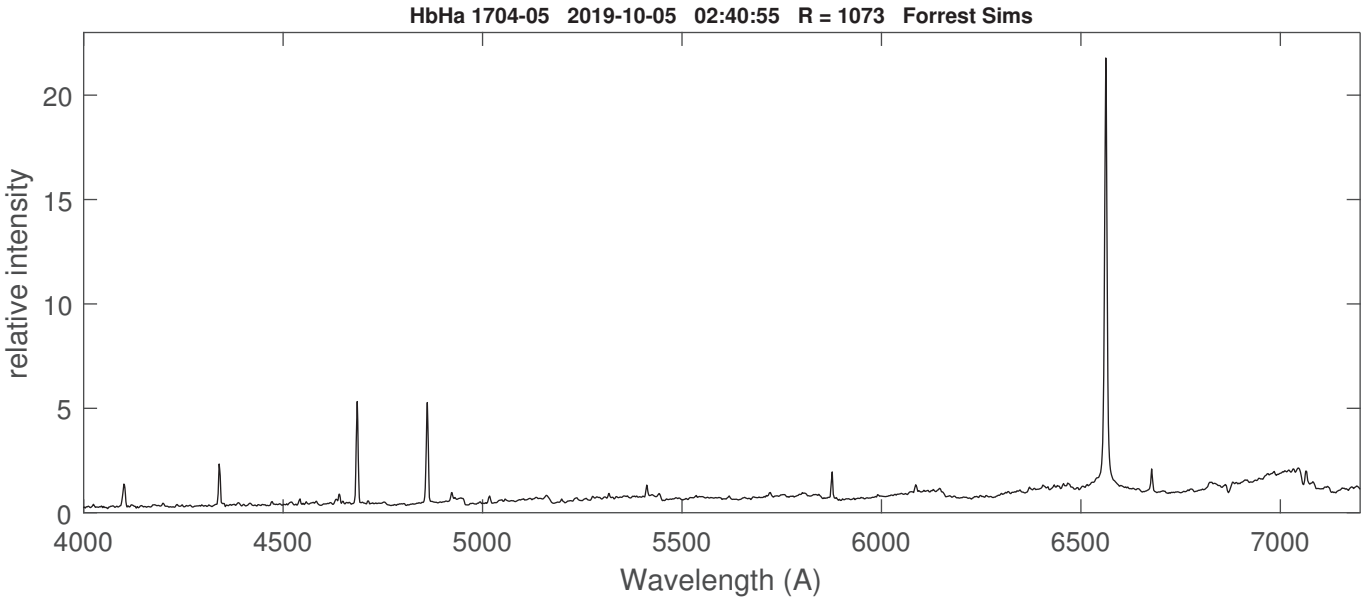

V426 Sge in quiescent state after its classical symbiotic outburst in 2019. The lightcurve clearly evokes an eclipse centered at JD 2458650.

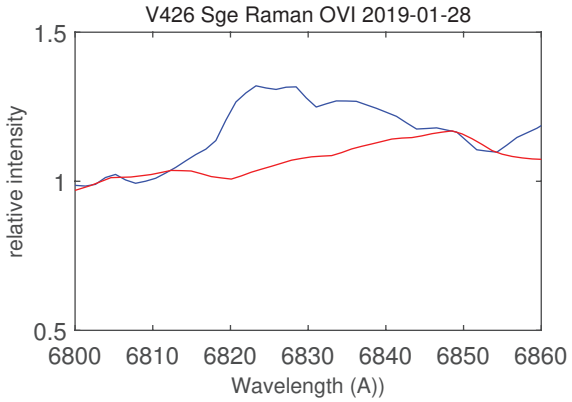

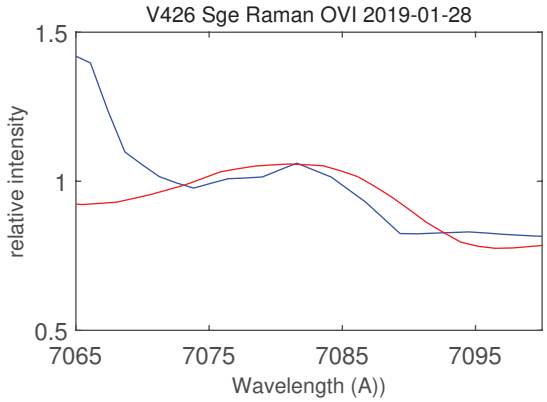

Raman OVI 6825 (left figure) has recovered after the 2019 outburst with an equivalent width of 3.5 while Raman OVI 7085 (right figure) remains indiscernable at most at that resolution. This is often the case in classical symbiotics for which the ratio OVI 6825/7085 is much higher than the theoritical value 2 and OVI l 7088 Å lies in the head of the TiO band 7080 Å

HM Sge

Coordinates (2000.0)	
R.A.	19 41 57.0
Dec	16 44 39.8
Mag V	12.3

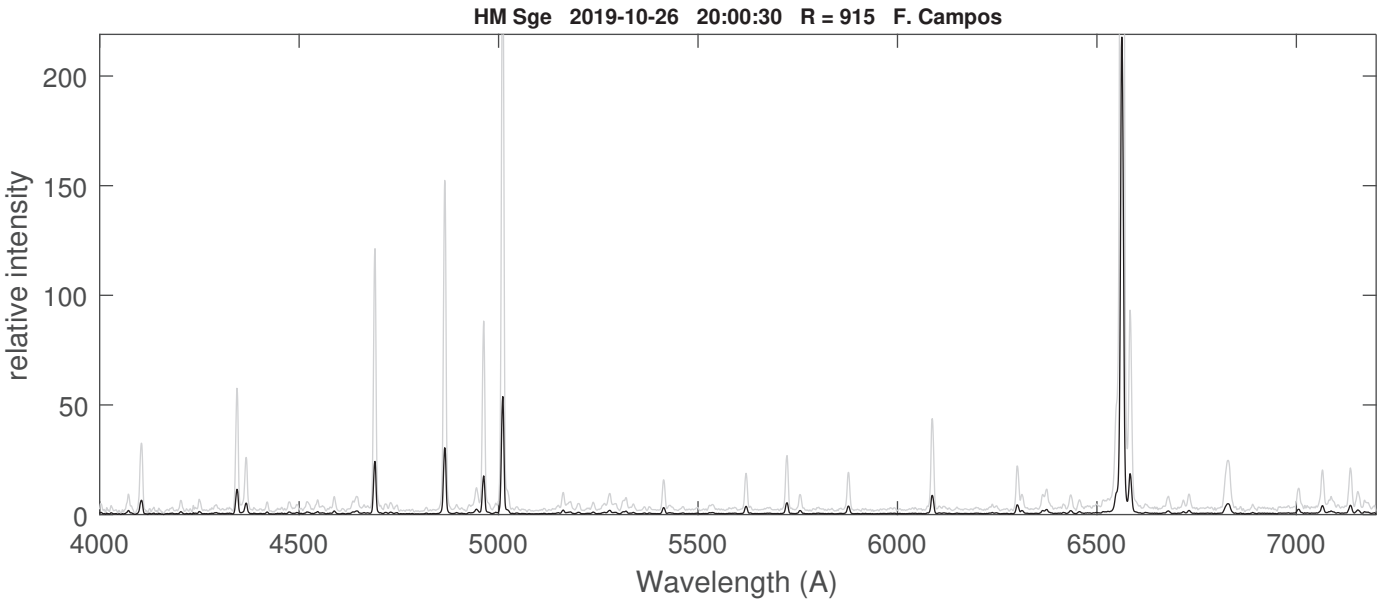

LT Del

Coordinates (2000.0)	
R.A.	20 35 57.2
Dec	+20 11 27.5
Mag V	13.2

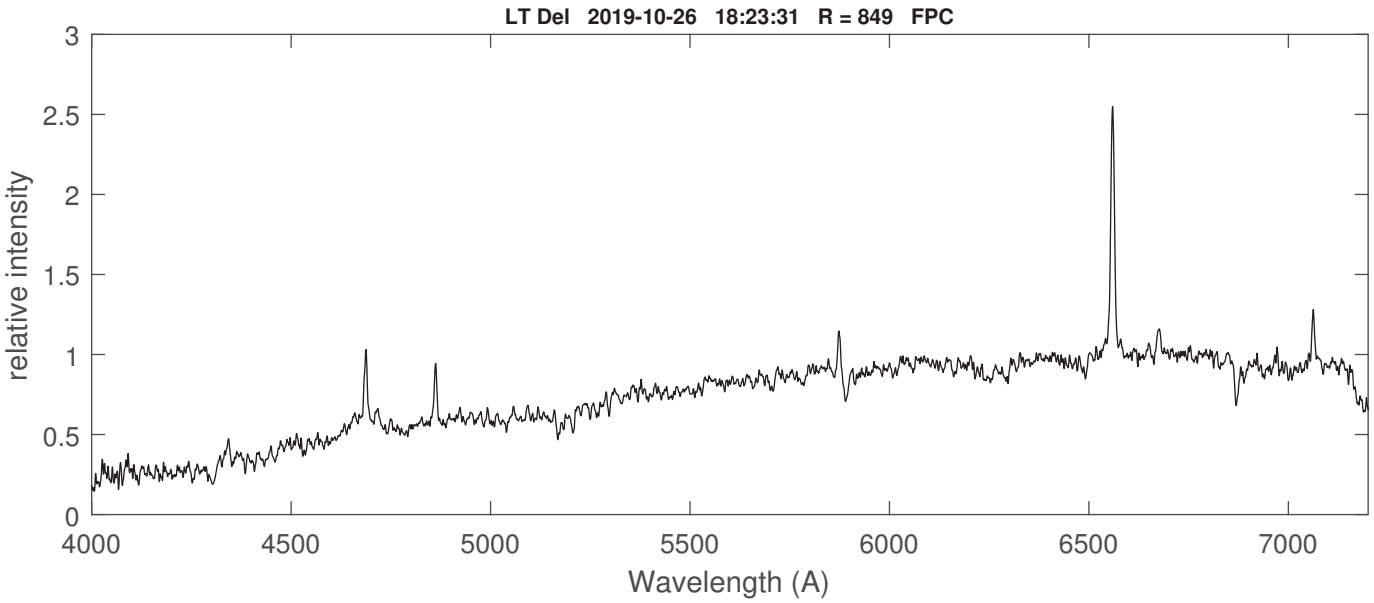

omi Cet

Coordinates (2000.0)	
R.A.	02 19 20.8
Dec	-02 58 39.4
Mag V	

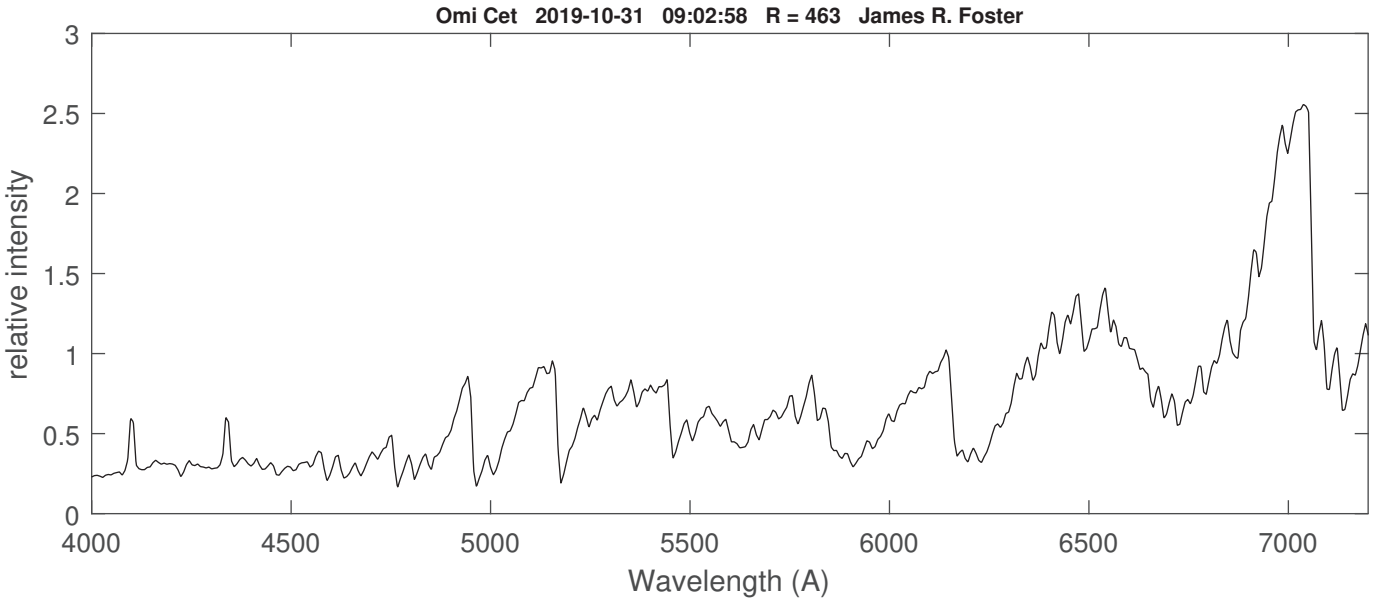

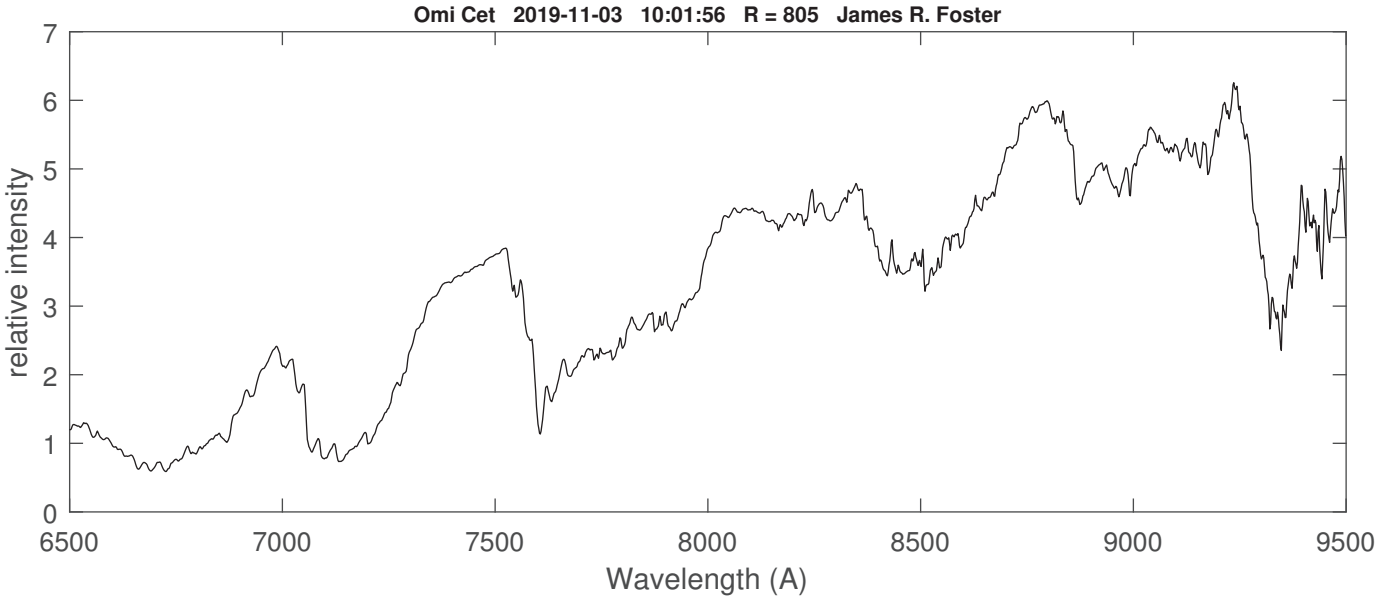

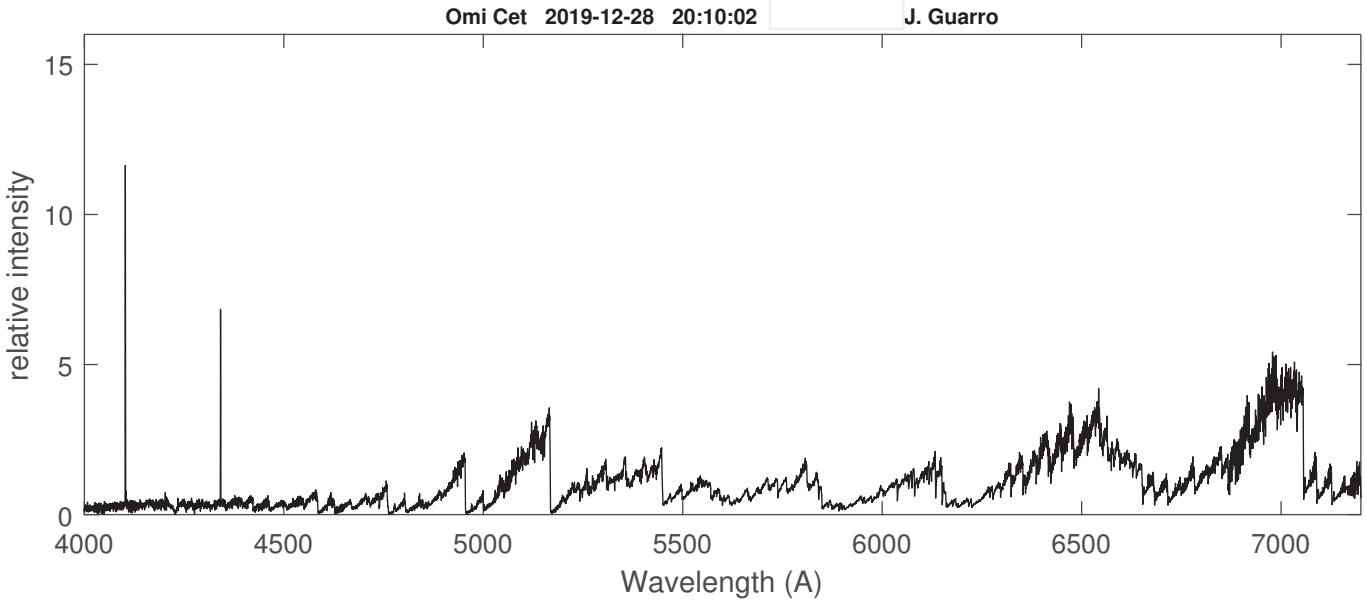
Omi Cet 2019-12-28 20:10:02 J. Guarro
relative intensity
Wavelength (A)
0
5
10
15
4000
4500
5000
5500
6000
6500
7000

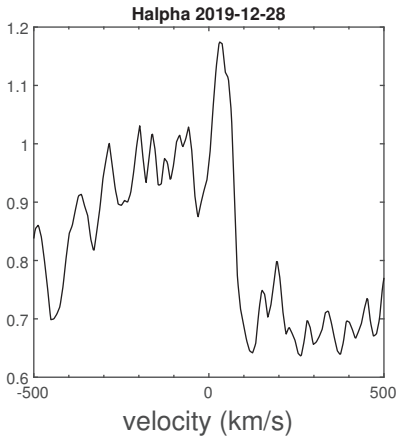
Halpha 2019-12-28
velocity (km/s)
0.6
0.7
0.8
0.9
1
1.1
1.2
-500
0
500

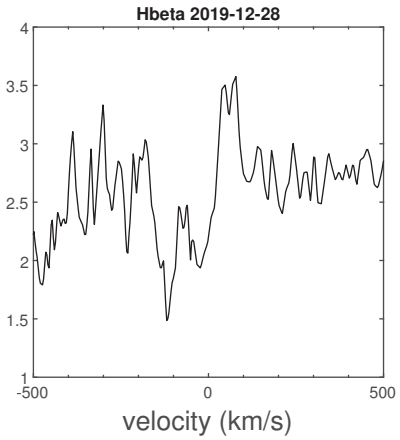
Hbeta 2019-12-28
velocity (km/s)
1
1.5
2
2.5
3
3.5
4
-500
0
500

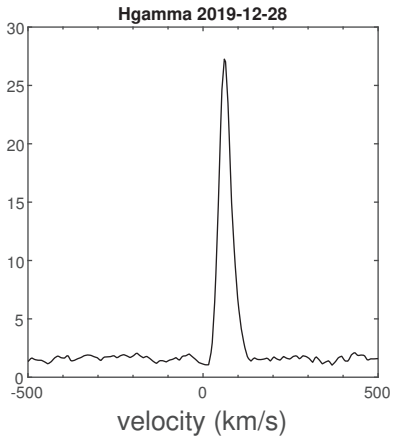
Hgamma 2019-12-28
velocity (km/s)
0
5
10
15
20
25
30
-500
0
500

R Aqr

Coordinates (2000.0)	
R.A.	23 43 49.5
Dec	-15 17 04.2
Mag V	12 (2019-12)

The symbiotic Mira R Aqr is in the decline of the pulsation of the red giant. The luminosity of the target during the current pulsation cycle is very low in comparison to previous ones. It suggests an eclipse. Margarita Karovska called for observations of the phenomenon. HST and CHANDRA observations are scheduled on 13th and 14th January, 2020.

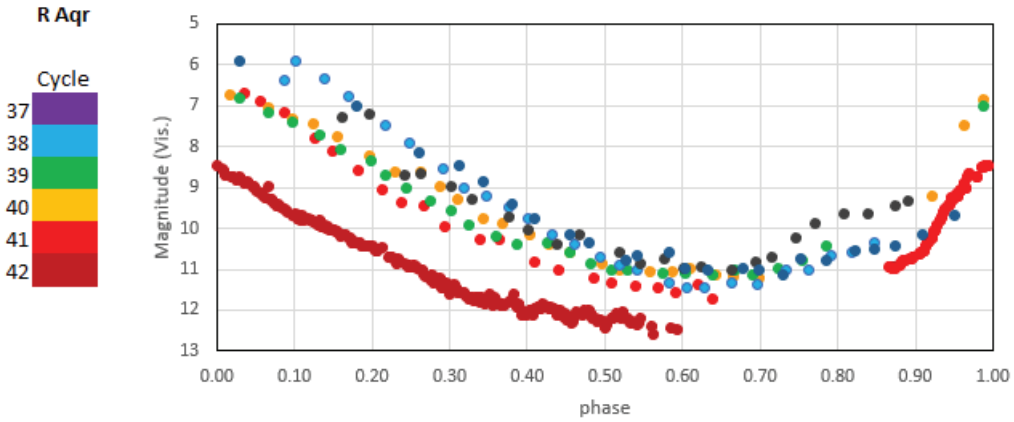

AAVSO Visual light curve (15 days mean) and V band (1 day mean) since phase 41.85 according to the pulsation phase of the Mira computed with Kholopov (1985) ephemeris: Max(V) = 2442398 + 386.96 x E - The pulsation period is slightly adapted (387.00 days) to avoid a shift. The luminosity during the current cycle (brown) is significantly weaker. The delta magnitude is about +2 magnitudes at phase 0.00 in comparison to the 3 previous cycles and +1.5 at phase 0.25.
Since phase ~ 0.39, the luminosity oscillates (ΔV ~ 0.25) with a rough period of about two weeks.

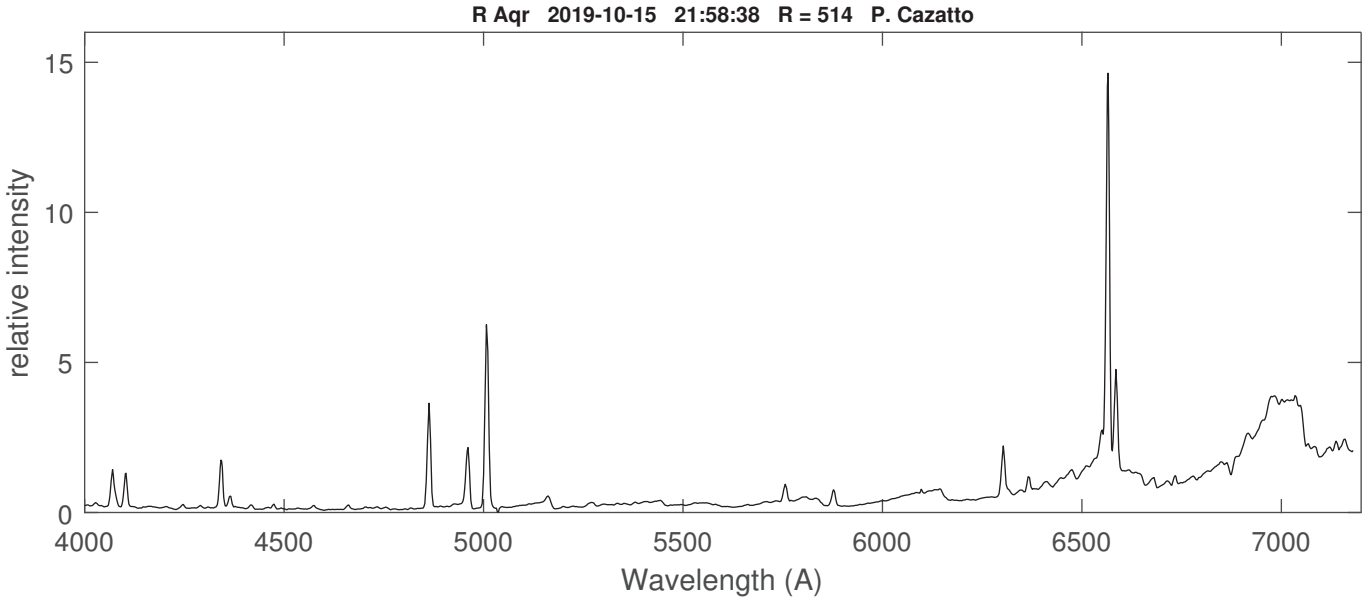

R Aqr, obtained by Paolo Cazatto on 2019-10-15 at phase 0.31 with an Alpy600

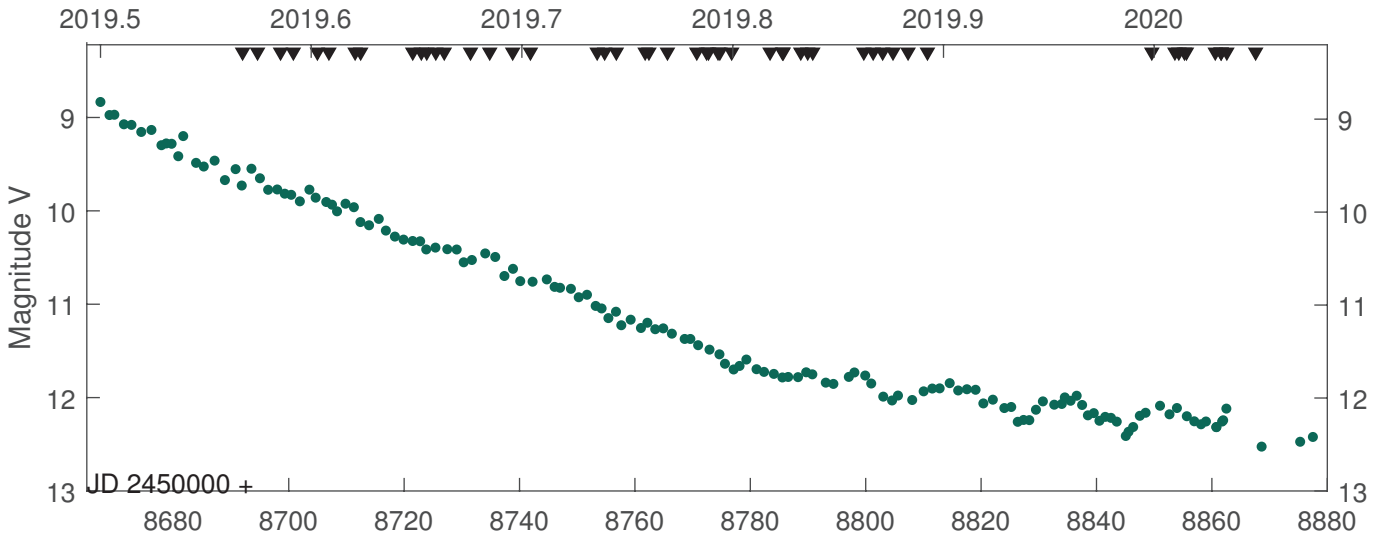

AAVSO V band lightcurve and ARAS spectra (triangles) from mid 2019 until mid 2020 January

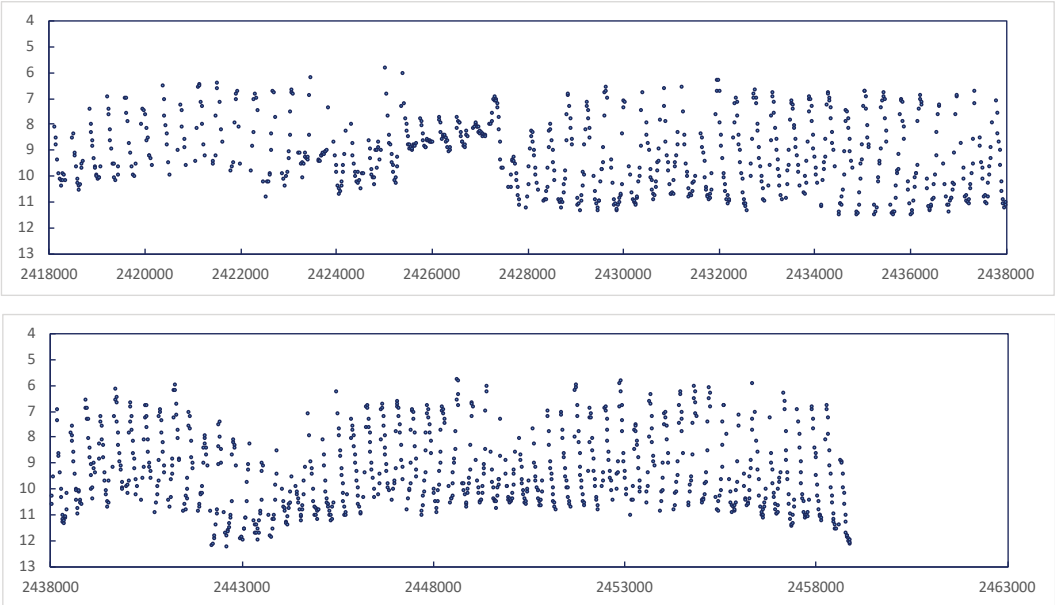

AAVSO Visible (15 days mean) from 1908 to 1962 (top figure) and 1962 to present (bottom figure)
The current state is very close to 1974 observations (JD ~2442000), about 46 years ago

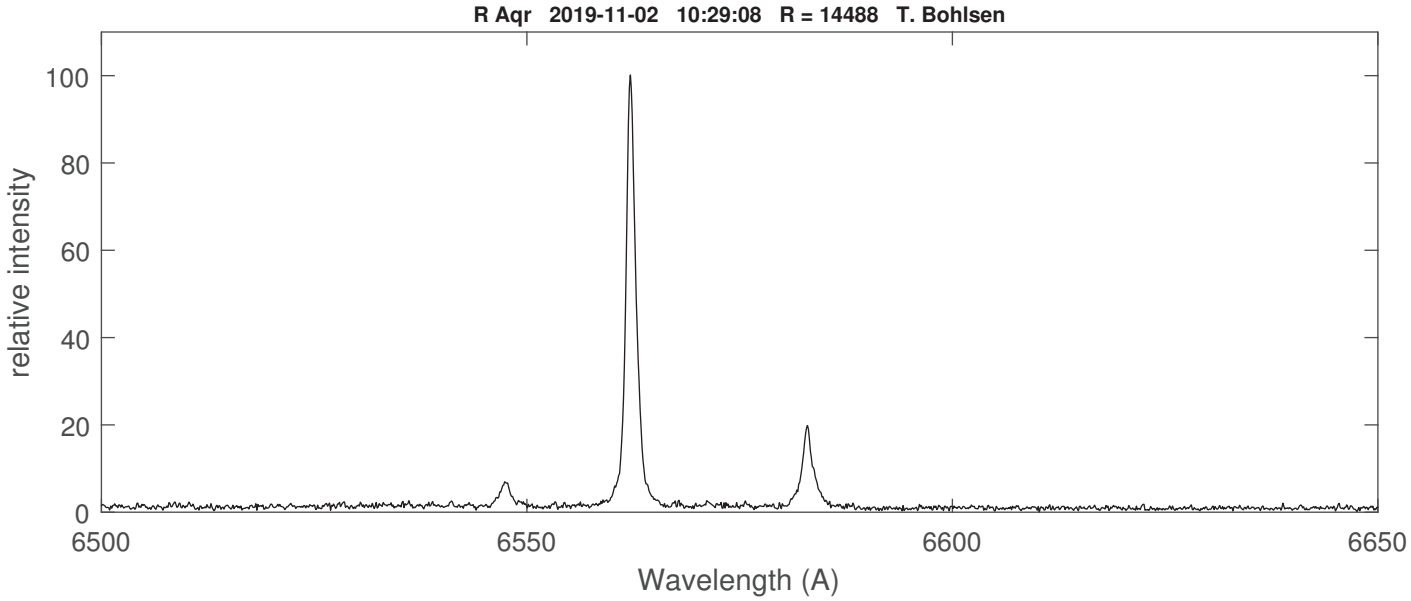

Hα region obtained by Terry Bohlsen with a Lhires III equipped with a 2400 l/mm gratings (R = 15000).
The FWHM of Ha is 55 km.s^{-1} and 1/2 FWZI = 110 km.s^{-1}
[NII] 6583 is slightly broader with a FWHM = 60 km.s^{-1} and 1/2 FWHI = 150 km.s^{-1}

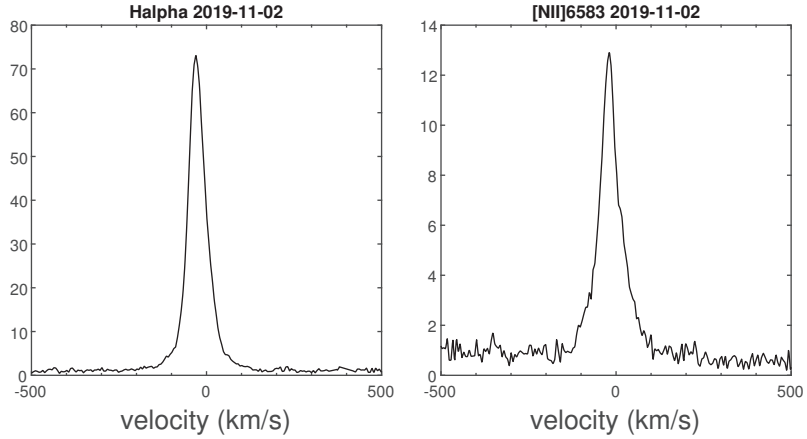

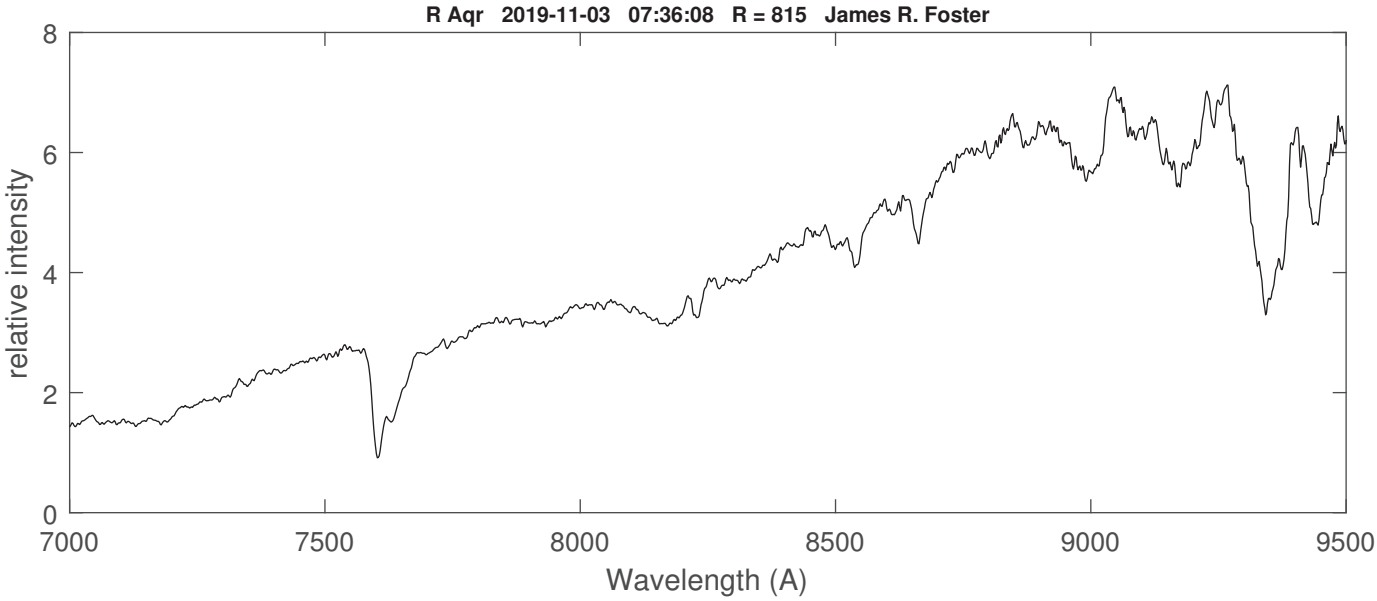

Near IR region obtained by James Foster with a LISA (R = 1000). No significant emission line appears.

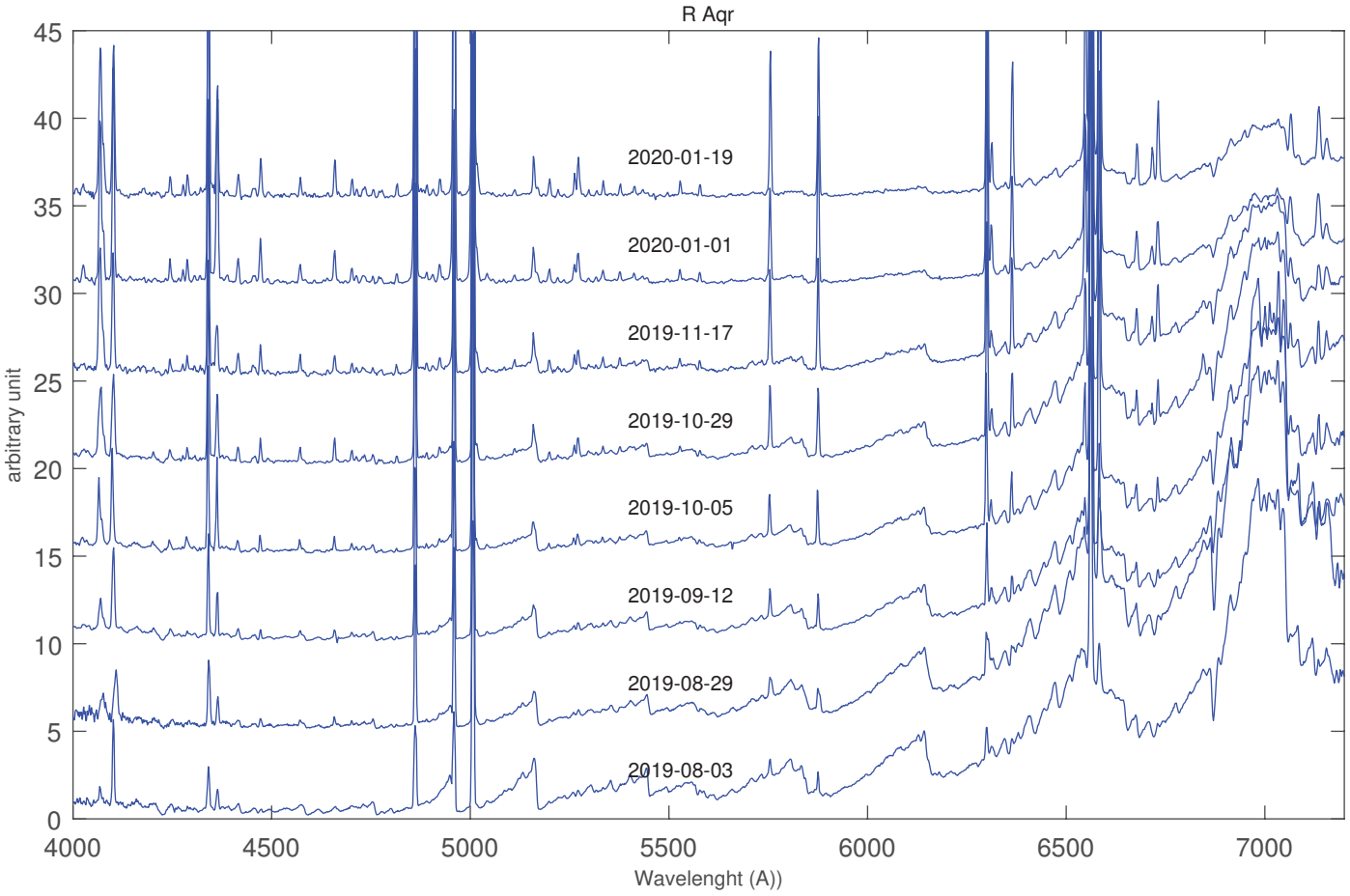

Evolution of the spectrum from phase 0.12 to 0.56 from LISA spectra obtained by Forrest Sims and Jacques Michelet

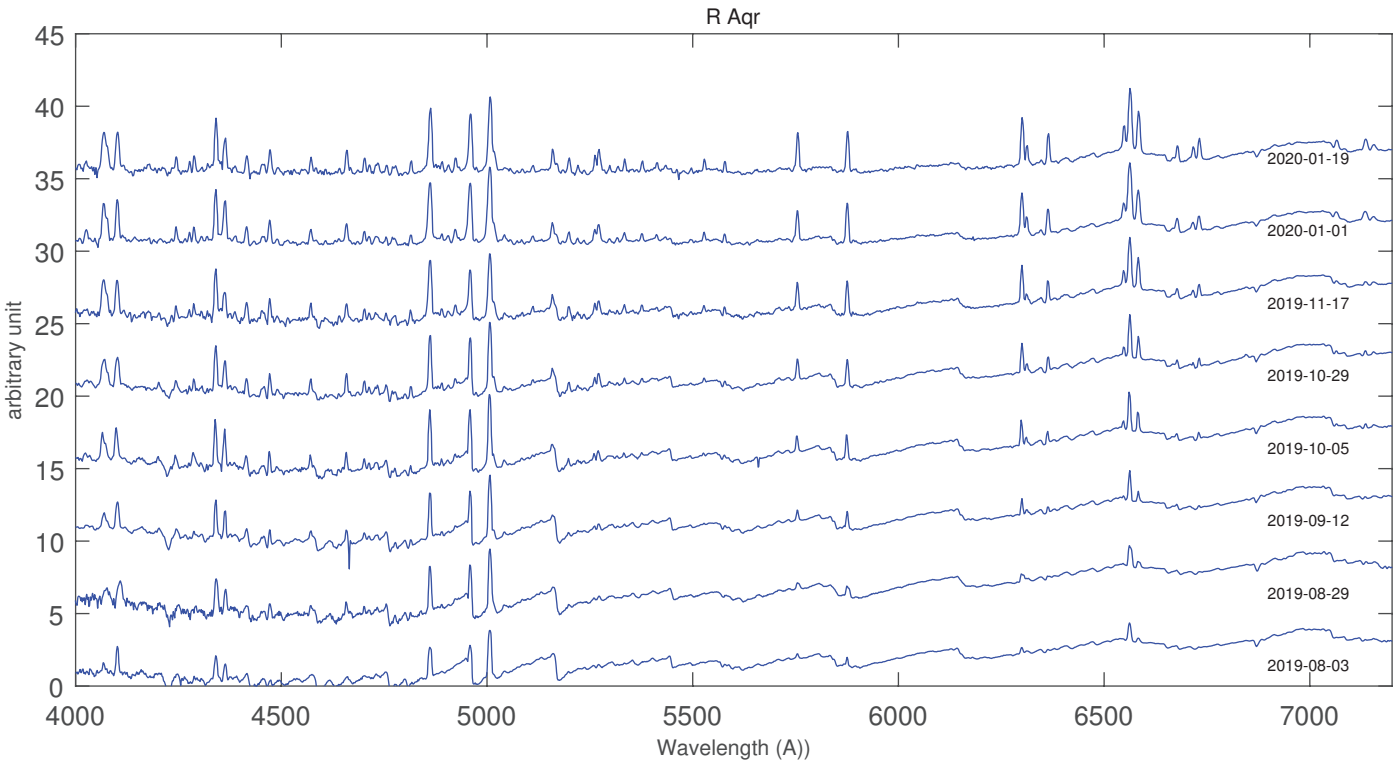

The same, in logarithmic scale

We note the the weakening of the TiO bands and the enhancement of number of recombination and forbidden lines according to the continuum.

The TiO1 index (as defined by Kenyon+, 1987) measured on LISA Spectra increases slightly to until phase 42.25 reaching 0.69 +/- 0.02 (equivalent to a MIII 4.6 red giant) and then declines to 0.40 +/- 0.02 (MIII 2 equivalent) at phase 42.5. It is stable in 2020, January.
The lack of data in 2019, December do not allow us to decide if the decrease remain ed linear until phase 42.5 or if a stepped variation happened.

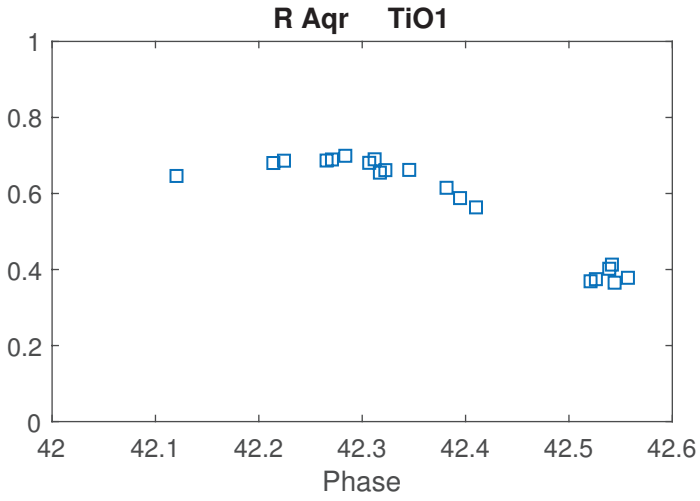

RS Oph

Coordinates (2000.0)	
R.A.	17 47 31.5
Dec	-06 41 39.5
Mag V	10.6 (2019-10)

Only one spectrum of the recurrent symbiotic nova RS Oph during this quarter. The target needs a better coverage in 2020 and until its next nova outburst (see N. Shagatova & A. Skopal in ESIL 2019-Q2).

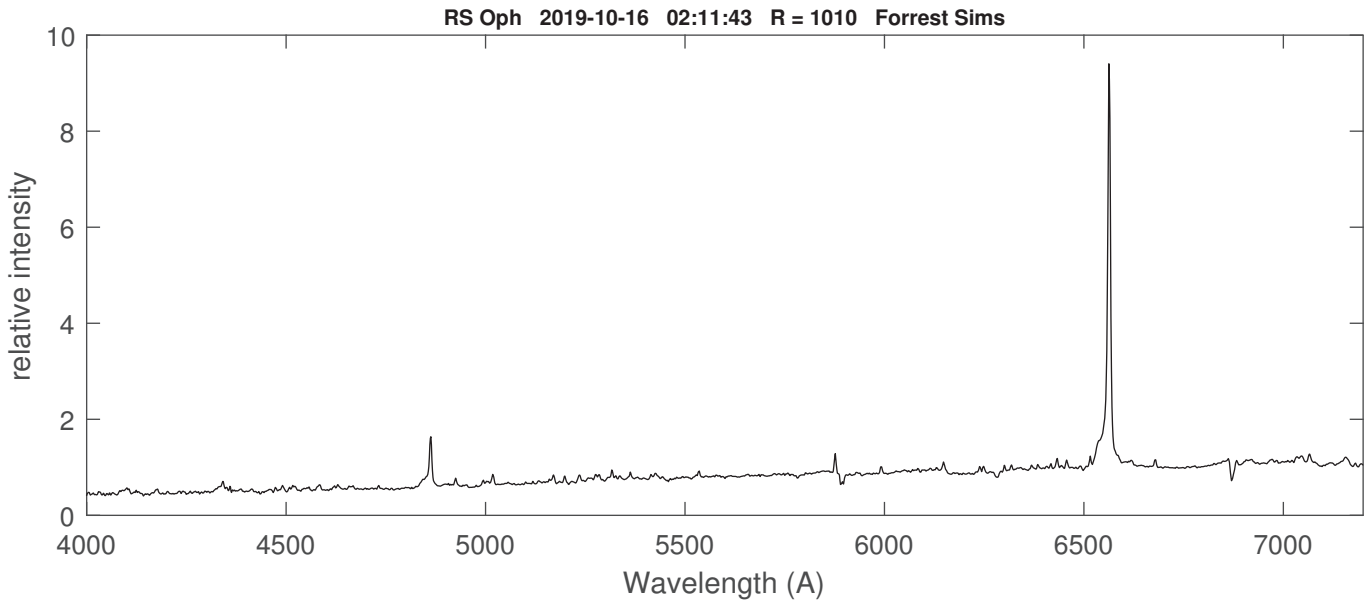

StHa 32

Coordinates (2000.0)	
R.A.	04 37 45.6
Dec	-01 19 11.9
Mag V	12.7 (2019-

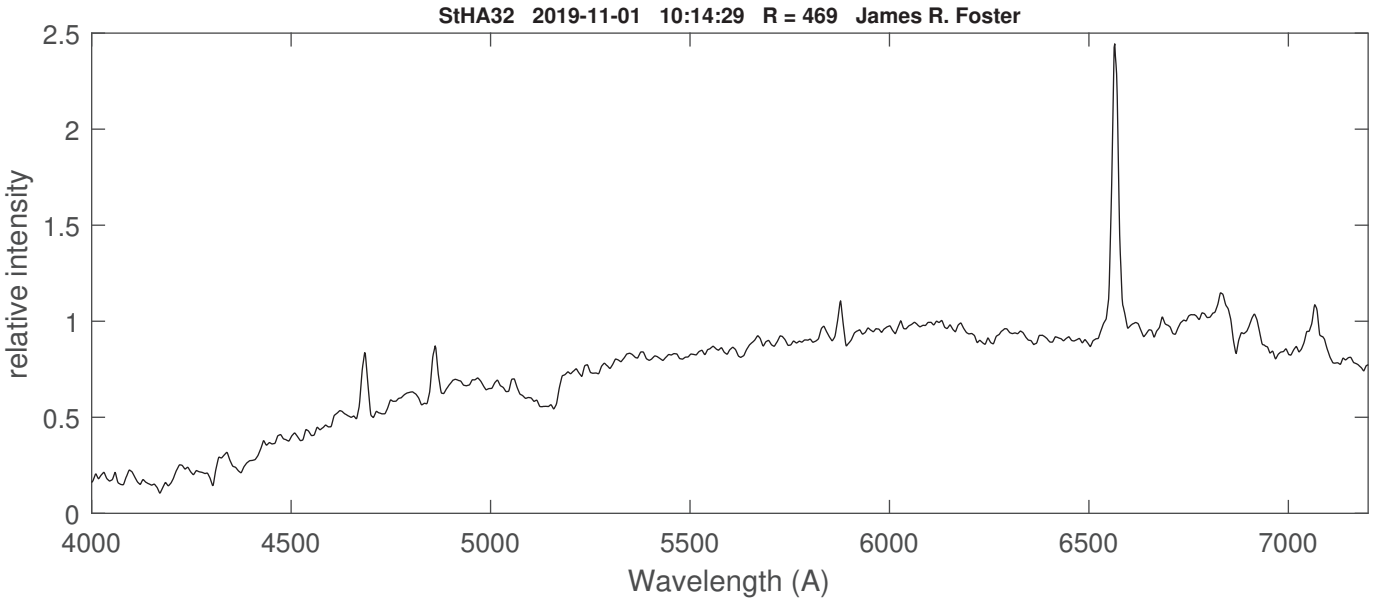

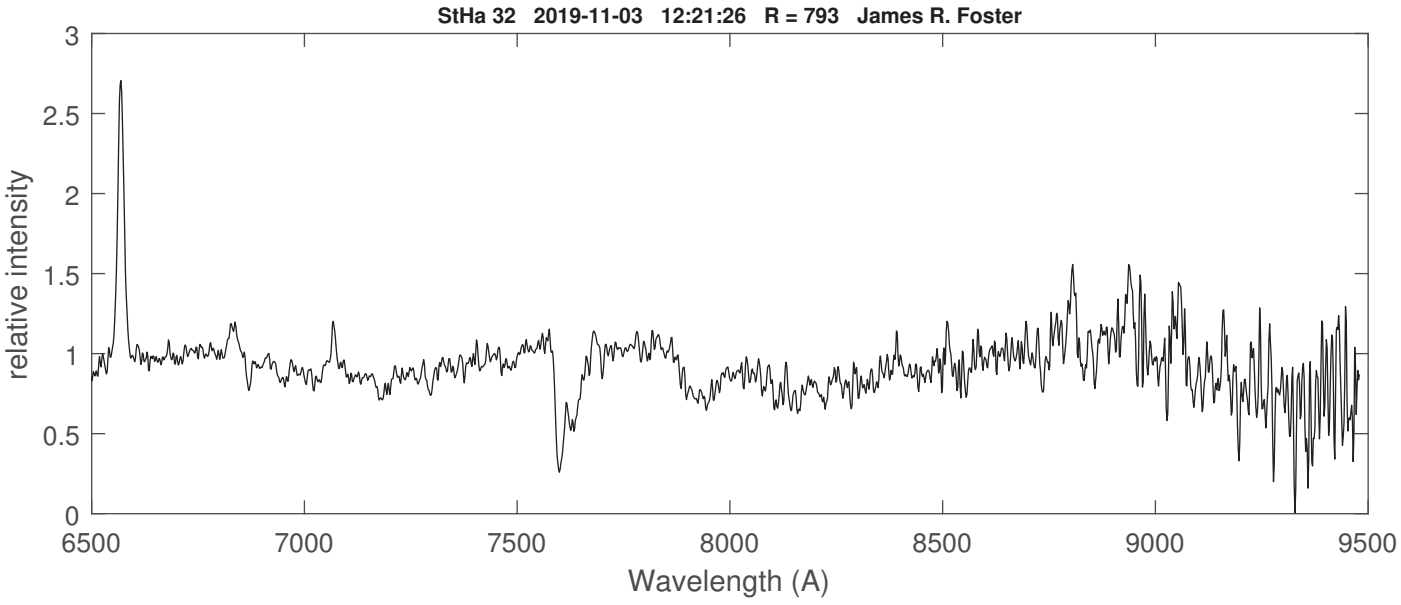

StHa 55

Coordinates (2000.0)	
R.A.	05 46 42.07
Dec	+06 43 47.07
Mag V	

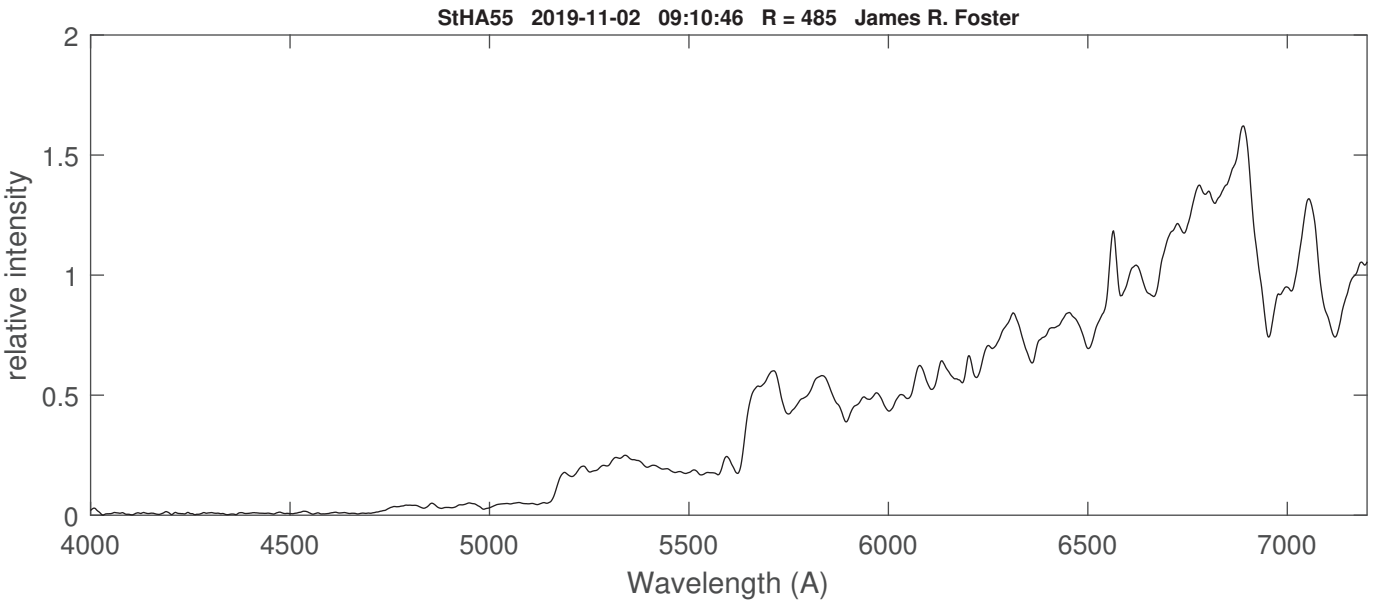

SU Lyn

Coordinates (2000.0)	
R.A.	06 38 45.7
Dec	+55 31 24.9
Mag V	

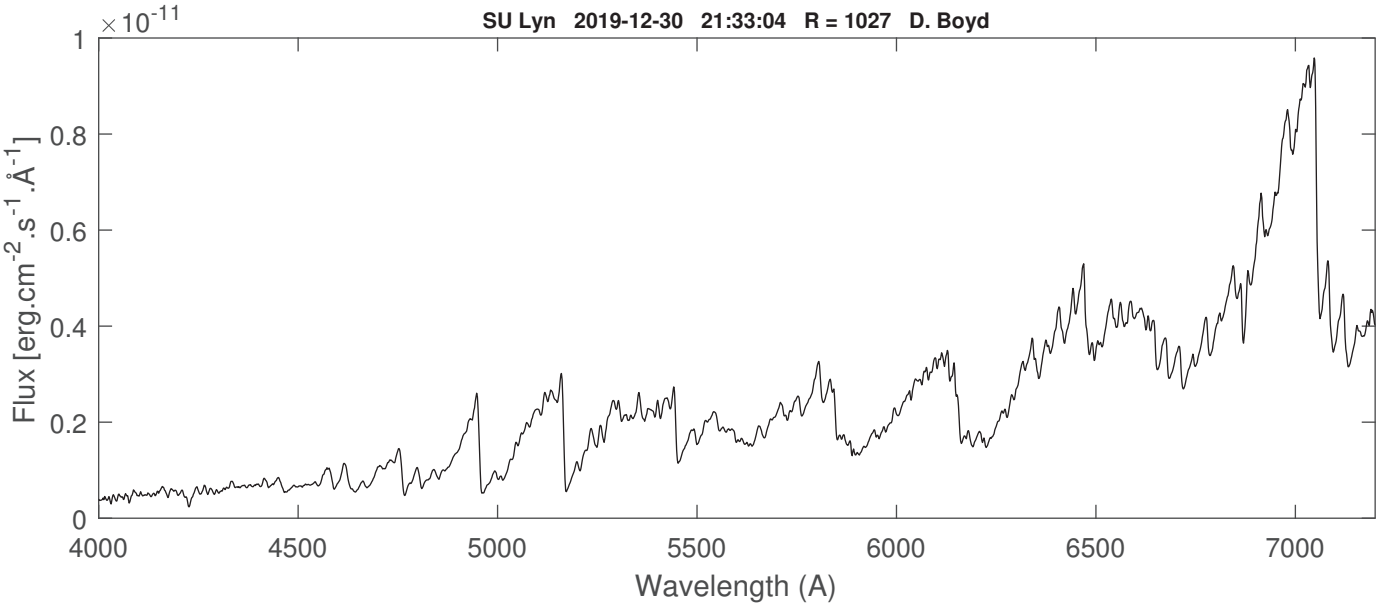

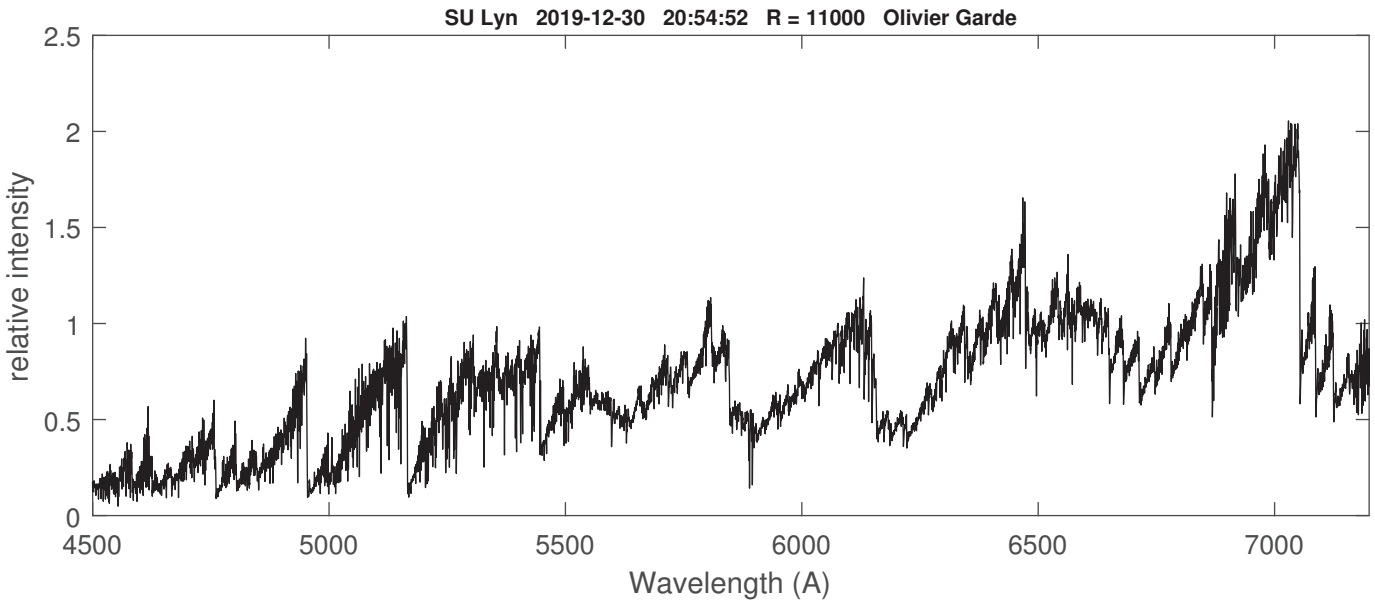

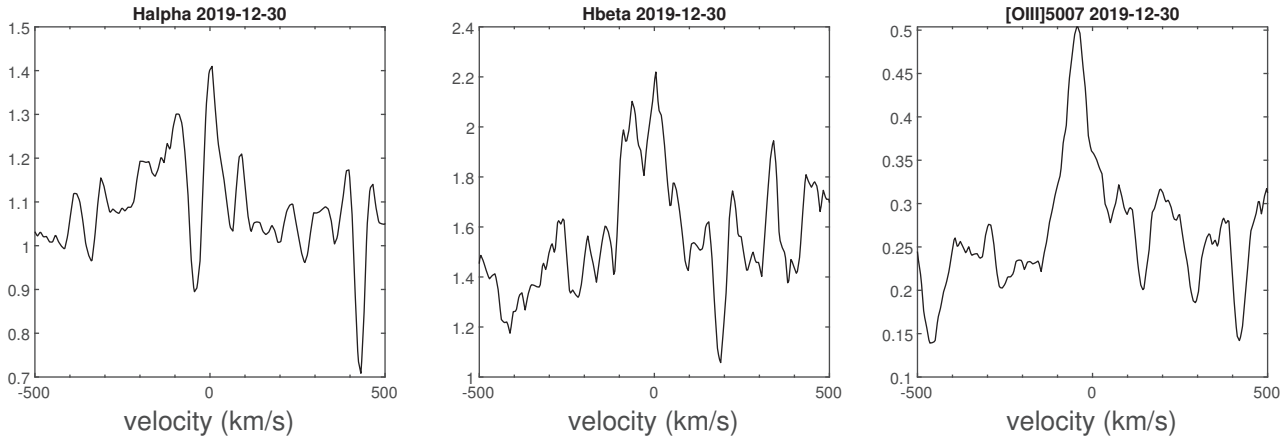

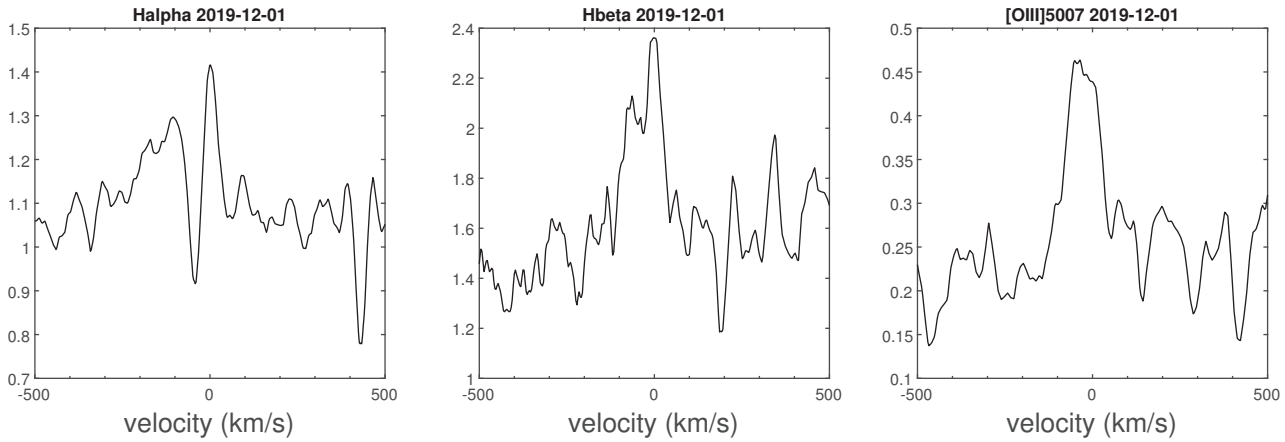

Line profiles. Top: Olivier Garde (2019-12-30) Bottom: François Teyssier (2019-12-01)
H alpha is very weak. Note the significant change in [OIII] profile

T CrB

Coordinates (2000.0)	
R.A.	15 57 24.4
Dec	+26 03 38.8
Mag V	9.8

Main target until the next nova event

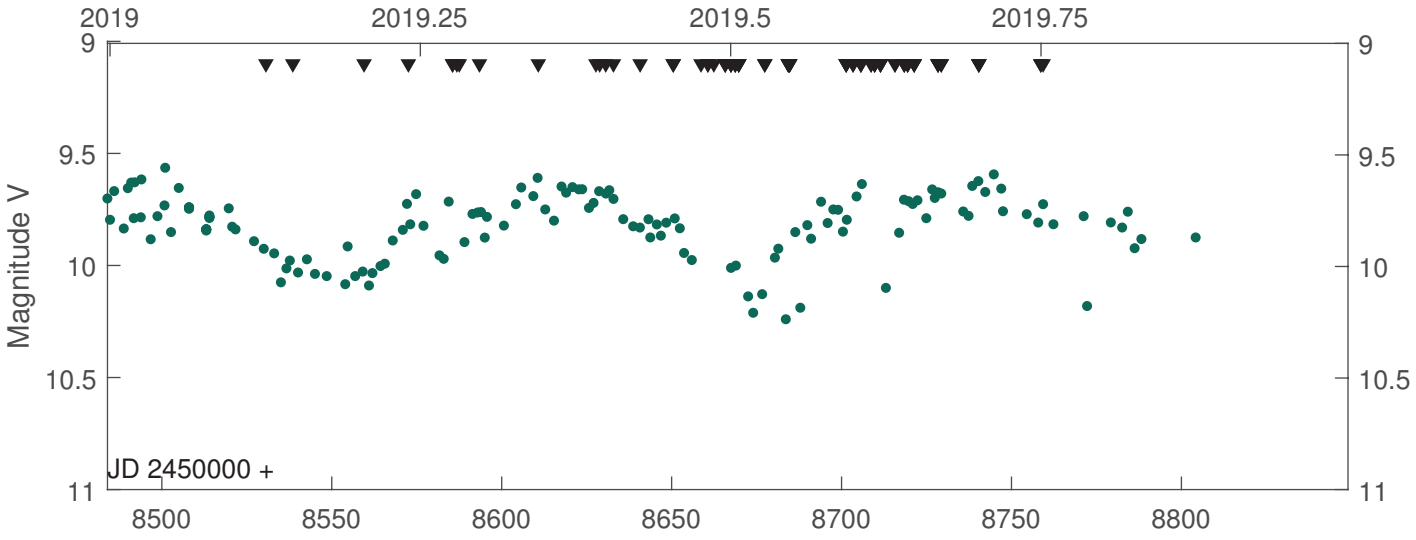

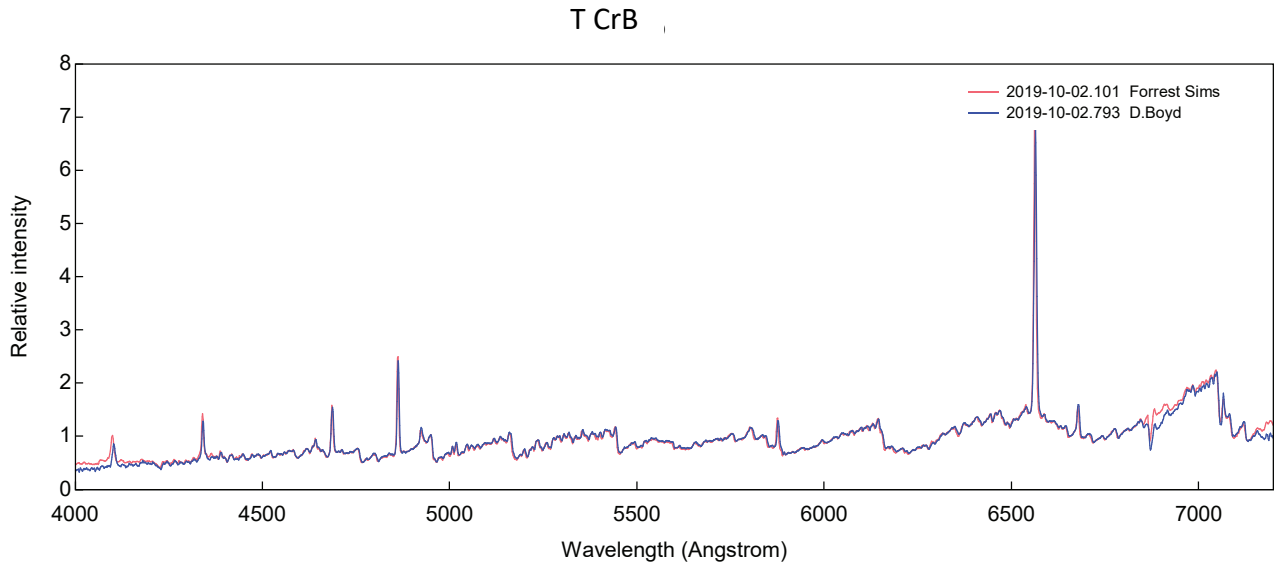

This figure illustrates the quality of the reduction of LISA (R = 1000) spectra of T CrB obtained by David Boyd and Forrest Sims at an interval of 0.6 day.

T CrB before the next nova event (Part 1)

T CrB is one of the four known recurrent symbiotic novae. Nova-type outbursts were recorded in 1868 and 1946 when the system reached magnitudes of 3 (Fig.1). The sytem consists in a massive M = 1.2 +/- 0.2 $M_{\odot}$ white dwarf with a low L = 40 $L_{\odot}$ luminosity (accreting powered symbiotic) and a M4-4.5 III type donor which fills its Roche Lobe. T CrB is one of the rare symbiotic stars in which hard X-rays have been detected and it flickers at a time scale of minutes or hours. Between nova outbursts, the activity of the system can be classified in quiescent state and active state [1], the later characterized by an enhancement of the blue continuum, increasing of the intensity of emission lines and appearance of high ionized lines such as He II λ 4686, [O IIII], CIII/NIII (Fig 2). Since 2015 T CrB is in active phase[2] [3] . From a comparison of the trends of the luminosity in B band of the pre-outburst phase (1946 and current) , B. Schaefer deduced that the next nova event[4] could happen in 2023.6 +/- 1 (Fig. 3). In this document, we present the current status of the system from ARAS observations.

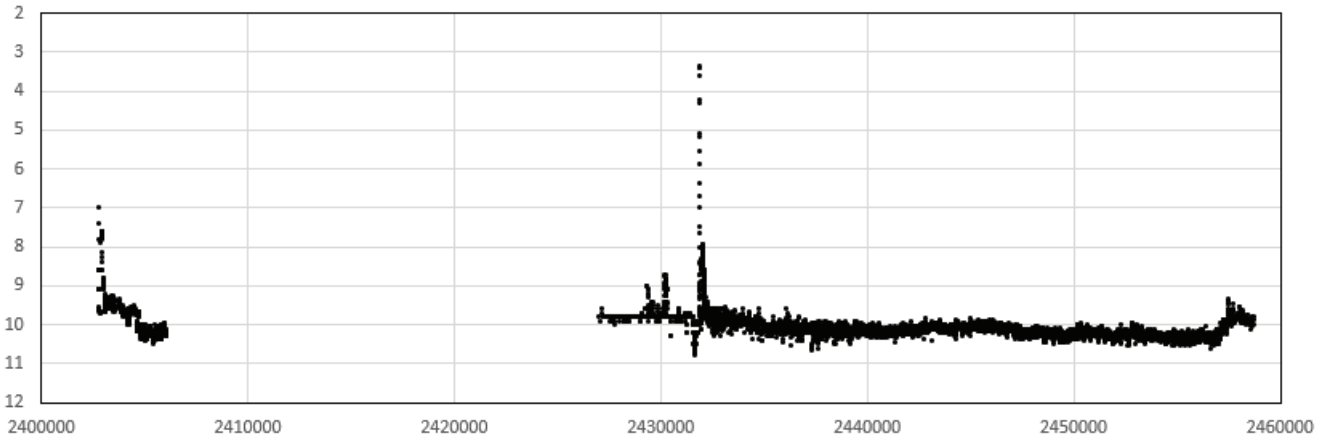

Fig. 1 - AAVSO historical lightcurve (Visual, 15 days mean) since 1866 nova-type outburst.

1 Iijima, T. 1990, Journal of the American Association of Variable Star Observers (JAAVSO), 19, 28.
2 Munari, Ulisse, Dallaporta, Sergio, & Cherini, Giulio 2016, \na, 47, 7.
3 Iłkiewicz, K., Mikołajewska, J. Stoyanov, K., Manousakis, A., & Miszalski, B. 2016, \mnras, 462, 2695
4 Schaefer, Bradley E. 2019, American Astronomical Society Meeting Abstracts #234, 234, 122.07

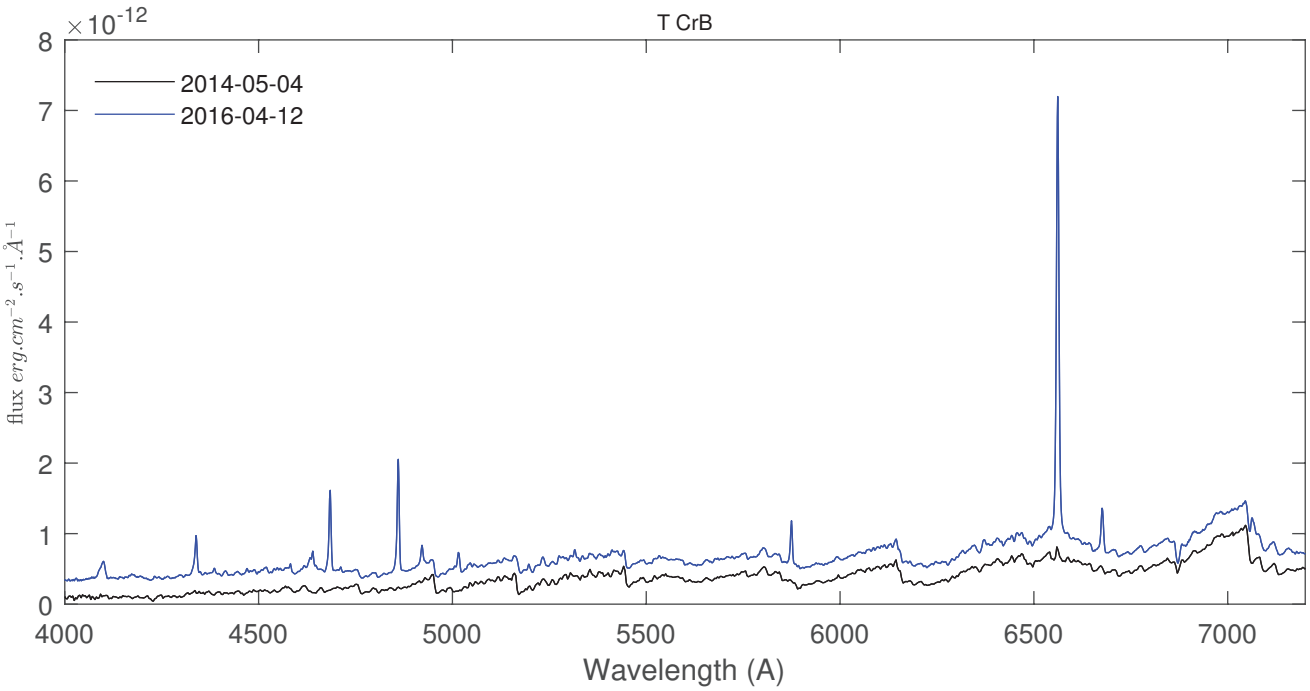

Fig. 2 - Comparison of the spectra in low state (2014-05-04, F. Teyssier) and high state (2016-04-12, D. Boyd). LISA Spectra (R = 1000)

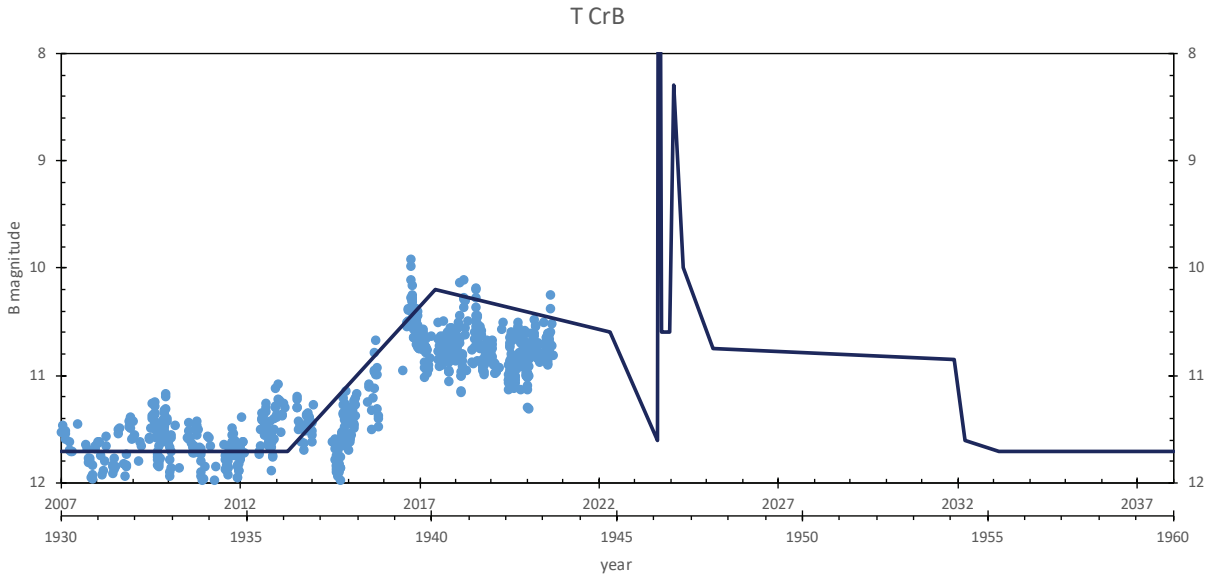

Fig. 3 - Adapted from Brad Schaefer's figure: B magnitude, comparison of the current state (AAVSO 1 day mean, blue dots) with the 1946 outburst (dark blue line). Updated on March, 2020.

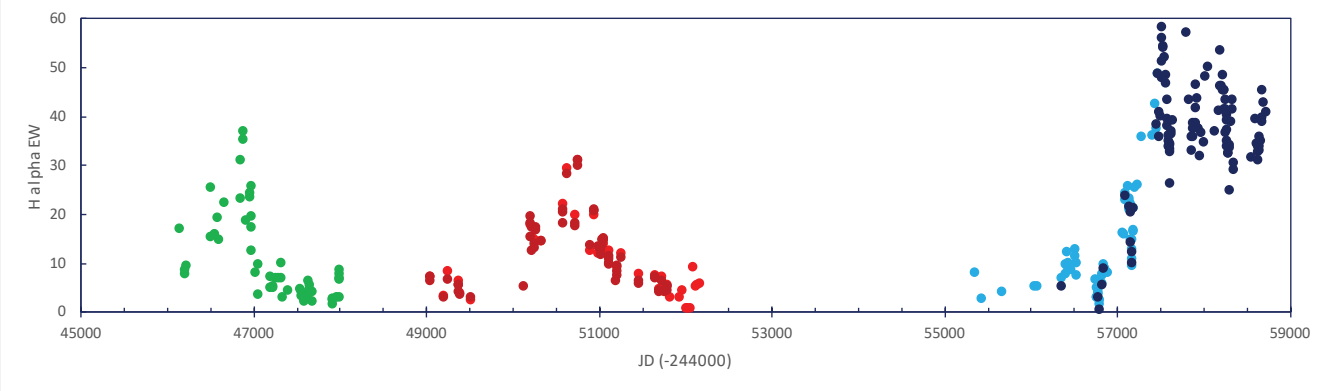

Fig. 4 - Equivalent width of H alpha compiled from various sources.

1 Anupama, 1991[1]
2 Stanishev, 2004[2]
3 Zamanov, 2001[3]
4 Ilkiewitcz, 2016[4]
5 Aras[5]

The current active phase is clearly longer and stronger than the two previous ones. The lack of published data does not allow determining if an active phase occurred between JD 245300 and 5500.

The EW(Hα) peaked at almost 60 near JD 2457600 and the global trend since then have been a slight decline which follows the decline of the B luminosity (fig. 3).

1 Anupama, G. C. & Prabhu, T. P. 1991, MNRAS, 253, 605.

2 Stanishev, V., Zamanov, R., Tomov, N., & Marziani, P. 2004, \aap, 415, 609.

3 Zamanov, R. & Marti, J. 2001, Information Bulletin on Variable Stars, 5013, 1.

4 Iłkiewicz, K., Mikołajewska, J., Stoyanov, K., Manousakis, A., & Miszalski, B. 2016, MNRAS, 462, 2695.

5 This letter

T CrB: Equivelent widths of the main lines since 2015

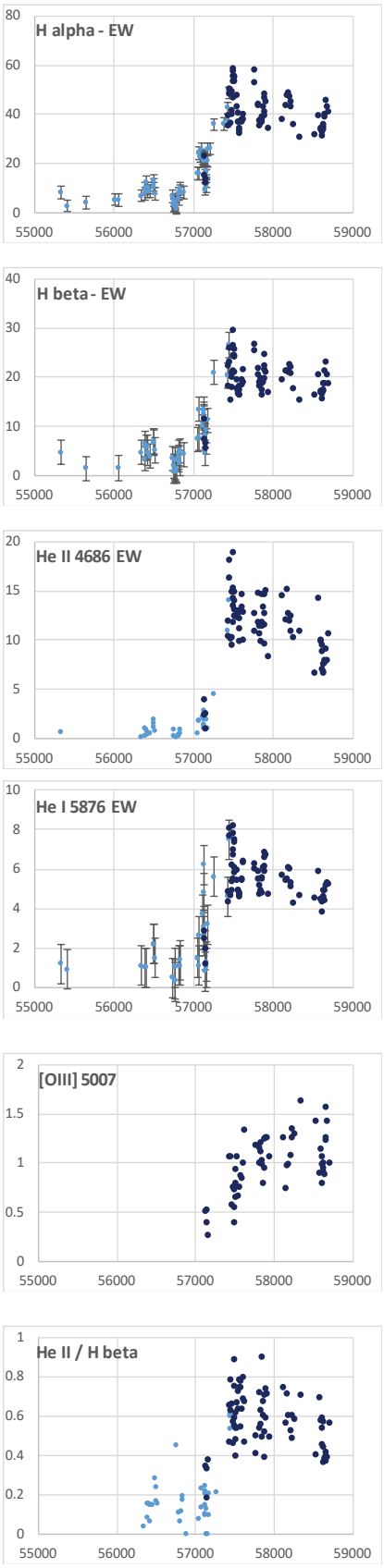

Fig. 5 - Equivalent widths of the main lines. Light blue dots : published values in Iłkiewicz+ (2016) . Dark blue: echelle spectra in the ARAS database

The equivalent widths of Hβ, He I and He II lines follows the same behaviour as Hα. The ratio He II λ 4686 Å / Hβ decreases since JD 2457500 which reflects the cooling of the hot component. We note the increase of EW(OIII λ 5007) which is anticorrelated to the decrease of the recombination lines.
In the next installment we'll produce the intensities of the lines from low and high resolution spectra.

JD - 2400000	Date	HeII 4686	Hb	Ha	He I 5876	He I 6687	[OIII]
57131.449	18/04/2015	4.0	11.4	22.8	2.9	1.8	0.5
57140.386	27/04/2015	2.5	7.4	15.3	2.5	1.2	0.5
57151.402	08/05/2015	1.0	5.5	12.2	1.9	0.6	0.4
57159.392	16/05/2015	2.5	6.7	13.6	1.2	0.9	0.3
57435.662	16/02/2016	12.0	18.3	39.3	4.8	4.2	1.1
57447.673	28/02/2016	18.1	23.1	50.4	8.1	6.7	1.1
57462.588	14/03/2016	10.1	15.3	36.5	4.6	4.1	0.6
57479.612	31/03/2016	10.3	18.0	41.6	5.4	4.9	0.8
57492.638	13/04/2016	14.9	20.0	49.1	6.2	5.4	0.4
57495.485	16/04/2016	18.9	21.4	53.1	6.7	6.3	0.6
57502.453	23/04/2016	15.3	26.0	58.7	8.2	7.0	0.7
57507.419	28/04/2016	14.3	26.5	57.3	7.8	6.1	0.8
57508.503	29/04/2016	14.9	24.2	54.7	7.4	5.5	0.7
57509.447	30/04/2016	12.4	25.7	55.7	7.5	5.4	0.9
57523.411	14/05/2016	14.0	21.0	53.5	6.1	4.7	1.1
57548.389	08/06/2016	12.9	17.8	47.8	5.9	4.3	0.7
57565.398	25/06/2016	13.0	16.6	40.7	4.9	3.8	0.8
57576.409	06/07/2016	12.2	16.5	36.7	4.6	3.5	0.9
57586.410	16/07/2016	11.1	17.5	34.4	4.8	3.5	0.9
57606.398	05/08/2016	14.7	18.5	38.2	5.4	4.3	1.0
57623.363	22/08/2016	12.8	19.1	40.0	6.4	4.7	1.3
57774.702	20/01/2017	12.8	25.4	58.1	6.3	4.7	1.2
57817.636	04/03/2017	14.7	20.6	44.1	5.5	3.9	1.0
57837.597	24/03/2017	11.4	18.2	37.4	4.8	3.8	1.1
57855.473	11/04/2017	14.6	16.3	37.0	4.8	4.4	1.0
57865.530	21/04/2017	11.8	17.5	38.8	5.5	3.7	0.8
57885.450	11/05/2017	13.4	18.9	43.2	6.1	5.6	1.0
57887.439	13/05/2017	11.6	22.3	48.5	6.8	6.8	1.2
57899.446	25/05/2017	14.6	19.8	40.9	6.1	4.4	1.3
57905.450	31/05/2017	15.0	21.1	45.3	6.7	4.9	1.3
57940.653	05/07/2017	8.3	16.8	34.1	4.7	3.6	1.1
58115.738	27/12/2017	14.5	19.4	38.1	5.7	5.9	1.3
58159.656	09/02/2018	12.0	21.3	43.8	5.4	4.1	0.7
58173.660	23/02/2018	15.1	21.3	47.8	5.5	5.7	1.0
58187.648	09/03/2018	12.7	21.0	48.8	6.1	5.3	1.0
58213.411	04/04/2018	11.9	22.6	47.1	6.0	4.0	1.1
58230.431	21/04/2018	12.4	20.6	43.1	5.1	3.5	1.3
58230.677	21/04/2018	10.9	22.2	45.4	5.3	3.9	1.4
58258.455	19/05/2018	10.2	17.6	35.8	4.3	3.4	1.3
58336.389	05/08/2018	10.9	15.4	30.7	4.6	3.6	1.6
58529.653	14/02/2019	6.6	16.5	31.8	4.6	4.0	1.4
58578.448	04/04/2019	14.2	20.5	39.5	5.9	5.8	0.9
58602.461	28/04/2019	9.9	17.3	34.5	4.5	4.0	1.1
58609.639	05/05/2019	10.0	17.0	33.9	4.5	4.1	1.1
58615.447	11/05/2019	8.9	16.6	33.0	4.4	3.6	1.0
58616.448	12/05/2019	7.0	15.5	31.1	3.9	3.6	0.8
58625.384	21/05/2019	9.5	16.7	33.2	4.4	3.7	1.0
58634.439	30/05/2019	6.8	18.6	36.0	4.9	3.9	1.0
58636.422	01/06/2019	7.6	17.1	33.9	4.6	3.2	0.9
58641.397	06/06/2019	6.7	17.3	35.1	4.6	2.9	0.9
58656.478	21/06/2019	7.9	21.3	39.8	4.9	3.4	1.3
58658.645	23/06/2019	7.7	18.6	39.1	4.4	2.9	1.2
58662.413	27/06/2019	9.1	23.0	45.4	5.2	4.1	1.6
58677.405	12/07/2019	8.0	20.6	42.8	5.3	3.8	1.4
58703.383	07/08/2019	10.6	18.7	41.1	5.2	4.5	1.0

T CrB before the next nova event

Call for observations by B. Schaefer

I would like to urge you to take many spectra of the recurrent nova T CrB, all leading up to its eruption in 2023.6 +- 1.0. Similarly, you can pass this recruitment around to your colleagues and collaborators, because the more observers the better. This is a wonderful opportunity; (1) because this is a frontline science target well in the range of your spectroscopy (V=10 or so), (2) because the professionals do not know and have not been monitoring the fast moving case, and (3) the nature of the very-high-energy pre-eruption plateau has no theoretical explanation and I could call it 'impossible'. It all begins with my >100,000 magnitude light curve, fully corrected to Johnson B and V, from 1842 to 2015:

This shows the 1866 and 1946 eruptions. We see a weird post-eruption plateau and a the still-mysterious second eruption half a year after the first, with the exact same structure being visible after *both* eruptions. We also see a whole complex of unprecedented and un-explained pre-eruption structure before the 1946 eruption. We also see that the light curve from 1955 to 2015 is essentially constant.

Let me show you a blow up of the weird stuff around the 1946 eruption. I'll only show the B light curve as heavily binned in time, and a superposed schematic shape meant to represent a smoothed light curve. The complex and totally-unique structure after the main peak (and the main peak itself) is identical from 1866 and 1946. This makes us think that the eruption physics will also duplicate the pre-eruption phenomena before every eruption.

Now let me update the T CrB light curve from 2015 to present:
[...] , from 1951 until 2014, the light curve has been holding flat, but suddenly in 2015, T CrB starts a determined rise followed by a plateau with a slight downturn. Egad, this is exactly what happened in 1936. The curve superposed is the same template from the 1946 eruption, just shifted 77.5 years (see Fig. 3, p. 48). Zounds, this means that T CrB started its pre-eruption plateau in 2014 or 2015. It also means that the next eruption will be in 2023.6 +- 1.0.

Now, the pre-eruption plateau from 1936–1946 has never been published, and every theorist that I've talked with has no understanding or even any ideas. I would even say that it is 'impossible' for the accretion disk (the undoubted site of the pre-eruption rise) would know that the base of the accreted material on the white dwarf (the undoubted site of the nova trigger) will blow up in a decade.

The pre-eruption plateau in 1936 had a variety of spectra taken and published [1] [2].
The ultraviolet continuum if incredibly strong, and there are high-excitation emission lines.

The old data is pitiful by modern standard. And that is where you can do greatly better than the heros of old. What is needed is many digital spectra throughout the complex developments of T CrB. You can provide wonderful very-high resolution spectra showing the detailed line profiles, and this will be critical for working out the flows of material inside the system. For this, you'll need spectra throughout the orbital period to get the Doppler shifts from many directions, and frequently to monitor the changes. The professionals are not doing it, but this is close to your sweet spot.

I urge you to redouble your efforts for T CrB, elevating it above just being one-of-a-lon- list-of-standard-targets. You might try to get people to push as far into the ultraviolet as possible, as there are some interesting lines well below 4000 Å. I can hope that you push into the solar gap, so that the Doppler shifts in the line profiles can be measured from many angles around its orbit. Indeed, for a middle-latitude northern observatory, T CrB can be recorded even through its solar conjunction, yielding full year-round measures.

[...] The intermediate questions are to measure the mass flows in the system, measure the disk properties, measure the photospheric temperatures, the size of the UV emitting region, and the luminosities; all as it varies over time. The high level question is what is making the pre-eruption plateau? The ultimate question is how and why the pre-eruption plateau is related to the nova event itself.

[...] No one had previously noticed or published the pre-eruption plateau before 1946, and no one has done more than note the rise starting around 2014-2015. (Previously, the only people who thought about the next T CrB eruption did nothing more than note that 1946-1866=80 years and apply the numerology that 1946+80=2026.) So the surity of an upcoming eruption (and its date) is new. This is providing the urge to follow the pre-eruption weird phenomena.

Bradley E. Schaefer, Louisiana State Univ. (Baton Rouge, Louisiana, United States)

1 Minkowski, R. 1943, PASP, 55, 101

2 Swings, P., & al., PASP, 52, 199

V1261 Ori

Coordinates (2000.0)	
R.A.	05 22 18.6
Dec	-08 39 58.0
Mag V	6.8

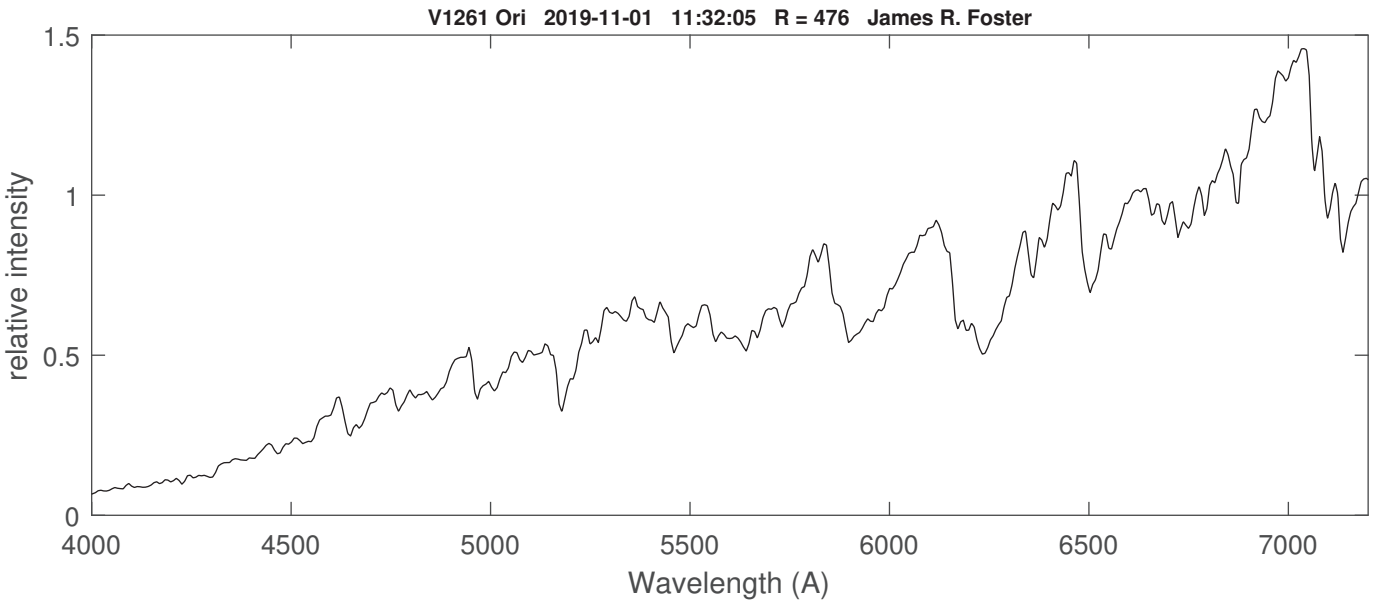

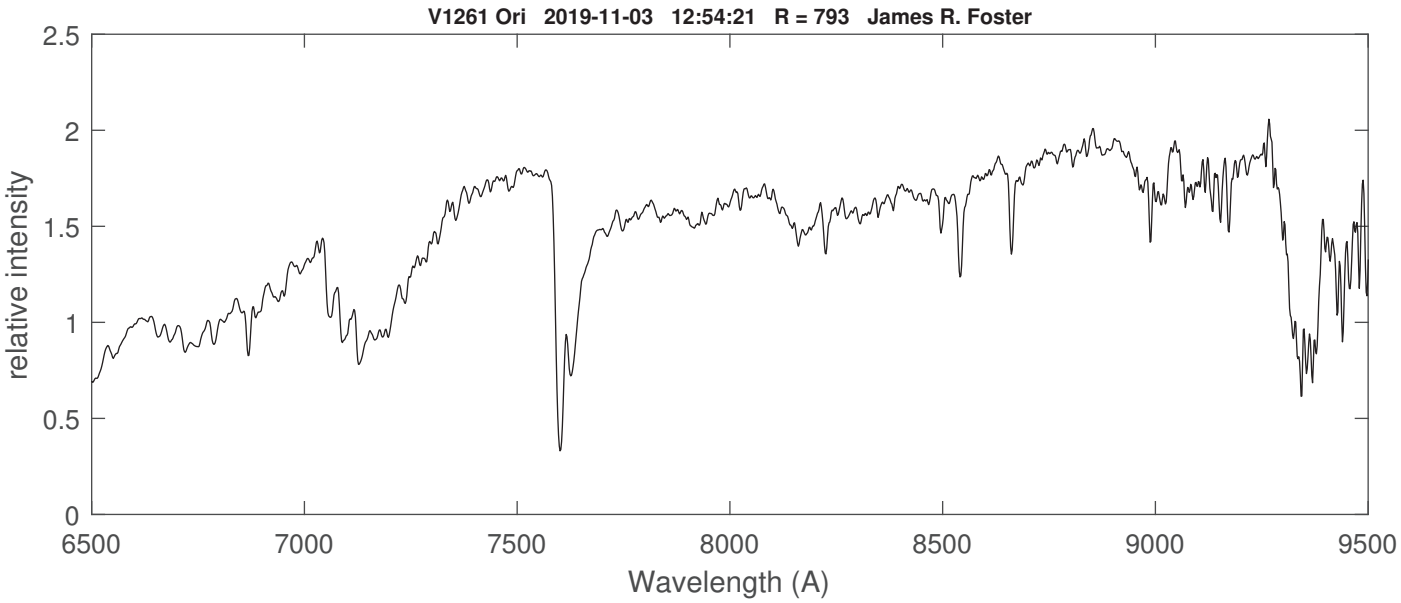

V1329 Cyg

Coordinates (2000.0)	
R.A.	20 51 01.2
Dec	+35 34 54.1
Mag V	

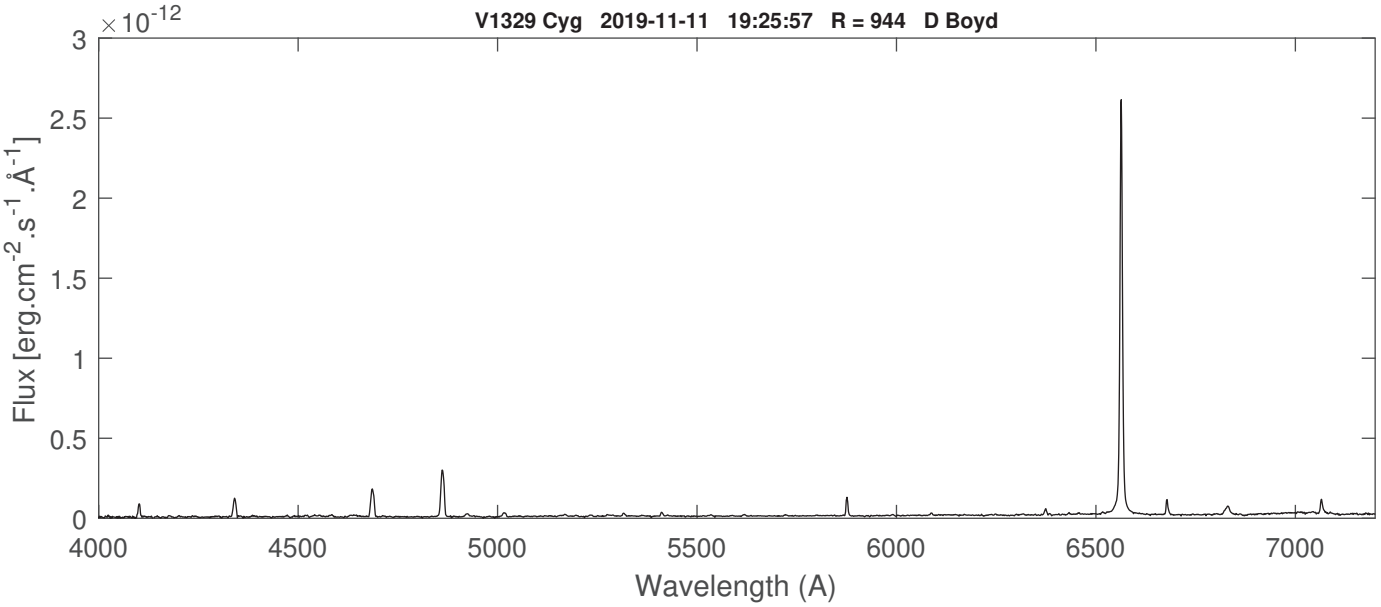

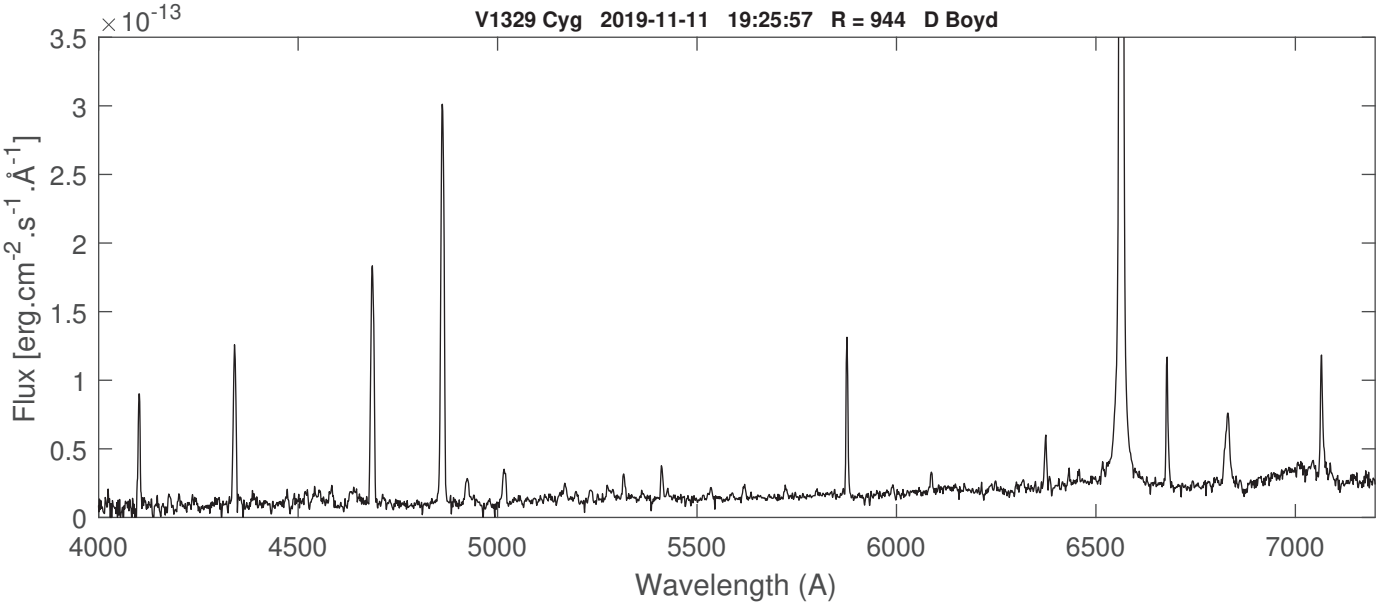

V443 Her

Coordinates (2000.0)	
R.A.	18 22 07.85
Dec	+23 27 19.9
Mag	~ 11.6 (vis.)

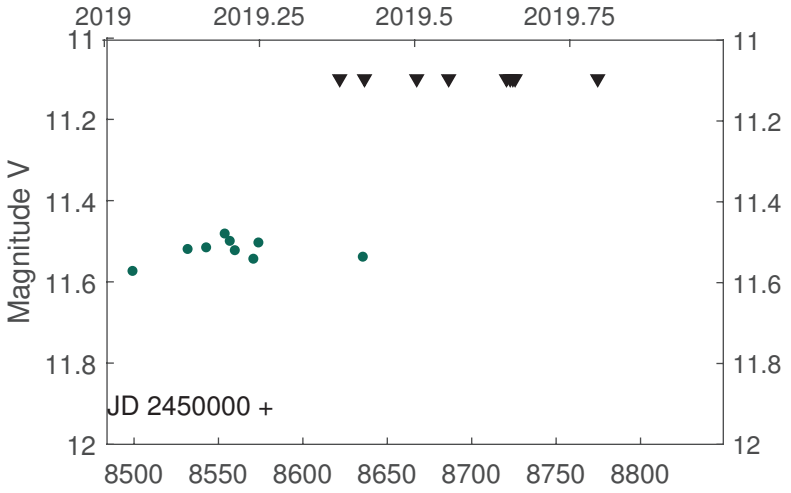

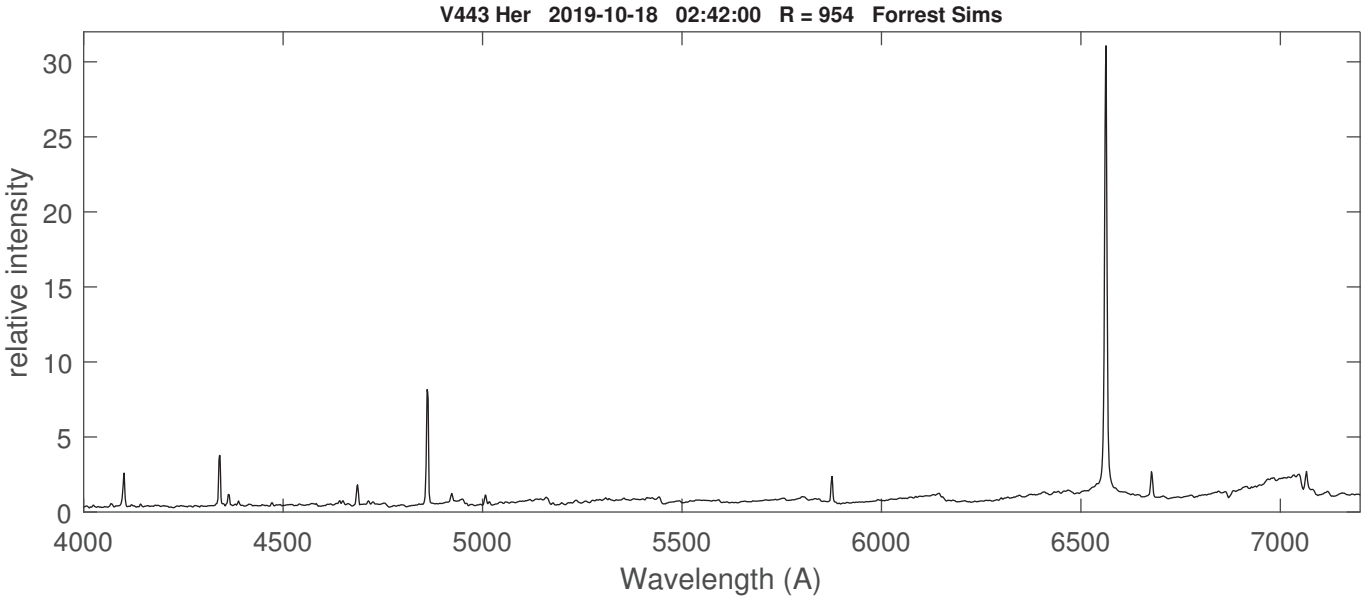

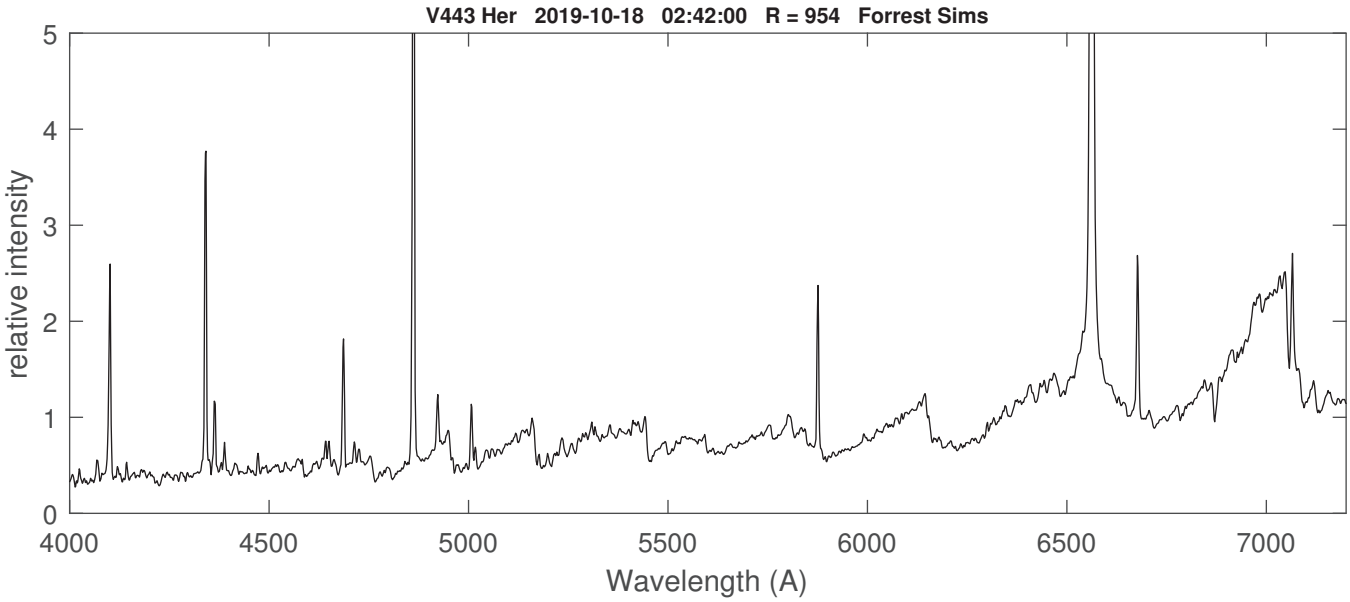

[Fe VII] is absent, the ratio He II/Hβ is very low (0.15)

V471 Per

Coordinates (2000.0)	
R.A.	01 58 49.7
Dec	+52 53 48.5
Mag	13.0

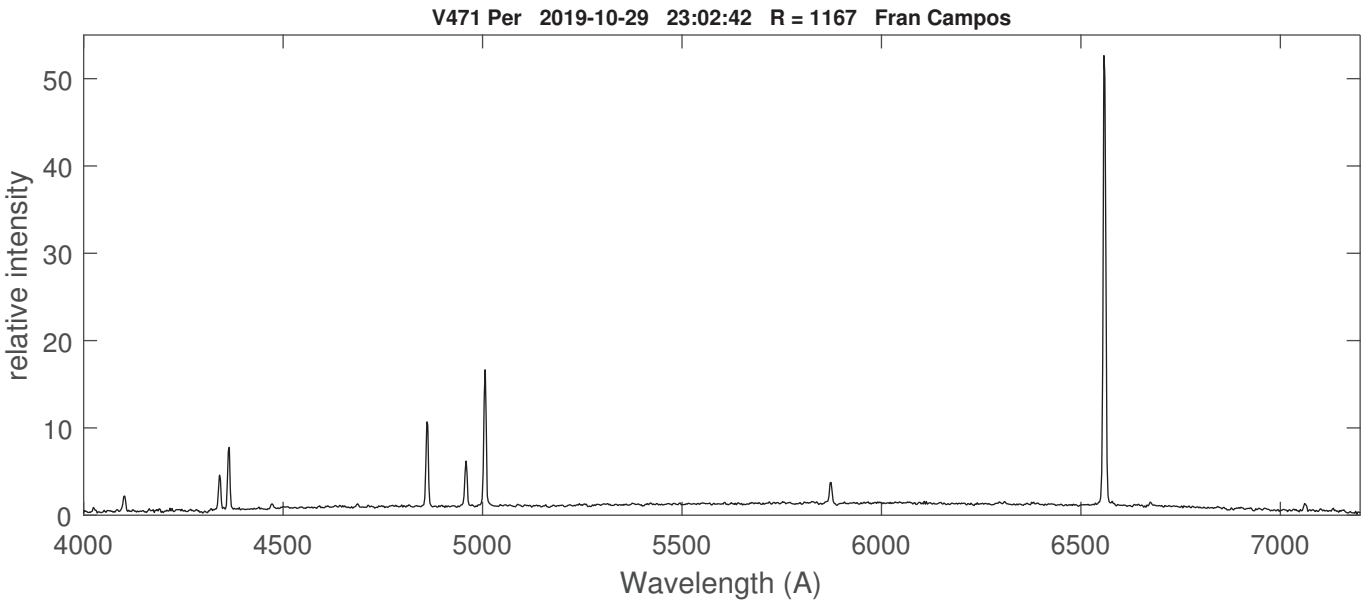

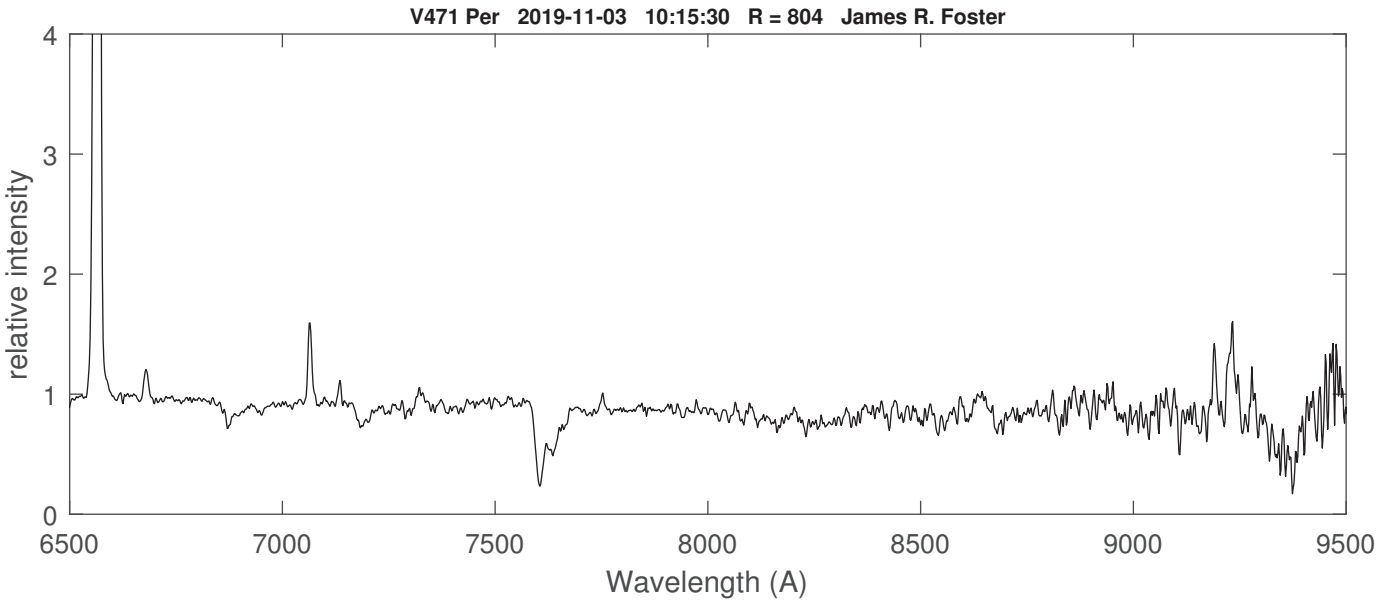

V627 Cas

Coordinates (2000.0)	
R.A.	22 57 40.96
Dec	+58 49 12.6
Mag	12.2

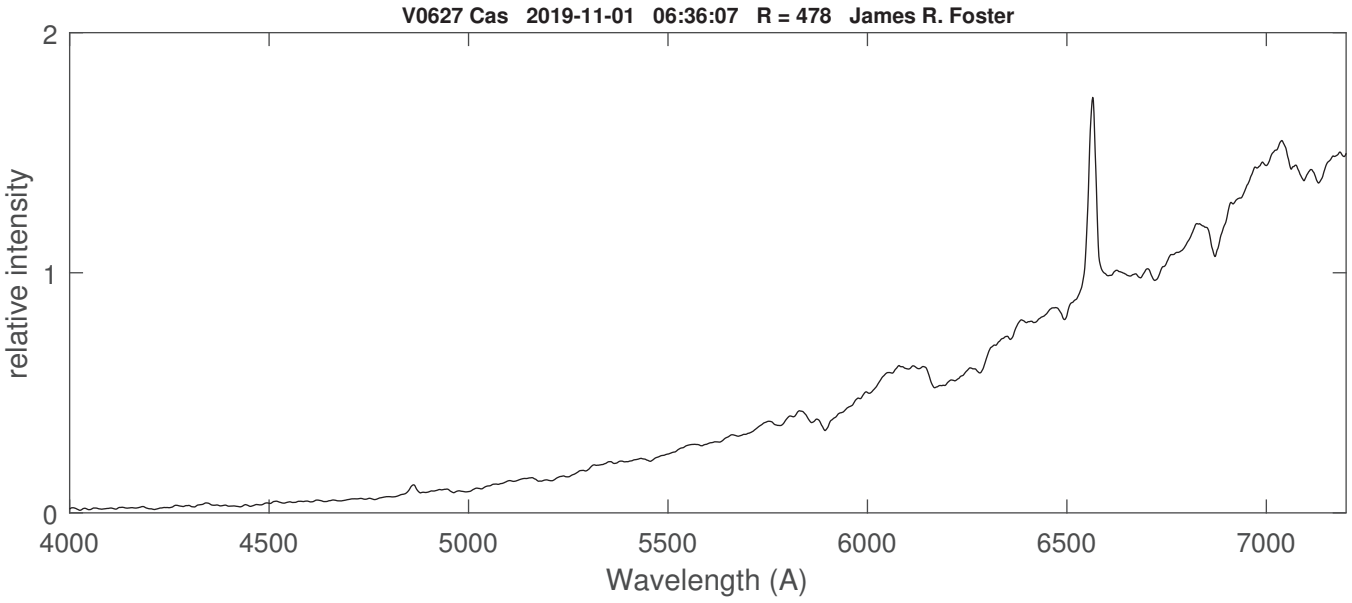

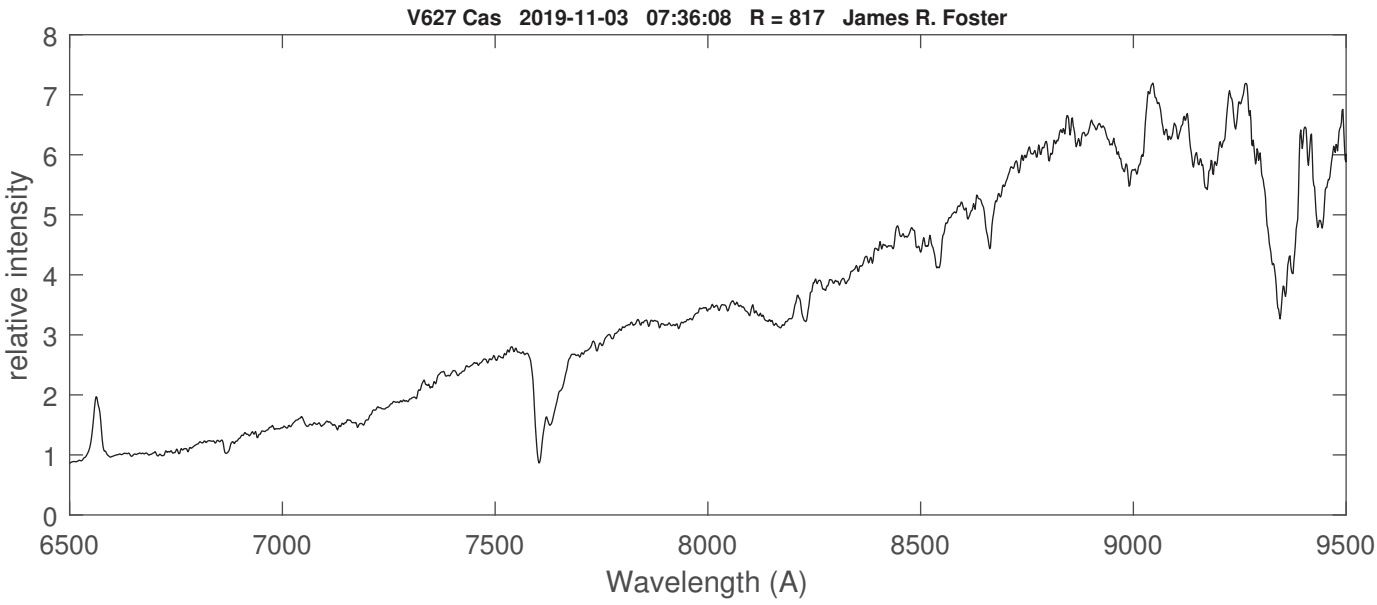

V694 Mon = MWC 560

Coordinates (2000.0)	
R.A.	07 25 51.28
Dec	-07 44 08.07
Mag	8.7 (2019-12)

Still very bright and increasing. It is the brightest luminosity ever recorded for this object. The previous record was mag ~ 9 in 1990 (see e.g. Leibowitz and Formiggini, 2015).

A special effort of observations in support to HST/STIS (Far UV) observations by C. Bruhweiler and B. Mc Collum (American University) on October, 23.

CHANDRA observations are scheduled January and March, 2020

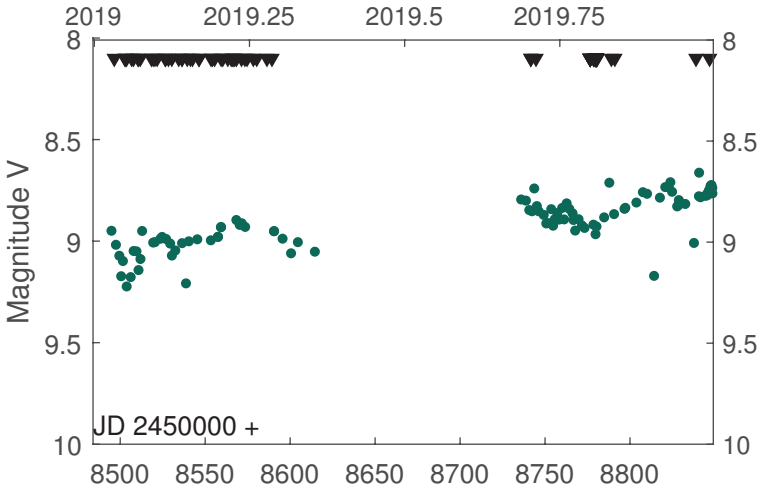

AAVSO (V) Light Curve and ARAS Spectra in 2019 (triangles)

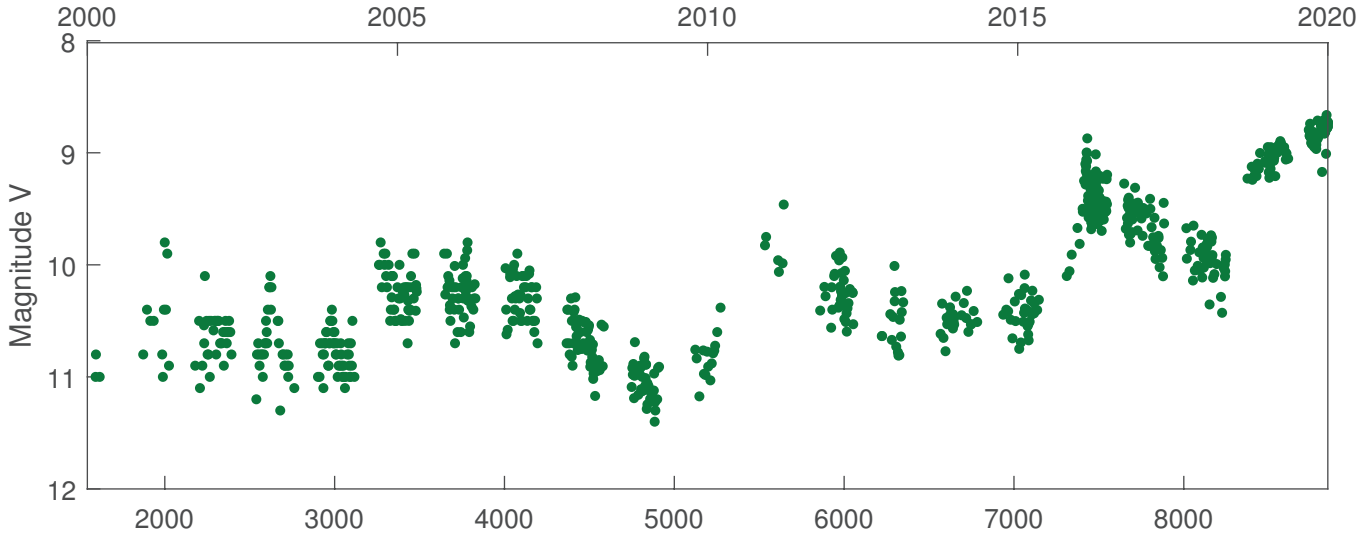

AAVSO Light Curve (V band, 1 day mean) since 2000

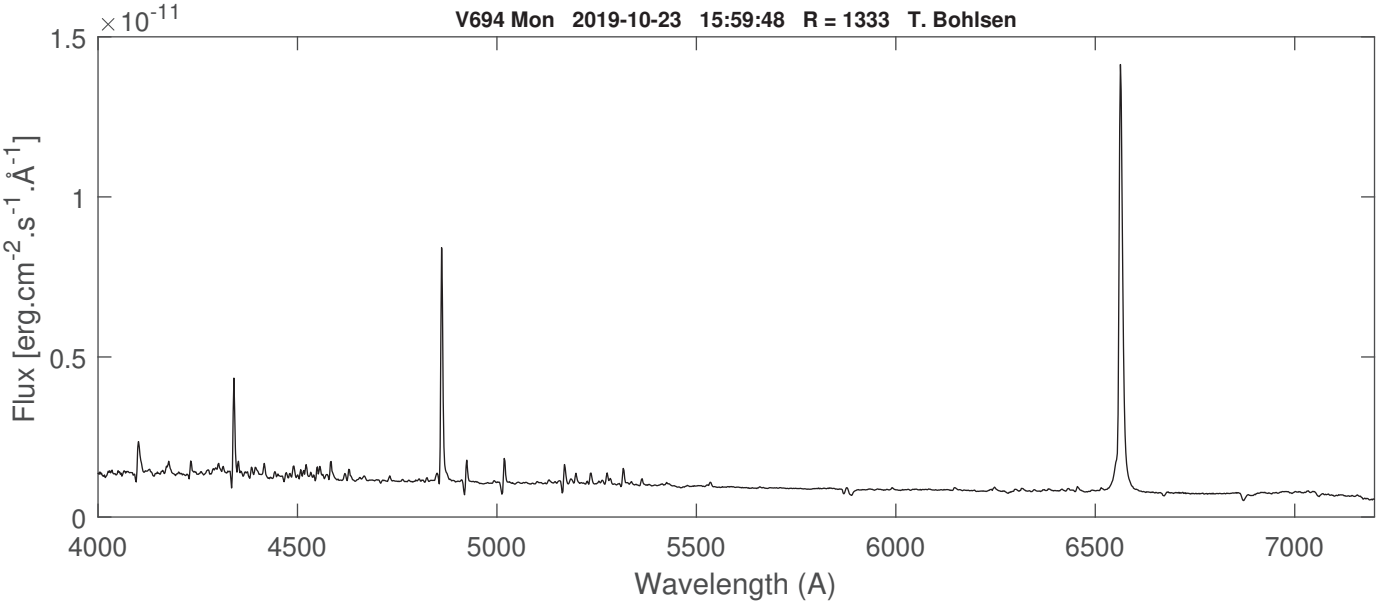

V694 Mon obtained by Terry Bohlsen with a LISA (R 1000)

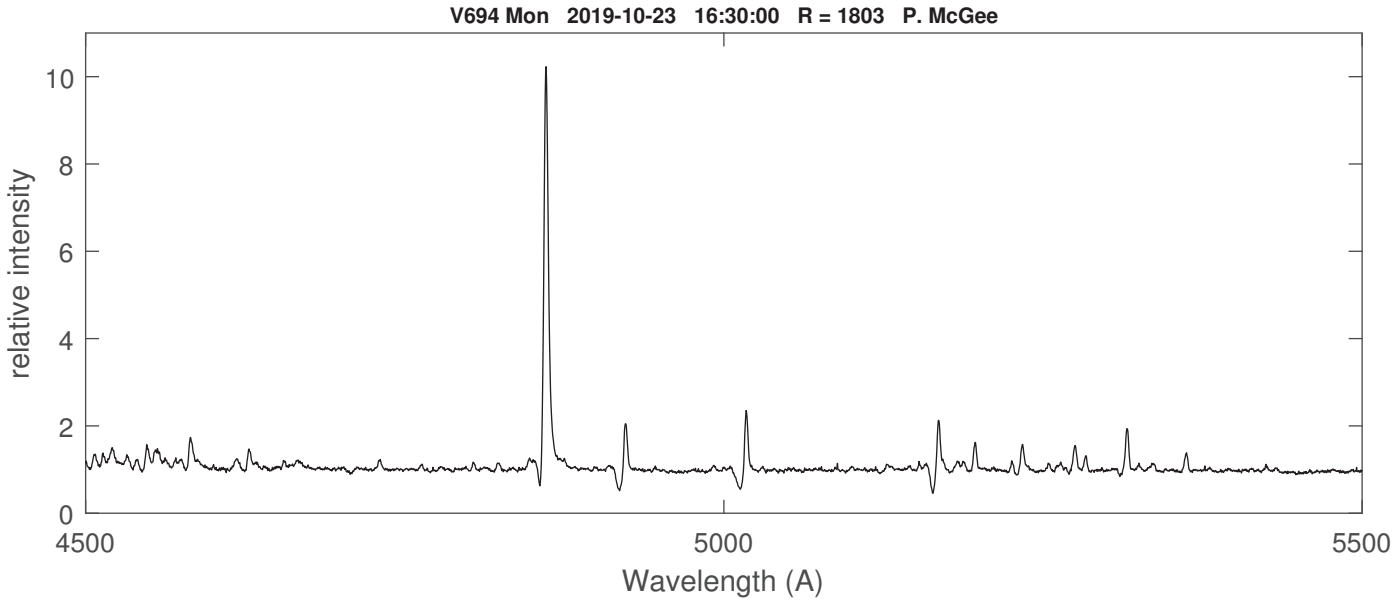

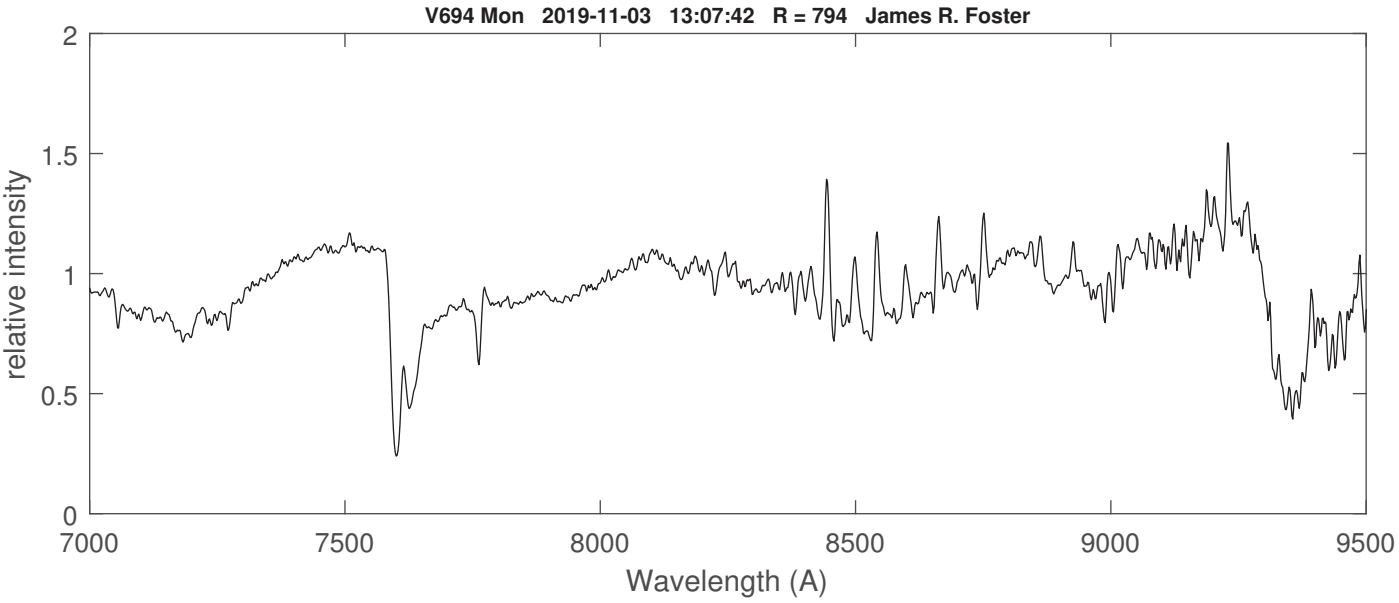

Th near IR spectrum obtained by James Foster with a LISA (R = 1000) shows OI λ 8448 Å and Ca II triplet in strong emission. Other lines identification

Time series obtained by Forrest Sims on 2019-10-23 at a time scale of 14 minutes.
12 spectra acquired from 11:34 to 12:56 UT
No significant variation can be detected

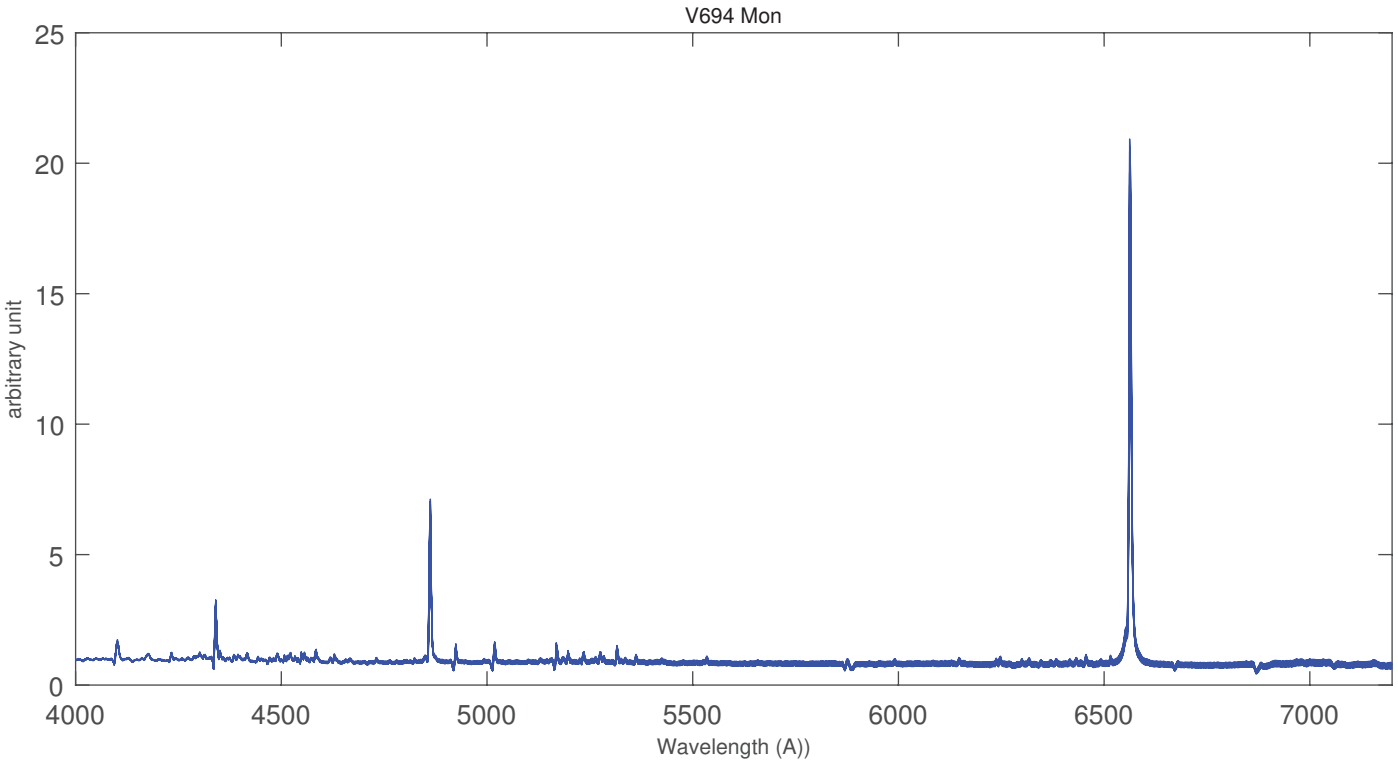

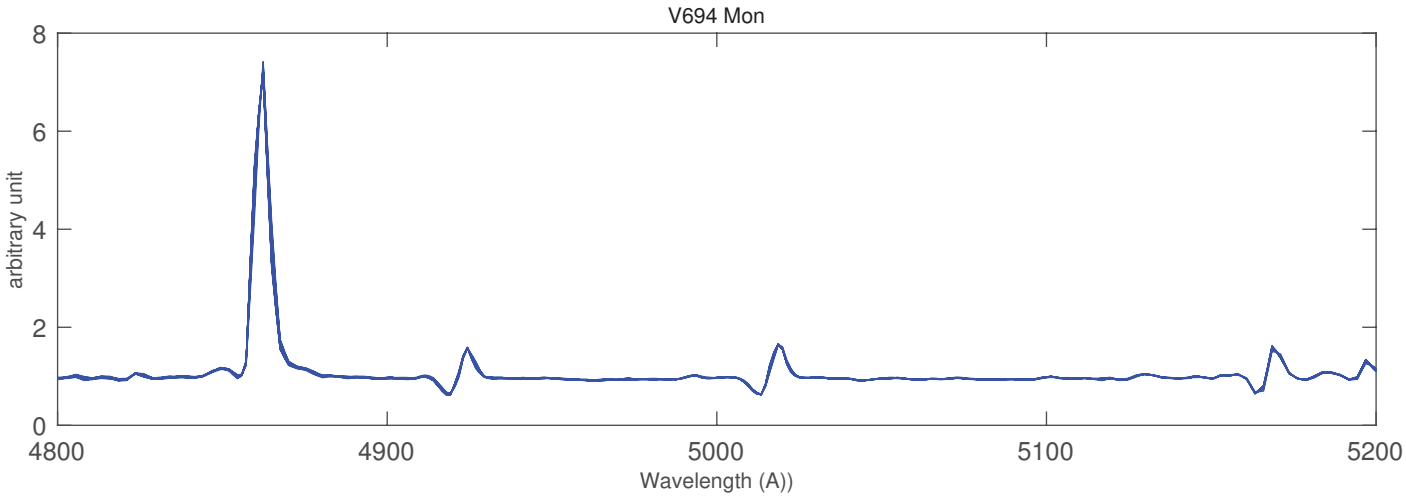

Crop on Hb and Fe II (42) region

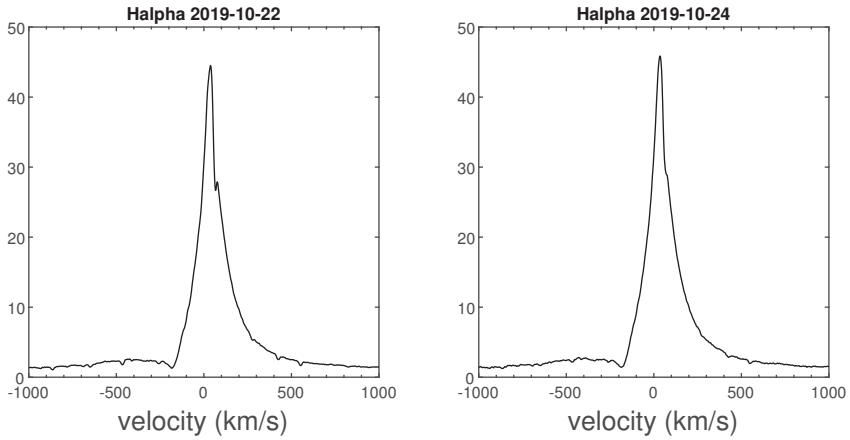

Hα profile obtained by P. Somogyi with a Lihres III 2400 l/mm (R = 15000)
The blue-shifted absorption is maximal at -180 km.s^{-1}.
A broad and faint emission component extends from -1000 to +1000 km.s^{-1}

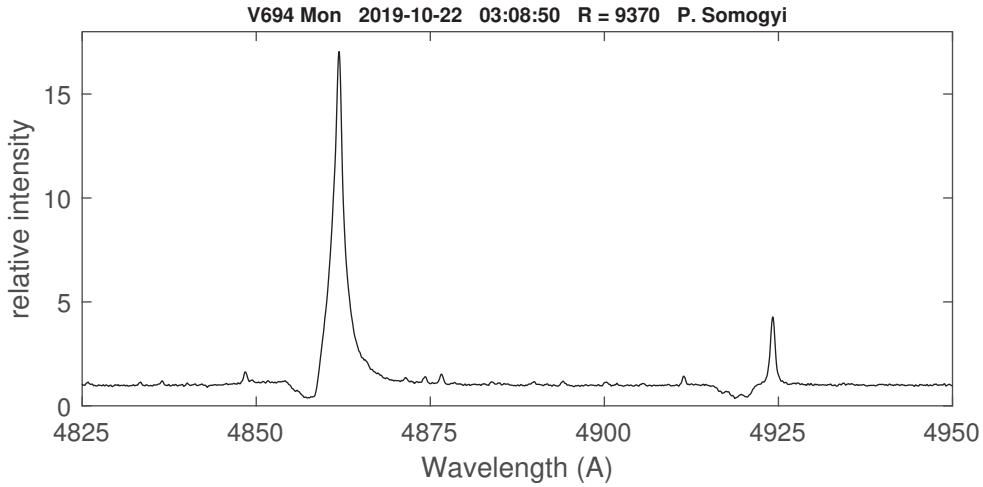

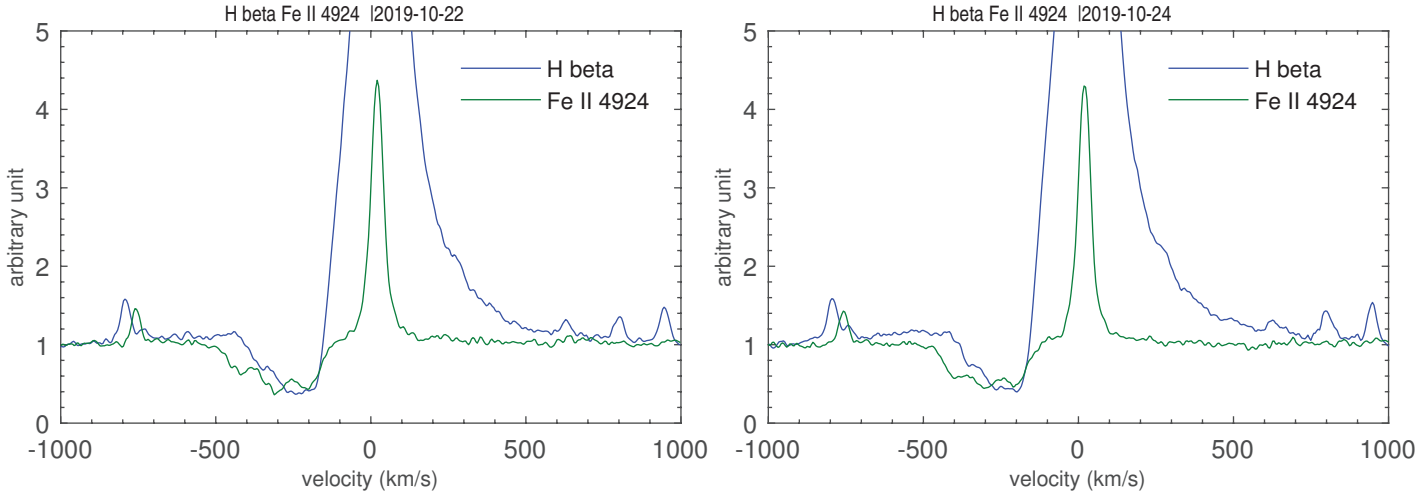

Comparison of Hβ and Fe II λ 4924 Å in the spectra obtained on 2019-10-22 and 24 by P. Somogyi
The maximum radial velocity of the blue-shifted absorption is - 440 km.s^{-1} for Hb and -530 km.s^{-1} Fe II λ 4924 Å

Z And

Coordinates (2000.0)	
R.A.	18 14 34.2
Dec	+20 59 21.2
Mag V	10.3 (2019-12)

In quiescent state after 2018 outburst

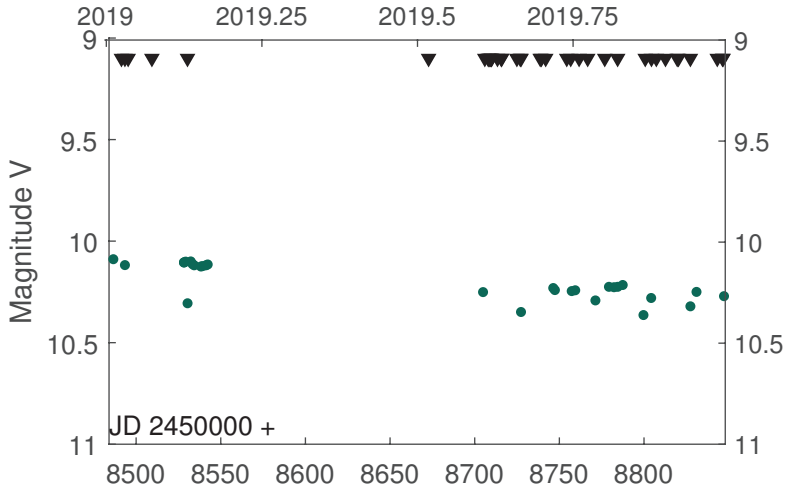

AAVSO V-band lightcurve and
dates of ARAS spectra (triangles) in 2019

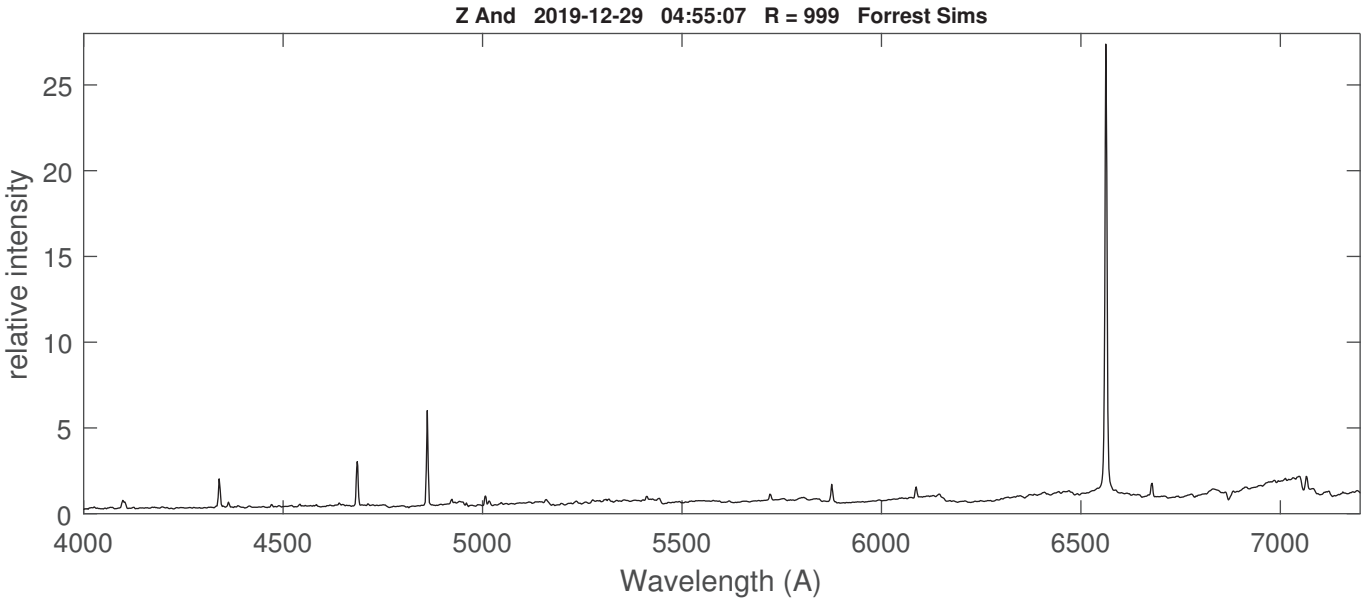

Evolution of the profiles of the main lines during 2019-Q4

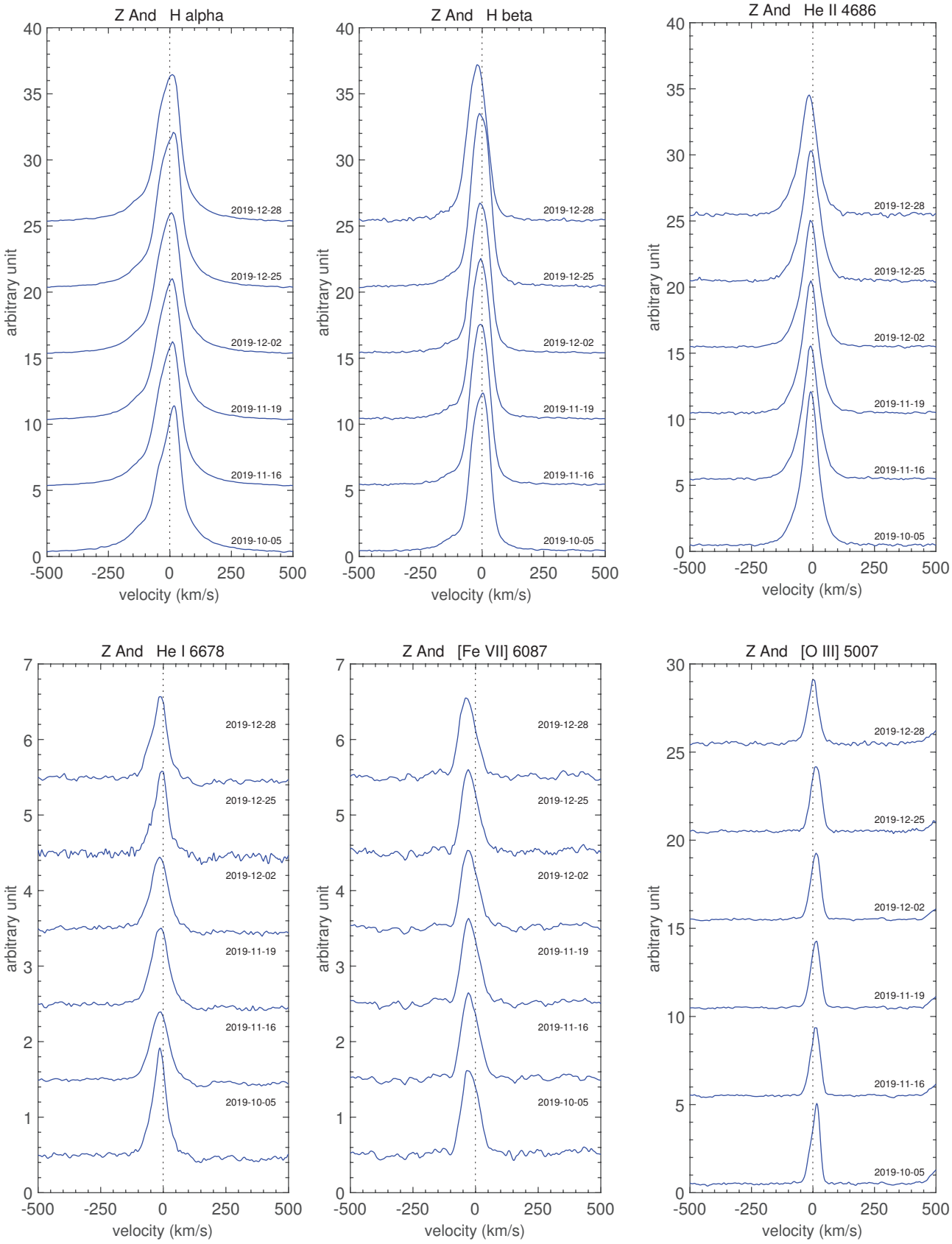

Eruptive stars spectroscopy
Cataclysmics, Symbiotics, Novae

Eruptive Stars
Information Letter n° 44 #2019-04 15-02-2020
Observations of Sep. - Dec. 2019

Spectroscopic observations of the Dwarf Nova TCP J21040470+4631129

Authors:
D. Boyd, F. Sims, P. Dubovsky, P. Berardi, F. Teyssier, U. Sollecchia, T. Lester, L. Franco, V. Lecocq

Abstract:
The very bright transient TCP J21040470+4631129 was detected by Hideo Nishimura on 2019-07-12.190 UT. As reported in the 2019-Q3 newsletter, it was identified as a dwarf nova outburst by F. Teyssier with an Echelle spectrum obtained on 2019-07-12.190 UT (ATel 12936,) and confirmed by Tim Lester in another Echelle spectrum obtained a few hours later.

Over a 6 month period from July to December 2019, the dwarf nova experienced one bright superoutburst followed by two short rebrightenings, a second full but less bright outburst followed by another short rebrightening and then, 3 months later a third full outburst. This behaviour is most unusual for a suspected WZ Sge-type dwarf nova.

A campaign to observe this object by amateurs and professionals using both photometry and spectroscopy was coordinated by Dr Vitaly Neustroev. Analysis of these observations will be published in due course. Further information was published in ATels 12947, 13009, 13122 and 13297.

Stars:

TCP J21040470+4631129

58 spectra were obtained between 2019-07-12 and 2019-01-03 and reported to the ARAS database.
http://www.astrosurf.com/aras/Aras_DataBase/Cataclysmics/Miscellanous.htm

TCP J21040470+4631129: dwarf nova with multiple rebrightenings

Coordinates (2000.0)	
R.A.	21 04 04.7
Dec	46 31 12.9
Mag V max	8
Mag V min	15

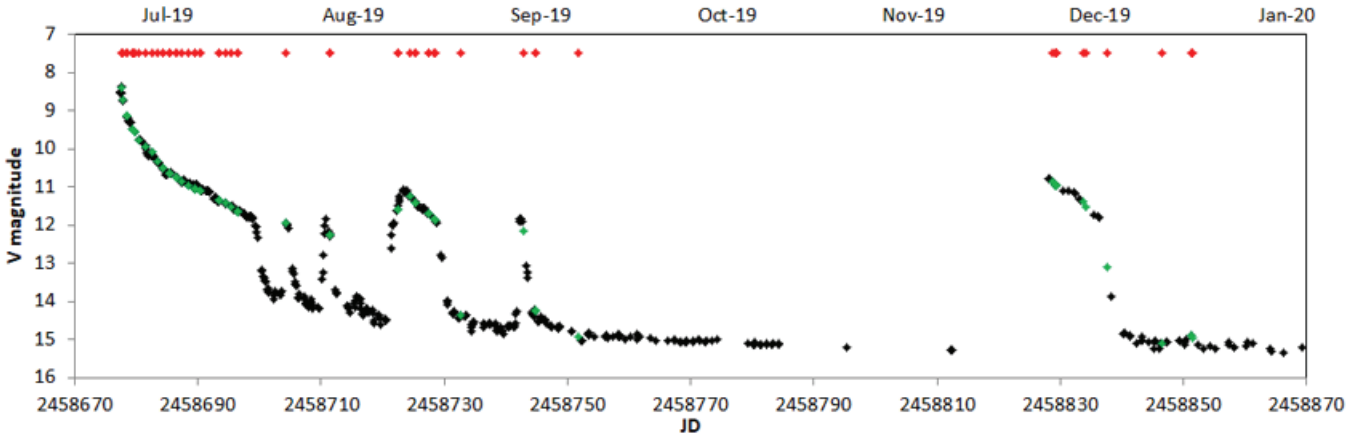

Fig.1 - AAVSO V band lightcurve (0.1 day mean, black), dates of ARAS Spectra (red) and interpolated V magnitudes (green).

47 spectra were flux calibrated using V magnitudes interpolated from AAVSO V band observations at the times of recorded spectra.

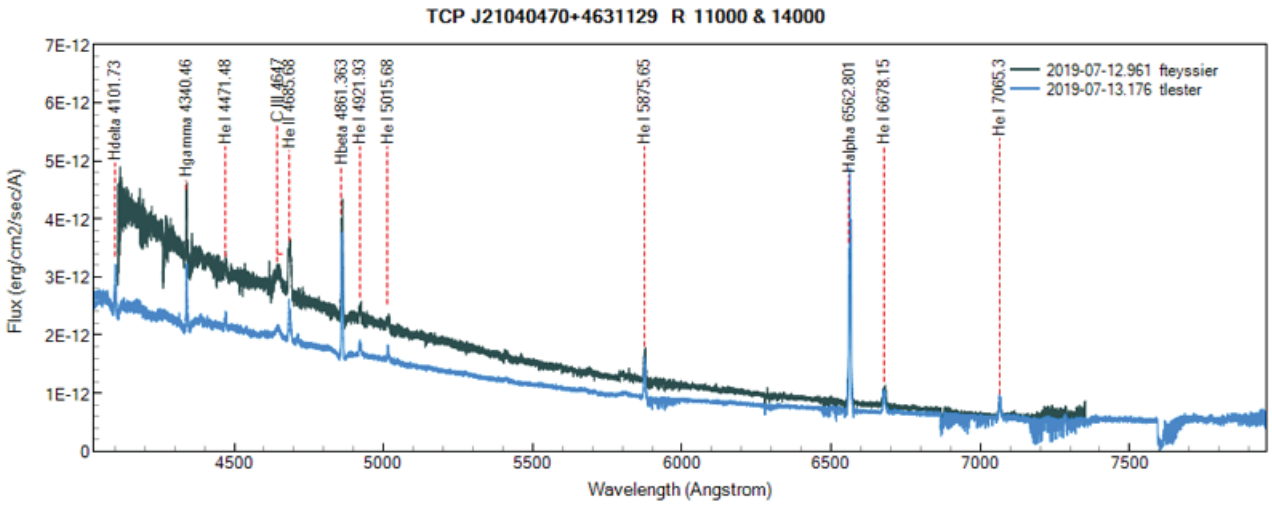

Fig.2 - High resolution spectra recorded immediately after the start of the superoutburst. A description of these early spectra can be found in the 2019-Q3 newsletter.

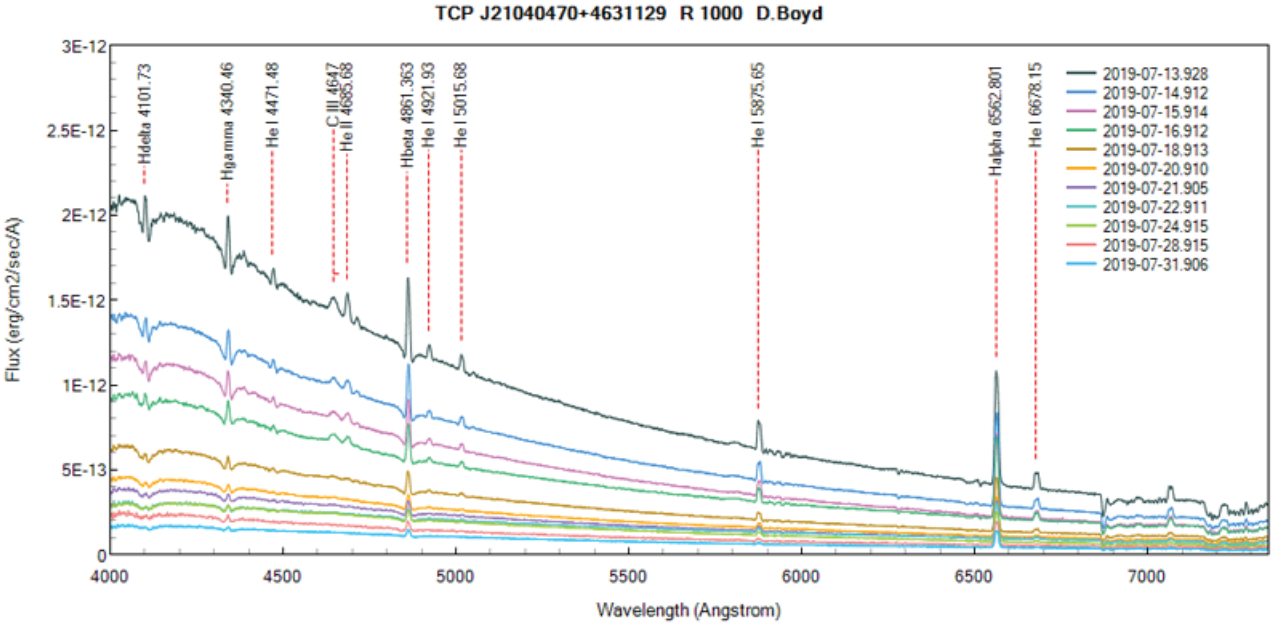

Fig. 3 - Sequence of spectra as the superoutburst declined showing gradual fading of emission lines.

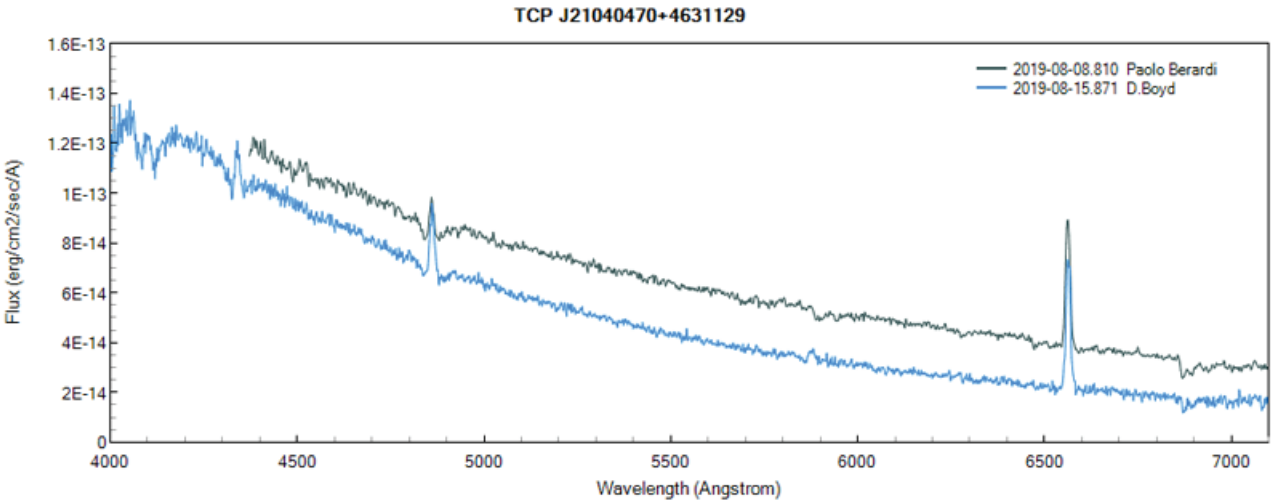

Fig. 4 - Spectra recorded during 1st and 2nd rebrightenings on 8th and 15th August.

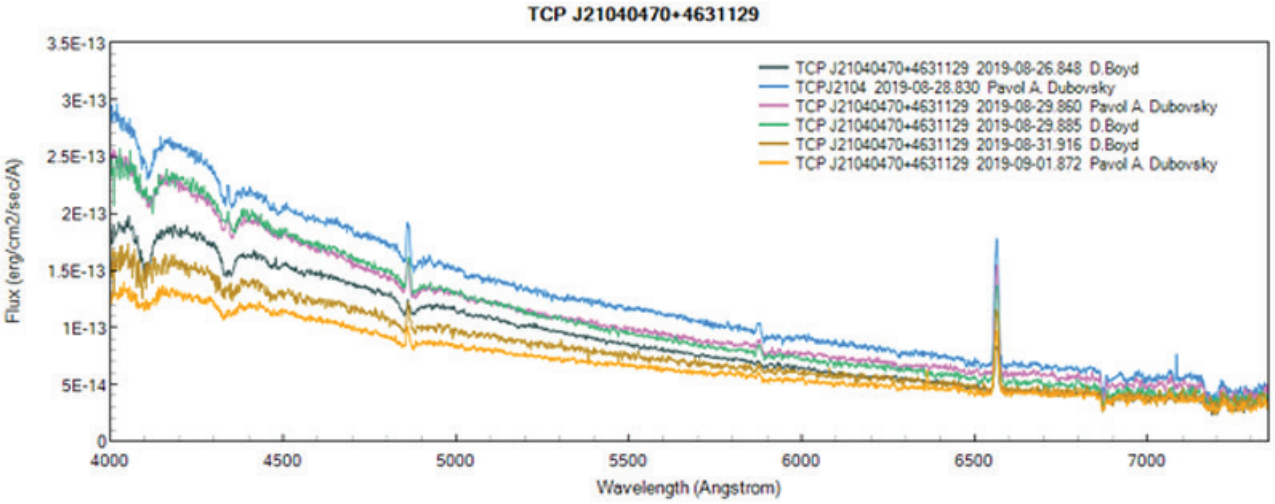

Fig.5 - Spectra recorded during 2nd outburst from 26th August to 1st September.

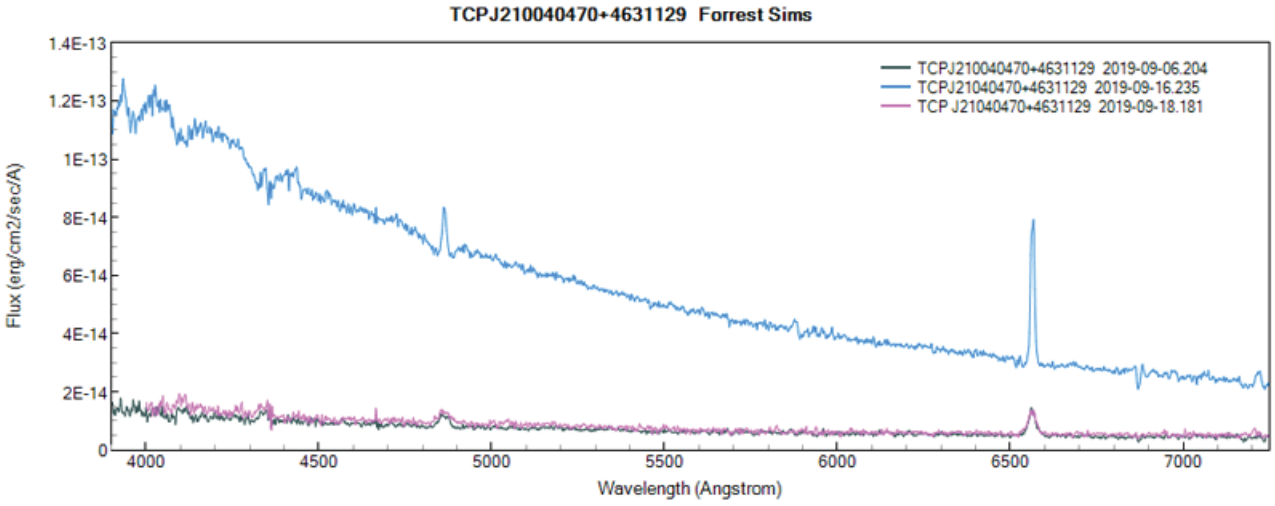

Fig.6 - Spectra recorded on 6th September following 2nd outburst, on 16th September during 3rd rebrightening and on 18th September after 3rd rebrightening.

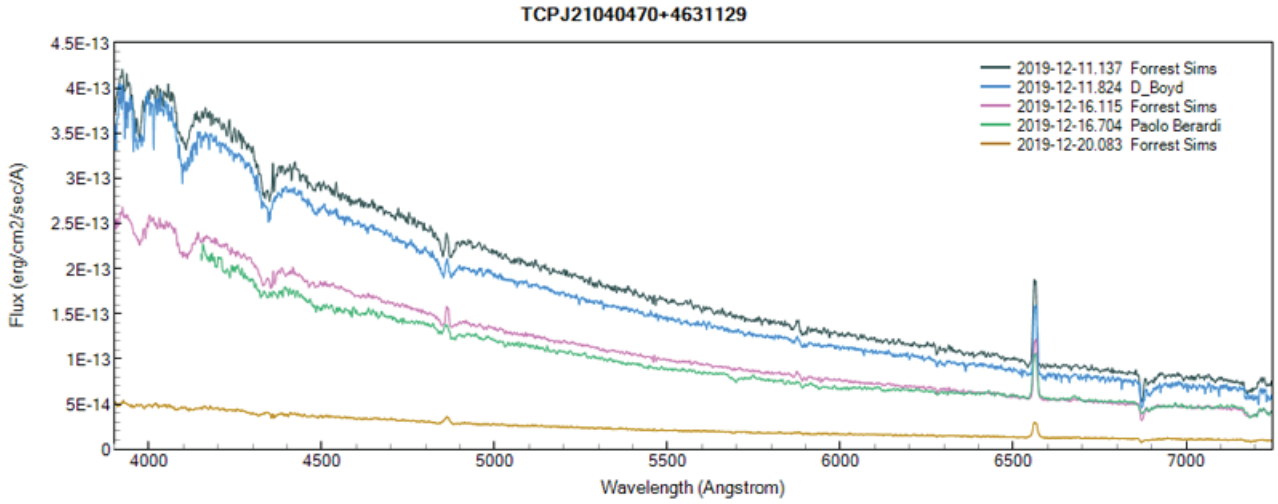

Fig.7 - Spectra recorded during 3rd outburst from 11th to 20th December.

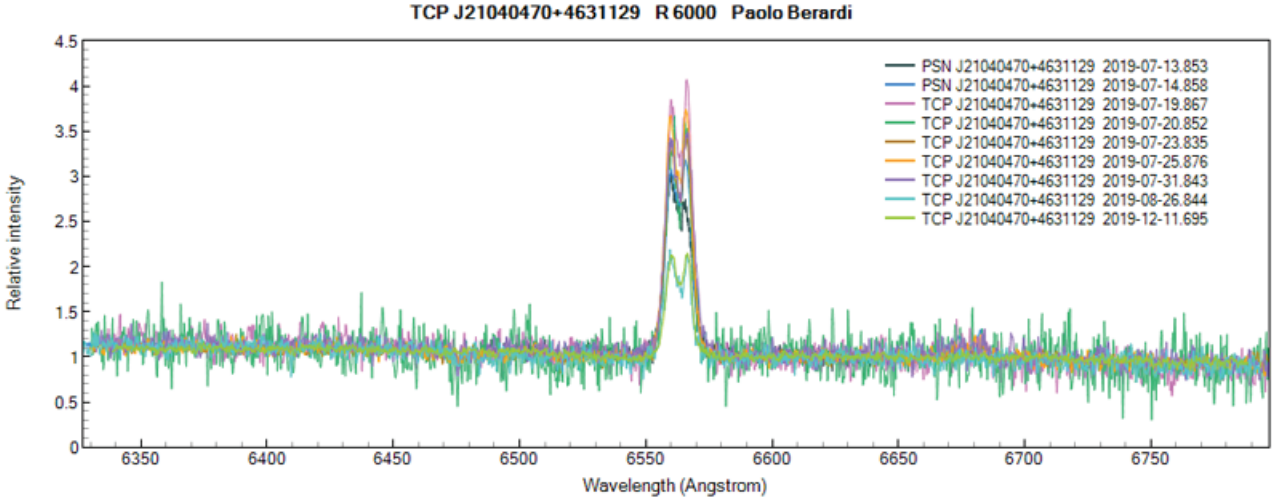

Fig. 8 - Series of rectified high resolution (R 6000) spectra of the Hα emission line between July and December showed the consistent double peaked profile expected of an accretion disc seen at high inclination. FWZI ~ 700 km/s.

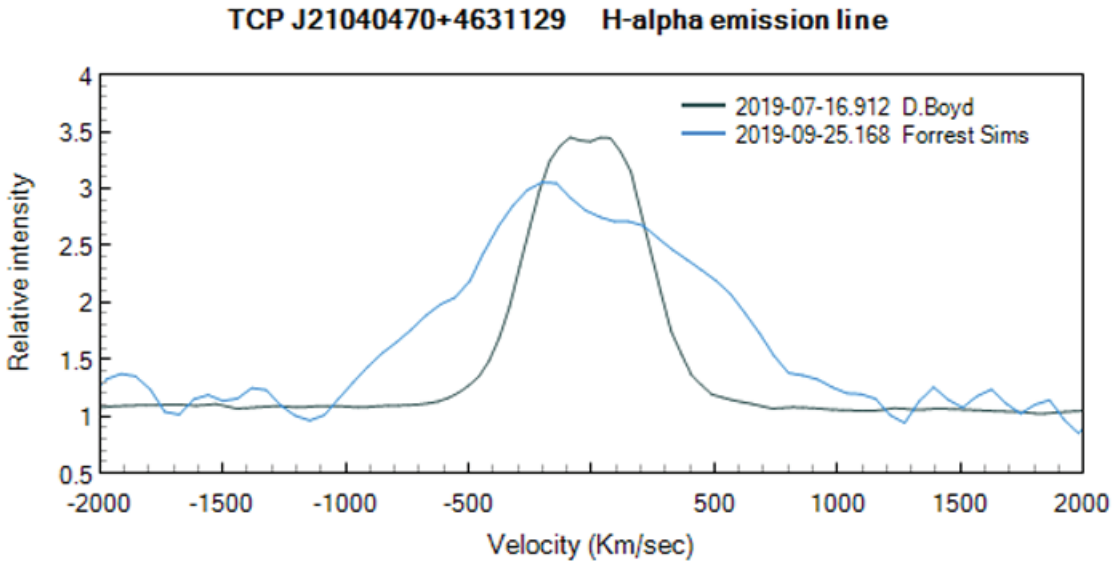

Fig. 9 - Comparison of Hα emission line profiles between outburst (2019-07-16) and quiescence (2019-05-25).

	Outburst	Quiescence
FWHM (km.s^{-1})	560	1096
FWZI (km.s^{-1})	768	1616

A report of time resolved spectroscopy of the Hα emission line by Paolo Berardi was included in the 2019-Q3 newsletter. An analysis of these Hα spectra by Neustroev et al. reported in ATel 13009 gave an orbital period of 77.07±0.02 min. This agreed well with the orbital period of 77.04±0.43 min derived from optical photometry over the same period (ATel 12947).

The initial superoutburst of TCP J21040470+4631129 was unusually bright for a dwarf nova and offered the possibility to directly measure the orbital period using low resolution (R~1000) time resolved spectroscopy. Series of 300 sec spectra with accompanying calibration frames were recorded on 5 nights between 13th to 18th July. On average 15 spectra were recorded each night covering approximately one orbital period of the dwarf nova. Heliocentric correction was applied to the times of all 73 spectra. Wavelength calibration included correction for temperature drift during each night. Subsequent spectra within each night were cross correlated with respect to the first spectrum to measure the time variation in their relative radial velocities. Zero point drift in radial velocity from night to night was accounted for by subtracting a nightly mean radial velocity. A period analysis of all 73 radial velocities gave a period of 76.81±0.20 min for the mean orbital period between 13 and 18 July, consistent with photometric measurements (Fig. 10).

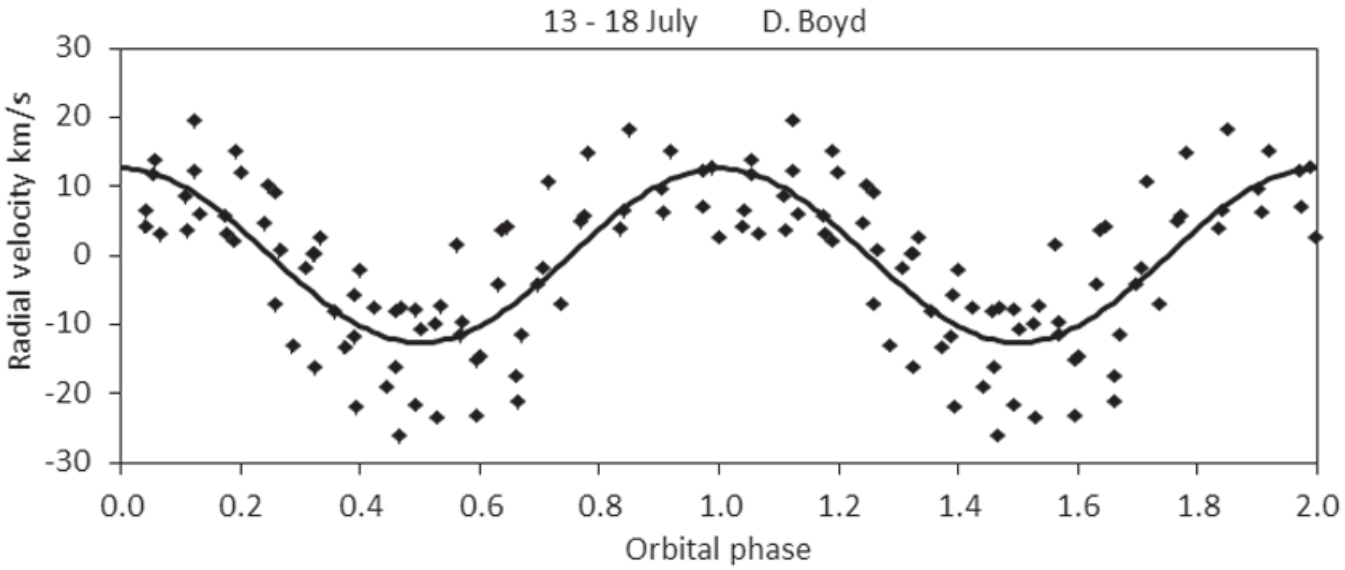

Fig. 10 - Spectroscopic radial velocities measured between 13 and 18 July phased on the orbital period of 76.81 min with a fitted sine function.

Some notes on shocks and diagnostics (part 2)

Steve Shore

The last installment covered the signatures of a shock passing through a dense circumstellar medium, the case of V3890 Sgr and other recurrent novae that resemble symbiotic stars. We got to the point of discussing the essential diagnostics of the early stages. In that early stage, then the radius of the front is on the same scale as the length on which the density of the red giant wind decreases, While the piston is deeply imbedded in the wind and expanding with velocities of thousands of km/s, strong X-ray and EUV emission from the matter that's already been engulfed by the shock produces a luminous ionizing precursor. But the density is decreasing with distance from the red giant, which means the shock is not slowing down as quickly as it would were the density constant. More to the point, the rate at which the atoms recombine depends very sensitively on the local density. So when the gas is ionized by the shock's hard irradiation, it stays ionized even as the emission weakens.

Shock precursors and photo-ionization fronts in diffuse media: from breakout to crush-ing

Let's go back, for a moment, to the mother of all interstellar nebular, the classic H II region. You know these from all of the images of regions like M 42 (Orion) and 30 Dor (``the Tarantula''). As a first pass approximation, these are regions where the gas is completely ionized by the continuous illumination of an imbedded hot single or cluster; think of the Trapezium θ^1 Ori).

Ambient neutral atoms are ionized by UV radiation (with wavelengths shorter than 912 Å, or energies above 13.5 eV). The number density of the medium is set somehow, it doesn't depend on the stellar properties, and in the locality of the source it's roughly constant. You can now imagine inscribing a sphere *completely* around the star. The *totality* of photons passing through any shell will pass through any other shell. If at each shell a photon is absorbed and ionized the atom, that photon is ``lost''. But don't despair, there's another coming along since it will be the *rate* of arrival that matters. That new arrival may find the medium already depleted in neutrals so it continues until it is absorbed. And so it continues. The ionized region continues to grow linearly in time. Were this all there is to it, in time every star would ionize a progressively growing region until it turns off. This is why rate matters. Since the gas is neutral, every ion produces a free electron at its inception and, therefore, that electron can be recaptured if you wait long enough. The farther you are from the central source, the lower the rate of arrival of ionizing photons but the rate of recombinations, the neutralizing events, is local and depends only on the local number density.

Closer to the source, the ionization rate overwhelms the recombination rate. Farther away, it begins to give way to the neutralization that means an atom is now available to absorb and re-ionize. You see that there is a unique radius, for a uniform gas, at which the two rates balance, depending only on the luminosity of the source and the density of the circumstellar medium. Called the *Strömgren radius*[1], this is the approximate size of the zone of influence of the star.

Outside the region, the neutral gas is invisible. Inside, the recombining electrons drop through all the

1 Stromgren, B. 1939, ApJ, 89, 526: ``The Physical State of Interstellar Hydrogen'', https://ui.adsabs.harvard.edu/abs/1939ApJ....89..526S/abstract

available energy levels of the atoms to eventually reach the ground stare, emitting photons with each step of the cascade. This doesn't mean they proceed like walking down steps; it's more like a crowd stumbling down any combination of steps screaming at progressively higher frequencies as they near the bottom.

For a pure hydrogen gas, the lines will be the complete ensemble of the line series, ending with the Lyman lines in the UV and also passing through the Balmer series. The latter are the familiar optical lines that begin with Hα ending at 3647 Å with the Balmer limit. It is this series that gives the regions their conventional name, *H II regions* (a misnomer because, in fact, the spectrum of ionized hydrogen is *not* emission lines but a thermal continuum). The denser the circumstellar medium, the more compact the ionized region. The same holds for the central star's luminosity. The emission lines from such regions, however, are not only formed by recombination.

The gas is never pure hydrogen and the stellar continuum doesn't simply truncate at the ionization energy for hydrogen. Several important elements have lower first, and even second, ionization energies and absorb photons that would otherwise produce a more extended H II region. These also have individual ionization zonation so different ions are formed at different distances from the central source depending on their atonic properties (the rate of capture of ambient electrons and their absorption efficiencies). You see this most clearly in planetary nebulae, individual ions come from stratified radial zones (He II is formed, for instance, closer to the central white dwarf than, say, [N II] or O I).

There is one more important difference between compact (dense) environments and the diffuse gas of the interstellar medium. Although really just more jargon, the physical distinction is simple to apply and basic. When inside a cloud, the ionization zone may be limited in size by the luminosity of the star. This is, in the business, referred to as '' ionization bounded''. Here you run out of ionizing photons before you run out of gas so the source may be surrounded by an extended neutral region. In contrast, should the density be low enough, the region may be ''density bounded'' such that the ionization breaks out of the locale and further affects the surroundings, much like a visible H II region around already visible OB stars in a region like, for instance, the Trapezium. It's not that the ionized gas extends forever and everywhere, just that it becomes very large and, if there is a density stratification around the star, exceeds the confines of that local gas.

What this has to do with the symbiotic precursor case we discussed last time is that a shock, propagating through a symbiotic star wind, passes from one of these extremes to the other and not spherically.

At first, because of the particulars of the orbit, the white dwarf is imbedded deeply in the giant's wind. The initial precursor-dominated region around the shock is compact and would rapidly recombine were the shock to stall. But if the piston keeps moving, and actually accelerating for the part that's moving outward in the wind, the ionized region expands rap-

idly ahead in the direction away from the giant while remaining more compact on the side facing it. Thus, because of the different densities, one region will remain ionized for longer than the other. As we discussed last time, the shock does indeed break out of the dense inner wind at which time it's luminosity falls off as the density drops. It remains, however, a strong source of X-rays and extreme UV. The gas not only becomes progressively more highly ionized, e.g., lines of [Fe XIV] or higher appear in the visible, but these persist because the gas only slowly recombines even after the shock has ceased to power the ionization. In other words, the gas is no longer in photo-ionization equilibrium and can remain highly ionzed and with emission lines that persist long after the event ends.

The other side, toward the giant, has the piston plowing into ever denser gas and slowing so there too it's a less potent ionising source. But more to the point, that inner wind gas recombines much more rapidly (we're talking about several orders of magnitude different abundances) so the very high ions aren't contributed from that zone. This has an important signature in your observations: you'll see different line profiles from different ions depending on the region over which they form. Remember, this isn't a static medium -- it's a wind, albeit a slow outflow -- with a velocity gradient and a density profile.

This has an important signature in your observations: you'll see different line profiles from different ions depending on the region over which they form.

Additionally, and perhaps the most attractive feature of the profile as a projection of the line formation, there must be a shadow zone from which the higher ions are excluded and that will not show the dynamics of the shock. This is the rear side of the giant, where during the pre-outburst stage the wind was shielded from the softer UV of the accreting white dwarf. Now it's like standing on the rear side of rocks in a harbour, the wave (shock) arrives and passes around the rocks. Yes, there is a diffraction of the shock but the star's rump side is shielded. Thus, while the shocked gas on one side of the wind shows the dynamics of the piston and the ionization of the precursor, the other side shows the chromosphere and slow wind of the giant. Depending on the angle of viewing these will produce shifting signatures in the observed combined profile.

Take a view of the receding shock from the side of red giant inferior conjunction (what would be the eclipse by the giant of the WD). The gas is neutral while the other wide is an H II region of sorts so one side absorbs against the other. The H I lines will show this effect and the Balmer lines should show this as phase modulations of the profile in time. We've discussed this some time ago regarding the normal variations of the Balmer profiles in the quieter symbiotic systems. ow you have this more dramatically because even the He I lines may show some effects. If the system is less violent than V3890 Sgr or RS Oph or V407 Cyg or other symbiotic-like recurrent novae, so take the case of Z And or CH Cyg, the lines formed by any shock will not be as dramatically broadened and the absorption can more seriously change the measured fluxes. This requires looking at different transitions of the Balmer series, He I, and also using the highest resolution possible.

Shock precursors, unlike the photo-ionization provoked by the hot com-

panion, render the formation of the emission lines during transient events much more difficult to interpret. It isn't unlike what happens in novae compared to planetary nebulae. Very strange ions, from states far higher than would normally be expected from the current conditions of the WD, can persist or just appear.

In novae, for instance, long after X-ray observations from Swift indicate that the white dwarf has ended its supersoft emission phase, the low density parts of the ejecta -- those with highest expansion velocity -- may still be visible and preserve information about what the illuminating continuum looked like. Take the case of ASASSN-17hx, also known as nova Sct 2017. The X-ray source was never detected yet, years after the event, the optical spectrum displayed strong lines of [Fe X+ and [Fe XI] that bespeak ionization by some source reaching at least 0.1 keV. Recombination was so slow that these spectra were still visible. Their excitation is particular: these are ground state lines so could still be excited by collisions with electrons at only a few eV but, because the density in the line forming region was so low, there wasn't a subsequent collisional de-excitation. Similar processes occur for a wide range of lines and in symbiotics this is made more complicated by the continuing weaker photoionization once an outburst ends. Thus, [O I] may form from recombination but the 6300 Å line can be collisionally excited. The same holds for [Ne III], [O III], [N II], and many other forbidden lines.

The Balmer and He I and II lines, in contrast, require much higher energy electrons for excitation and are purely recombination so, again, these trace different emission zones in the wind of the giant. The advantage in outflows, like winds, and ejecta is that the velocities help separate these regions while in an unresolved H II region, such as the emission from a star forming site in an external galaxy, this isn't possible.

One last thing should be mentioned regarding H II regions, and tis also applies to planetary nebulae. While we carry in our heads a picture of a smooth, uniform medium, even if there's a density stratification, that surely isn't true in detail. High contrast imaging, whether in visible or radio bands, shows networks of filaments and blobs. The Helix nebula is a well known example where ''cometary'' structures are observed with tails pointing away from the central star. In the shadow regions, the UV is screened out and you can observe lines from lower than expected ions. Forbidden lines may be suppressed in the higher density knots while the diffuse gas shows them, and even recombination lines may be differently weighted because the local emission depends on the density.

While we carry in our heads a picture of a smooth, uniform medium, even if there's a density stratification, that surely isn't true in detail.

Usually we talk about filling factors, the fraction of a volume that's filled by gas, when converting from the intensity to mass of the structure, as in nova ejecta. Bu the inter-filament part of the structure isn't empty, just lower emissivity, so what you see is a sum over all of these. If the individual knows are visible, that helps and in nova ejecta that is the case. But again, when there is little systematic motion, these knots may superimpose and be indistinguishable. This also changes how you convert between the emis-

Don't forget that although we talk about adiabatic shocks, meaning that their energy is constant, it isn't really.

sion in the line and the number of photons emitted by the central source.

The same hold for shocks, both the precursor and the post-shocked gas. Different zones of the shock have different temperatures and densities, the gas cools after it's been accelerated, and between collisional excitation and de-excitations and recombinations, the inhomogeneities in the swept-up gas will make their presence known. Don't forget that although we talk about adiabatic shocks, meaning that their energy is constant, it isn't really. The gas is always cooling even if its luminosity is a negligible drain on the energy of the shock at any moment. As the expansion proceeds, this emission continues to drain energy from the post-shocked gas and eventually can dominate the energetics and dynamics, as we discussed in the last instalment.

Boundary and bow shocks

Bow shocks and *asterospheres* are our final, promised example of shocked flows. There's no precursor, they are too slow or weak for that, but they have some remarkable signatures. First, the radiative shock structure forms when a star moves through the ISM. Or, in our previous picture, when the medium moves past the star. A stellar wind is a fuzzy boundary, incident gas can enter the boundary but, ultimtely, must come to rest or pass out the downstream side. The point where the dynamical pressures balance is a stalled shock, standing off at a distance that depends on the mass influx from the diffuse environment and the rate of stellar mass loss. To a pretty good first guess, the shock is a sort of cylindrical parabola with the windy star at its apex. Here the flow is deviated sothere's a slip between the two regions and that's what's responsible for the broadening of the opening angle with distance. The heliosphere, while more complicated because of the essential role played by the stellar magnetic field and the extremely weak outflow, nonetheless has a boundary shock beyond 40 AU (or about 3000 $R_{\odot}$). The difficulty with this simple picture for stars like the Sun is the collisionless nature of the gas; the densities are so low, a few cm-3, and the flow speeds high enough that collisions are suppressed and neutrals can slip into the inner heliosphere. I'll leave this aside because, aside from possible visibility at the very low radio frequencies achievable with LOFAR, there's no emission observable fro these.

But when the star has a stronger wind, and for OB stars that's six or seven orders of magnitude greater than the Sun and with hiher velocities, things get more interesting. The rate of excitation of the Balmer lines is sufficient to render the arcs visible. The higher the differential velocity relative to the surrounding ISM, the stronger the shock and the greater the compression and collisional excittion. There regions, like the front of a blunt-nosed ship, form a compression zone, a bow shock. It behaves very much like an H II region. If dense and opaque enough, the flow passing the stand-off distance is now ionized. It might already arrive at the shock ionized, the shock itself rdiates in the XR and EUV so could prepare the upstream gas. Examples are accumulating in the Galaxy, the best observed is λ Cep but others have these bow structures. A cute feature, as you might guess from the example of a wind sock, is that the direction of the vertex lies in the direction of the star's motion. Using the radial velocity and (if available) proper

motion in RA and DEC, the three dimensional velocity follows and, then, the strength of the wind can be measured from the cone structure. This is still a developing procedure but, especially after the Gaia results, it's becoming a tool of great promise. The most extreme examples, the so-called runaway stars (those young stars whose space velocities are hundreds of km/s) are massive stars ejected from associations through multiple close passes with nearby cluster members (or, in some cases, from systems in which a star exploded as a core collapse supernova). A few leaving the Galactic center are even faster, one at about 1000 km/s from the central parsec or so has been detected and there are surely more. If possessed of a strong wind these are like supernovae in the background ISM.

I realize your head is likely splitting by now, and these issues are more technical in nature than our usual discussions. But you should always bear in mind that what we see is always smoothed out by the spatial resolution of our instruments and the inhomogeneities of real cosmic nebulae can only be disentangled by using as many diagnostics as possible. When you get inconsistent answers from different tracers it may not be wrong: they may be revealing structure. This is yet another reason why spectroscopy is such a powerful tool and I hope inspires your imagination as you ramble in the astronomical garden.

When you get inconsistent answers from different tracers it may not be wrong: they may be revealing structure

Eruptive stars spectroscopy
Cataclysmics, Symbiotics, Novae

Spectroscopic monitoring of eruptive stars (e.g. symbiotic binaries, classical novae) by amateurs around the world, in both the northern and southern hemispheres, is a fundamental activity of the ARAS (Astronomical Ring for Amateur Spectroscopy) initiative. The group of volunteers demonstrates what can be accomplished with a network of independent, very small telescopes (from 20 to 60 cm), furnished with spectrographs of different resolution, from 500 to 15000, and covering the range from 3600 to 9000 Å. The observing program concentrates on bright symbiotic stars (64, to date) and novae (41, to date). The main features of the ARAS activity are rapid response to alerts, long term monitoring and high cadence. A part of the program involves collaborations based on requests from professional teams (e.g. CH Cyg, AG Dra, R Aqr, SU Lyn, T CrB) for long term monitoring or specific events.

Submit your spectra:

Please :
- respect the procedure
- check your spectra BEFORE sending them

Resolution should be at least R = 500
1/ reduce your data in accordance with standard procédures
(notably offset, dark, flat,
correction of atmospheric and instrumental response)
2/ the header must be compliant with BeSS file format
3/ name your file as: _novadel2013_yyyymmdd_hhh_Observer
Example: _chcyg_20130802_886_toto.fit
4/ send you spectra to francoismathieu dot teyssier at bbox dot fr
for inclusion in the ARAS database

ARAS database:

http://www.astrosurf.com/aras/Aras_DataBase/DataBase_EruptiveStars.htm

Conditions for use of data in publications

Note there is a first level validation check prior to adding spectra to this table.
Users should verify the quality of the spectra.
Use of these data in research publications is encouraged subject to the following conditions:

*ARAS DataBase Eruptive Stars should be acknowledged with reference to http://articles.adsabs.harvard.edu/pdf/2019CoSka..49..217T

* Observers' contribution must be acknowledged

* Observers contributing a significant amount of data or whose data are pivotal to the findings of the paper should be included as co-authors.

Please contact François Teyssier (francoismathieu.teyssier [at] bbox.fr) before submitting the publication .

The Letter is prepared by François Teyssier (FR), David Boyd (UK), Forrest Sims (US)

Download previous issues of the Eruptive Stars Information Letter:

http://www.astrosurf.com/aras/novae/InformationLetter/InformationLetter.html

The letter in the SAO/NASA Astrophysics Data System

https://ui.adsabs.harvard.edu/abs/2019ESIL...43...19T/abstract

Your observations, taken with higher cadence than usually followed in the literature will be key to understanding thisin a broad range of systems.

S. Shore, 2015

… the presented results showed also the importance of professional/amateur collaborations. ARAS Group is a perfect example that such collaboration can be very successful and can bring important results. Thanks to amateur photometric and spectroscopic data, we are now able to monitor the evolution of symbiotic systems on timescales which were not previously available.

R. Gàlis& al., 2019

We are grateful to all of the amateur astronomers that contributed their observations to this paper. In particular, we are thankful to members of the ARAS group for theirwonderful work.

K. Ilkwiecz & al., 2015